BEHAVIOUR OF ULTRA-HIGH PERFORMANCE CONCRETE AS A JOINT-FILL MATERIAL FOR PRECAST BRIDGE DECK PANELS SUBJECTED TO NEGATIVE BENDING

by

David Rodrigues Coelho Amorim

A Thesis submitted to the Faculty of Graduate Studies of

The University of Manitoba

in partial fulfilment of the requirements of the degree of

MASTER OF SCIENCE

Department of Civil Engineering

University of Manitoba

Winnipeg

This page intentionally left blank

Abstract

This thesis investigates the behaviour of UHPC as a fill material for precast deck panels subjected to negative bending. Two full-scale test specimens were constructed. The transverse joints between the panels, the shear pockets, and the deck haunches were all filled with UHPC. A total of four tests were performed including two static tests to failure and two fatigue tests, one of which was performed to failure. Testing consisted of a loading apparatus acting upwards on the deck soffit in an attempt to impose tensile stresses across the transverse joints, representing the conditions that a transverse joint in the negative moment region of a continuous bridge deck would experience. It was concluded that the transverse UHPC joint performed satisfactorily by transferring bending stresses and shear stresses across the joint from one panel to the adjacent panel. Overall, the test specimens displayed performance levels expected from conventional cast-in-place concrete deck alternatives.

This page intentionally left blank

This Thesis is dedicated to my loving wife Kayla for her continuous support throughout my graduate studies. I am constantly amazed by her dedication and perseverance and I would not be motivated to complete this project were it not for her daily support.

This Thesis is also dedicated to my family, especially my mom and dad, Maria and Laurentino Amorim for all the love and support that they have provided me with. I would not be the person I am today without them and I am eternally grateful for all that they have done to try to provide me with the best life possible.

Thank you.

This page intentionally left blank

Acknowledgements

I would like to acknowledge the guidance provided by my advisor, Dr. Dagmar Svecova throughout my graduate research. Her insight and support were most valuable. I would also like to acknowledge Dr. Aftab Mufti and Dr. Baidar Bakht for their technical guidance and Dr. Chad Klowak and the W.R. McQuade Structures Laboratory technical staff for their efforts throughout the course of this project. I must acknowledge Manitoba Infrastructure and Transportation (MIT) for providing me with an opportunity to conduct this exciting research as well as for their significant financial contribution to the project. Given my passion for structural engineering, especially bridge design and construction, I am very grateful to have collaborated with MIT on a project that has a very direct contribution to the engineering community in Manitoba. Thank you to all those at MIT I collaborated with, especially Mr. Evan Fer, for your assistance throughout the course of my studies.

This project could not have been completed without the assistance and input of the many individuals involved. I cannot acknowledge every last one due to space restrictions but I must acknowledge Dr. Hugues Vogel of Stantec Consulting, who was the Red River Bridge Design Engineer; Mr. Ryan Sanders of M.D.Steele, who assisted with test specimen construction; and Mr. Gaston Doiron and Mr. Kyle Nachuk of Lafarge Ductal, who provided the UHPC and supervised its preparation and placement.

I would also like to acknowledge all of the organizations that have supported my graduate research financially through scholarships and fellowships including the UofM, NSERC, ACI, AGA, CPCI, TAC, and NPCA. Without your help, this project would not be possible.

Table of Contents

List of Figures

List of Tables

List of Symbols

E_s = Elastic modulus of steel

f_{pu} = Ultimate strength of prestressing strands

δ_{max} = Maximum deflection achieved

δ_{perm} = Permanent deflection of specimen following unloading

δ_{ult} = Deflection corresponding to ultimate load

Ω = Ohm

List of Abbreviations and Acronyms

AASHTO = Association of American State Highway and Traffic Officials

ABC = Accelerated Bridge Construction

ASCE = The American Society of Civil Engineers

ASTM = American Society for Testing and Materials

CIP = Cast-in-Place

CSA = Canadian Standards Association

c.t.c. = Center-to-Center

CV = Coefficient of Variance

DAQ = Data Acquisition System

DOT(s) = Department(s) of Transportation

ESG = Electrical Strain Gauge

EVA = Ethylene-vinyl Acetate

FHWA = Federal Highway Administration

FRP = Fibre Reinforced Polymer

HFL = Highways For Life

HPC = High Performance Concrete

HSC = High Strength Concrete

HSS = Hollow Structural Section

HRWRA = High Range Water Reducing Admixture

IDOT = Iowa Department of Transportation

LRFD = Load Resistance Factored Design

LVDT(s) = Linear Variable Displacement Transducer(s)

MDOT = Minnesota Department of Transportation

MB = Manitoba

MIT = Manitoba Infrastructure and Transportation

MTO = Ministry of Transportation of Ontario

NCHRP = National Cooperative Highway Research Program

NSC = Normal Strength Concrete

NYSDOT = New York State Department of Transportation

PPCP(s) = Precast Prestressed Concrete Panel(s)

PTH = Provincial Trunk Highway

SHRP2 = The Second Strategic Highway Research Program

SD = Standard Deviation

TRB = Transportation Research Board

TS1 = Test Specimen #1

TS2 = Test Specimen #2

UHPC = Ultra High Performance Concrete

UHS FRC = Ultra High Strength Fibre Reinforced Concrete

UofM = University of Manitoba

WisDOT = Wisconsion Department of Transportation

w.r.t. = With-Respect-To

Chapter 1

Introduction

1.1 Overview

The Report Card for America's Infrastructure assigned a C+ grade to America's bridges reporting that one in nine bridges are rated as structurally deficient as the nation's average bridge age approaches 42 years (American Society of Civil Engineers, 2013). To address the crumbling bridge infrastructure, an estimated $20.5 billion must be spent every year for the next 15 years. Although the Federation of Canadian Municipalities has recently started publishing its own infrastructure report card, the condition of the nation's bridges is not directly addressed (Federation of Canadian Municipalities, 2012). However, it is safe to say that Canada's bridge infrastructure is also in dire need of attention.

While the direct construction cost of addressing these crumbling bridges can be easily quantified, the indirect costs, such as those incurred due to closures of major transportation routes for construction purposes are harder to estimate but must also be considered. The American Society of Civil Engineers (ASCE) reports that over two hundred million trips are taken every day across structurally deficient bridges in the United States alone (American Society of Civil Engineers, 2013). The replacement or rehabilitation of one of these deficient structures requiring the closure of the major transportation routes they are a part of can have severe consequences to the nation's economy.

Naturally, the desire to construct new bridges or rehabilitate existing bridges in shorter amounts of time with less of an impact on the surrounding environment and transportation

network evolved. This has led to the development of Accelerated Bridge Construction (ABC) practices. While many ABC methods, such as the use of precast concrete girders for example, have been around for decades, the concept of ABC as it is known today is relatively new.

ABC is a broad term covering a variety of construction methods however ABC projects generally take on two main forms (Transportation Research Board, 2013): firstly, the prefabrication of bridge elements for the in-place construction of structures; and secondly, the use of bridge-moving technology to *move* completed bridge structures into place from their construction location typically adjacent to the completed alignment. In addition, either of these two main forms may involve other practices such as the tendering and procurement of certain materials, separately and in advance of the main construction contract. Only the first form of ABC projects involving the prefabrication of bridge elements, will be discussed here forward.

1.1.1 Precast Bridge Deck Panels as a Solution

A major element of ABC projects is the use of modular precast bridge components. These precast components regularly include girders but may also include abutments, piers, pier caps, and bridge decks (Transportation Research Board, 2013). In particular, precast concrete bridge decks have become a very common component of ABC projects. Whether the project is the construction of a new structure, or the rehabilitation of an existing deteriorated structure, implementing precast bridge deck panel systems can greatly accelerate the project schedule.

Reports on completed construction projects indicate that the construction time of bridge structures can be reduced by as much as 50% to 75% by using precast concrete bridge deck panels versus conventional cast-in-place (CIP) concrete decks (J. Fowler, 2008). However, a reduction in construction time is not the only advantage of these precast panel systems as these systems also offer increased quality, reduced structure weight, and reduced lifetime costs (Precast/Prestressed Concrete Institute, 2011).

Precast concrete bridge deck panel systems have been used in many jurisdictions across North America with projects dating back as early as 1965. While the use of these deck panel systems has increased since its earliest applications, they are still not as widely used as conventional CIP deck systems. Reasons for this include higher initial construction costs for precast systems, lack of knowledge by design engineers, lack of uniformity and consistency in design details, and more importantly, concerns over long-term performance and durability due to a lack of understanding of how these systems perform long-term under loading (Precast/Prestressed Concrete Institute, 2011).

1.1.2 Use of Precast Bridge Deck Panel Systems in Manitoba, Canada

Manitoba Infrastructure and Transportation (MIT), the governing transportation body for the Province of Manitoba (MB), completed a major bridge rehabilitation project in 2014/2015 involving the use of full-depth precast prestressed concrete bridge deck panels (PPCPs) to replace the existing deteriorated CIP concrete deck on the Red River Bridge. This project was the first structure in the Province of Manitoba to incorporate this full-depth and full-width precast deck system.

The existing Red River Bridge was constructed in 1968 and consisted of a steel-reinforced concrete deck acting compositely with four lines of haunched steel I-girders. The structure is located on Provincial Trunk Highway (PTH) 23, a secondary rural arterial highway, serving to connect PTH 59 to PTH 75. Due to extreme Red River flood events that may potentially occur during the spring and early summer months, PTH 75 (the main north-south highway connecting MB with the USA) can be closed resulting in a significant increase in traffic being routed along PTH 23 through Morris, MB. Due to the fact that PTH 23 becomes a lifeline for the Town of Morris during these extreme flood events, MIT considered it essential that the structure remain in operation year round including during times of flooding and seeding or harvesting of grains (MMM Group Limited, 2012).

As part of the preliminary design for the rehabilitation, MMM Group Limited (MMM) conducted two visual inspections of the existing structure in July and September of 2011. MMM reported that the 191 mm thick concrete deck with an asphalt overlay of varying thickness was in generally poor condition. The deck showed signs of spalling, cracking and delamination and it was ultimately recommended that the deck be replaced (MMM Group Limited, 2012).

Stantec Consulting Limited (Stantec) was retained to complete a detailed design for the rehabilitation of the bridge. The proposed rehabilitation included the replacement of the existing deteriorated concrete bridge deck utilizing full-depth and full-width PPCPs. Since this was the first application of its kind in Manitoba consisting of PPCPs in combination with

ultra-high performance concrete (UHPC) fill material, MIT desired to have experimental testing performed to evaluate the performance of the proposed system.

1.2 Objectives and Scope

The first objective of this research was to conduct a thorough literature review to obtain a clear understanding of: the history of precast bridge deck panel systems, the current state-of-practice and any research completed on similar systems. Current code provisions from both the AASHTO LRFD Bridge Design Specifications, specified by the Province of Manitoba for use on provincial projects, and the CSA/CAN S6-06 Canadian Highway Bridge Design Code, specified by the remaining Canadian provinces and territories, and other guidelines pertaining to the use of PPCP systems were also reviewed.

The second objective was to examine the constructability of the proposed PPCP system. MIT constructed a full-size mock-up of the bridge deck system to assess the constructability and to allow local contractors to familiarize themselves with the proposed system prior to bidding on the rehabilitation contract. A full-scale testing program was then developed consisting of the construction and static/cyclic testing of specimens constructed using three 6007 mm x 2415 mm PPCPs made composite with two 1538 mm deep steel plate girders; the PPCPs and the steel plate girders were supplied by MIT. The construction of the test specimens was well documented and observations regarding the general constructability of the system were made. It should be noted that while the researchers attended the MIT full-size construction mock-up, the mock-up was not ultimately a part of this research program and is not discussed further.

The third objective was to determine the performance of the transverse joint detail subjected to cyclic loads and static overloads. The test specimens were tested with the load applied to the deck soffit pushing up on the deck to induce negative bending moments in the test specimen. Strains in the vicinity of the transverse joints were measured, cracks were identified and monitored, and the strength of the joint relative to that of the panel was determined.

The fourth and final objective was to monitor the composite performance of the system, specifically the composite performance between two adjacent panels as well as between the panels and girders. Extensive monitoring instrumentation was incorporated into each test specimen to obtain an understanding of the behaviour of the system.

1.3 Research Significance

While there have been many projects completed using PPCPs, it is important to note that there exists many types of precast bridge deck systems. Throughout the years, performance issues with these systems has led to innovative solutions, that while solving the performance related problem, introduced undesirable complexity and in turn cost to a project. One example is the evolution of longitudinally post-tensioned precast panel systems in the 1970s and 1980s. Longitudinal post-tensioning allows the transverse joints to be put into compression under service loads thereby mitigating many durability issues seen on earlier projects. However, panels became more complex to construct and the on-site post-tensioning process increases construction time and overall cost. After years of progressive innovation, today's commonly used PPCPs and UHPC fill material system, similar to that used on the

Red River Bridge, appears to have solved many performance related issues, however its use has been in-most part limited to simply supported structures.

Due to the desire to design bridges made continuous for live load, a technical knowledge gap exists in the use of UHPC jointed PPCP deck systems in areas of negative bending, as is the case over and in the proximity of an interior sub-structure of a continuous bridge. In addition, due to the relatively recent development of these systems, there does not exist sufficient long-term performance data. Therefore, this research involving the static and fatigue testing of full-scale models in negative bending serves to fill a current research gap and will provide transportation authorities with additional performance data to allow these systems to be comfortably implemented in future projects.

1.4 Organization of Thesis

This thesis has been divided into five chapters as follows: Chapter One introduces the research project, its objectives and scope, and its significance to industry; Chapter Two details a literature review conducted on various aspects of the research program; Chapter Three outlines the research program in detail including descriptions of the test specimens, their construction and instrumentation, and details of the testing scheme; Chapter Four provides the experimental results and analysis of the data; and finally, Chapter Five summarizes the research program and offers conclusions and recommendations based on the findings of the research presented herein as well as recommendations for future work.

Chapter 2

Literature Review

2.1 Introduction

The following Chapter provides a summary of the literature review for this project. In particular, typical PPCP bridge deck systems are described, past research conducted on precast bridge deck panel systems is presented, UHPC as a material is briefly defined and characterized, and current code provisions relating to the design and construction of PPCP bridge deck systems are discussed.

2.2 Typical Precast Panel Bridge Deck System Description

Precast concrete bridge deck panels come in many forms ranging from partial depth to full depth systems. Only full depth precast panel systems will be discussed here forward. Panels can potentially span the full width of the structure in the transverse direction, or be half width or less, therefore requiring multiple panels in the transverse direction introducing longitudinal joints into the system. Although using full-width panels is desirable, when staged construction is necessary or when the structure width exceeds approximately 15 m, half-width panels are typically used. Ultimately, panel sizes are governed by transportation and handling requirements (Precast/Prestressed Concrete Institute, 2011).

The precast panels are designed for transverse flexure and are reinforced with mild reinforcement, prestressed reinforcement, bonded post-tensioned reinforcement, or any combination of these. The panel thickness is limited to a minimum of 175 mm but is usually

thicker depending on the reinforcement used, transportation and handling requirements, or its anticipated loading conditions (Precast/Prestressed Concrete Institute, 2011).

The concrete panels are typically anchored to the girders by means of positive attachment such as shear stud clusters located in discrete full-depth shear pockets filled with a grout material (Chavel, 2012); this allows for composite action between the girders and panels thereby increasing the structural efficiency of the system.

In composite systems, the concrete deck serves as part of the top flange of the girder, increasing the strength and stiffness of the system. In addition, the panels serve to provide continuous bracing of the top flange of the girder and also serve as horizontal diaphragms able to transfer horizontal loads applied to the bridge superstructure (Chavel, 2012). While composite action is desired, many early systems have been designed such that the deck does not act compositely with the supporting girders. A non-composite system would result in a less costly and simplified construction process as shear pockets would not be required; however, relatively larger girders would be necessary to carry design loads as the girders would not benefit from the increased strength and stiffness provided by the precast panels. It is widely considered that composite systems are structurally and economically more efficient and thus more desirable (Precast/Prestressed Concrete Institute, 2011).

In the case of full-width panels, only transverse joints are present. Many joint configurations, joint reinforcing details, and joint fill materials have been researched worldwide with the

goal of improving overall joint performance. If panels are used that are less than the full-width of the structure, longitudinal joints between the panels are introduced to the system.

In order to improve the performance of transverse joints, post-tensioning is frequently utilized to ensure that the joint remains in compression under service conditions (Chavel, 2012). However, due to the complex, lengthy, and costly post-tensioning process, joint systems have been designed using innovative materials and concepts resulting in narrow joints that do not require post-tensioning.

To ensure that the panels sit at the correct elevation to obtain the desired profile, panels typically include leveling devices. Many styles of leveling devices exist however all serve to level the panel and seat it at the correct elevation. The panels are commonly leveled by tightening threaded rods that penetrate the precast deck panel and sit on the underlying girder.

Once all of the panels are installed, the transverse joints, longitudinal joints (if any), shear pockets, and haunches are all grouted to achieve the desired composite action between the elements. Once the fill material has sufficiently cured, a riding surface may or may not be added to the structure and the bridge can then finally be opened to traffic.

2.3 Challenges Associated with the Precast Bridge Deck Panel Systems

Precast concrete bridge deck panel systems have faced many challenges that have limited their widespread use. As previously mentioned in Sub-section 1.1.1, these challenges include

higher initial construction costs, lack of knowledge by design engineers, lack of uniformity and consistency in design details, and concerns over long-term performance and durability when compared to conventional systems (Precast/Prestressed Concrete Institute, 2011). These challenges are gradually being addressed and as a result, the use of precast bridge deck panels has significantly increased in recent years. However, designers and contractors still face difficulties, specifically when dealing with the design and construction of shear pockets and transverse joints, and with the selection of fill materials. The following is a brief introduction into these challenges.

2.3.1 Shear Pocket Design

Shear pockets are needed to develop composite action between the precast panels and the underlying girders. These full-depth pockets are typically circular or rectangular in shape and provide discrete positive attachment – through shear stud clusters in the case of steel girders or hooked bars in the case of concrete girders – to the underlying girders. The spacing of these discrete pockets becomes of particular interest during the design of the system.

The pockets must be spaced close enough to ensure that the horizontal shear forces can be adequately transferred from the panels to the girders. Naturally, it is desirable to maximize the spacing of the pockets to: reduce the amount of blockouts required during fabrication of the panels; reduce the volume of fill material required; and reduce the overall congestion of the reinforcement in the panel. However, if spacing of the pockets becomes too large, a significant number of welded shear studs would be required per pocket and cracking may

occur at the panel / girder interface due to the lack of reinforcement across the interface between discrete pockets.

Current code provisions in the AASHTO LRFD and CAN/CSA S6-06 do not adequately address the design of shear pockets for precast concrete bridge deck panels. Therefore, significant research has been conducted worldwide to examine the behavior of these shear pockets and to determine the optimal spacing and reinforcement configuration to ensure that the system behaves compositely. Due to the fact that the behavior of these discrete shear pockets is not addressed specifically in the bridge codes, owners will frequently require testing programs to ensure that the proposed precast systems maintain acceptable composite behavior given their specific loading conditions.

2.3.2 Joint Design

The joints between precast bridge deck panels have long been considered the weakest link in the precast bridge deck system. Due to their generally poor field performance in which many joints have cracked, debonded and leaked, researchers have attempted to develop a joint with satisfactory performance. While a grouted female-female joint post-tensioned to ensure it remains in compression throughout the lifetime of the structure was eventually found to exhibit relatively good performance (Issa et al., 2000), the task of post-tensioning the joint introduced complexity, added cost and prolonged construction time. Due to the nature of ABC construction, a system with satisfactory performance without the need for post-tensioning is desired.

The post-tensioning through the joint can be replaced by mild reinforcement, however the joint has to be significantly wider to adequately develop the yield strength of the reinforcing bars projecting into it. A wider joint exhibits increased shrinkage and therefore increased potential for cracking, debonding and leakage. Therefore, new joint designs were developed using innovative fill materials that allow for very narrow joints without the need for post-tensioning.

These narrow joints take advantage of the properties of UHPC that allow significantly shorter reinforcement development lengths. However, due to the relatively limited use of UHPC joints, owners typically require laboratory testing prior to field implementation to ensure the UHPC joints will demonstrate acceptable structural performance and durability given the expected loading conditions for the proposed structure.

2.3.3 Selection of Fill Material

The type of fill material used for the joints has a significant effect on the performance of the joint. Engineers have many different choices for possible joint-fill materials ranging from epoxies to grouts to innovative materials such as UHPC. Due to the large selection of materials available to engineers, it is of the upmost importance to understand how the fill material will perform and what its durability will be given the service conditions.

2.4 Previous Research on Precast Concrete Bridge Deck Panel Systems

Due to the modular nature of precast concrete bridge deck panel systems, the design of the resulting transverse joints and in some cases longitudinal joints is of concern. Historically,

deck panel joints have performed poorly requiring continual maintenance over the life of the structure. As such, the area of precast concrete deck panel joints has benefited greatly from extensive research over the years. The following are significant research programs in the area of precast concrete bridge deck panel joints. It should be noted that many similar research programs have been conducted and only the ones deemed to be most significant are described in the following.

2.4.1 Historical Field Performance of Transverse Joints in the United States of America

In 1995, a major research program was completed consisting of an extensive investigation into the field performance of precast concrete bridge deck panels (Issa et al., 1995). The investigation included structures in the states of Alaska, California, Connecticut, Illinois, Iowa, Maryland, New York, Ohio, Pennsylvania, Virginia and Washington D.C. and consisted of two main tasks. First, a visual inspection of the precast concrete bridge deck panel joints, deck to supporting system connection, and overlay system was conducted for every structure. Secondly, state engineers were interviewed to discuss their thoughts on the design, construction, and performance of the precast concrete bridge deck panel system.

Overall, the condition of the deck joints varied significantly. Several structures inspected were performing adequately with little-to-no apparent damage to the joints. These structures performing in a satisfactory manner mainly consisted of decks with sufficient compressive forces (typically achieved with the use of longitudinal post-tensioning) at the joint to prevent debonding, cracking and leakage of the joint. Structures with bridge decks lacking post-tensioning were frequently observed to have poor performing joints showing signs of

debonding, cracking and leakage (Issa et al., 1995). Overall, it was observed that post-tensioned decks implementing female-female transverse joints were exhibiting the best performance.

Upon completing the investigation into the field performance of the precast concrete bridge deck panel joints, researchers came to the conclusion that many jurisdictions in North America had been using precast concrete bridge deck panels for several decades with varying levels of success. The lack of a unified and consistent approach to the use of precast concrete bridge deck panels in addition to the lack of code specifications led to the development of many different joint systems; some of these systems performed well while others exhibited performance issues when implemented in the field (Issa et al., 2000).

2.4.2 Post-Tensioned Transverse Joints

An important observation from the extensive field investigation (Issa et al., 1995) into the performance of transverse joints in the United States of America was that joints under compressive stresses exhibited improved performance. This observation led engineers to realize the potential of post-tensioning the panels to impose compressive forces at the joints thereby improving the overall performance of the system.

Experimental testing was performed to verify the effectiveness of longitudinal post-tensioning and to attempt to develop code requirements for post-tensioning levels (Issa et al., 2000). The experimental testing consisted of ¼ scale tests on three specimens modeled after a four-span continuous prototype bridge in the state of Virginia. One model contained no post-

tensioning while the other two models were post-tensioned (one to 1.43 MPa and one to 2.62 MPa); this was done to compare the effect of post-tensioning on the performance of the transverse joint. The models were tested under both static and fatigue loading. Fatigue loading consisted of at least 2 million cycles of simulated AASHTO HS20 loading to observe the cyclic performance of the joints.

It was reported that the performance of the models greatly improved with the increasing levels of prestress applied to the system. The post-tensioning was instrumental in delaying crack initiation of the joint and panels and substantially increased the cracking load of the models by 300% under cyclic loading relative to the non-post-tensioned model (Issa et al., 2000).

In 2005, construction began on the replacement of a state owned twin bridge structure over Door Creek on Interstate I-90 near McFarland, Wisconsin. The Wisconsin Department of Transportation (WisDOT) directly compared the performance of a conventional CIP concrete deck with a precast prestressed concrete bridge deck panel system by constructing the eastbound structure with a CIP deck and the westbound structure with precast bridge deck panels (Markowski, 2005).

The construction of the westbound precast panel structure utilized female-female transverse joints consisting of a 25 mm opening at the top of the joint to allow for the easy placement of non-shrink grout and a 6-13 mm opening at the bottom of the joint to allow for panel misalignment and dimensional growth. This joint detail was selected based on the

performance of similar joints on previous projects and on research conducted by several institutions. The joints were also designed to be post-tensioned to eliminate tensile stresses across the joint, thereby keeping the joint tightly sealed (Markowski, 2005).

Prior to construction of the twin structures, a research program was developed to determine appropriate post-tensioning levels for the transverse joints to be used on the Door Creek structure. The joint tightness and stiffness under the prestressing level recommended by the bridge designers were also examined in the laboratory (Markowski, 2005). A full-scale test on the proposed transverse joint was conducted to determine the post-tensioning level required to keep the female-female joints tight under service vehicle loads. Testing was conducted by loading the joint until it was observed that the joint began to open. The panels were then loaded to cause failure in the transverse joint.

The specimen female-female joints were cast using Dayton Superior Non-Shrink Grout. Once the grout had sufficiently cured, the joints were post-tensioned to 1.06 MPa. Fatigue loading consisted of 2 million cycles applied at 2 Hz with intermittent static tests taken every 400,000 cycles (Markowski, 2005). The testing program results indicated that the precast panel system to be used on the Door Creek Bridge performed sufficiently well to be used as an alternative to the CIP system. The post-tensioning level suggested by designers was found to have a factor of safety of 1.5 against cracking. The post-tensioned female-female detail previously described was recommended by researchers and it was noted that while post-tensioning may be more costly and time consuming, the benefits on the performance of the transverse joints makes post-tensioning worth while (Markowski, 2005).

Additional research on the performance of post-tensioned joints includes a full-scale bridge deck constructed at the Virginia Tech Structures Laboratory to examine the construction and behavior of precast bridge deck panel systems. In this research program, two transverse joint details, specifically epoxied male-female joints and grouted female-female joints were examined. The joints were post-tensioned to ensure they remained in compression throughout the testing program (Sullivan, 2007).

The transverse joints were initially post-tensioned to 1.85 MPa using twelve 13 mm diameter strands. The transverse joints on the live end were male-female joints epoxied using Sikadur® 31 SBA Slow Set while female-female joints used on the dead end were grouted using Five Star® Highway Patch Set. The testing program consisted of initial static tests, cyclic testing up to 2 million cycles at 2 Hz with intermediate static tests and final static tests. Water was also ponded on the transverse joints before each of the load tests.

Results from this research program indicated that from a purely construction standpoint, the grouted female-female joint was more desirable than the epoxied male-female joint due to the tight tolerances required when dealing with the epoxied male-female joint. Due to the nature of the grouted female-female joints, this joint would be more forgiving with a higher tolerance to construction error or deformation of the panels. Additionally, the grouted female-female joint system would allow for quicker construction of the bridge deck.

Ultimately, it was concluded that a decision between the two joint details would be due to constructability and not structural performance as both joint details performed sufficiently

well during the static and cyclic testing program. It was also determined that the post-tensioning value of 1.85 MPa was sufficient to keep the transverse joints in compression throughout the testing procedure.

2.4.3 Post-Tensioning Free Transverse Joints

While the use of precast concrete bridge deck panels with longitudinally post-tensioned joints was increasing, AASHTO recognized the cost, time and complexity implications of post-tensioning panels in the field. Therefore, AASHTO requested that the Transportation Research Board (TRB) research a panel system exhibiting satisfactory performance without the need for longitudinal post-tensioning. Therefore, as part of the National Cooperative Highway Research Program (NCHRP), NCHRP Report 584 on full-depth precast concrete bridge deck panel systems was developed (Badie and Tadros, 2008).

Report 584 provides guidelines for the design, fabrication and construction of full-depth precast concrete bridge deck panels written in an AASHTO LRFD language, stemming from research conducted by the George Washington University, the University of Nebraska-Lincoln and Tadros Associates, LLC (Badie and Tadros, 2008). Report 584 examines historical methods used for panel-to-panel connections and presents two new panel-to-panel connections for both steel and concrete girders. These new connections allow the longitudinal bars in two adjacent panels to be spliced and the yield strength of the bar to be fully developed while minimizing the reinforcement embedment length. Both connection details utilize a new confinement technique and do not require longitudinal post-tensioning.

In order to validate the performance of the proposed post-tensioning free confined transverse joint detail, an experimental program was conducted. A full-scale bridge specimen was constructed and several confining joint details were tested for comparison. The bridge specimen was fatigue tested for 2 million cycles at 2 Hz as per ASTM D6275 under ponded water conditions. The loading arrangement selected simulated the center axle of an AASHTO HS20 truck (Badie and Tadros, 2008).

Report 584 reports that the connection details performed well with no water leakage of the joint before, while, or after the 2 million cycle fatigue load was applied. In addition, no tension cracks were observed at the underside of the transverse joint, no concrete crushing was observed at the top of the joint, no separation between the grout and the vertical surface of the joint was observed, and it was concluded that no stiffness deterioration had occurred due to the fatigue load (Badie and Tadros, 2008).

Researchers determined that this new confinement detail using hollow structural section (HSS) tubes for the transverse joints adequately confines the joint, meaning post-tensioning is not required (Badie and Tadros, 2008). However, as later reported in subsequent joint research projects, concerns regarding the constructability, complexity and cost of the connection system led to its limited use in field applications (Graybeal, 2010).

2.4.4 Use of Ultra-High Performance Concrete Joints

During the mid 1990s, Danish architect firm Dall and Lindhartsen and Danish consulting firm Carl Bro Associates developed an innovative building system. The building system

consisted of prefabricated components joined by ultra-high strength fibre reinforced concrete (UHS FRC) or ultra-high performance concrete (UHPC) as it is commonly referred to today. This building system is frequently referenced as the first serious use of an ultra-high performance concrete joint-fill material in practice (Hansen and Jensen, 1999). The UHS FRC joint material, developed at the Aalborg Portland University Cement and Concrete Laboratory, allowed 200 mm precast concrete slabs, supported by columns, to be made continuous for live load. No floor beams were used as part of this system (Hansen and Jensen, 1999).

Due to the properties of the UHS FRC used in the joints, significantly shorter joints were possible as rebar anchorage lengths decreased with the use of UHS FRC compared to conventional concrete or grouts. Several tests were performed to validate the structural performance of the UHS FRC as a joint-fill material for the innovative building system. Testing concluded that casting the UHS FRC joints is a relatively simple process and that the use of UHS FRC joints adds significant ductility to the structure. The anchorage length of an 8 mm bar with a tensile strength of 550 MPa was found to be only 60 mm therefore indicating that shorter anchorage lengths are possible with UHS FRC (Hansen and Jensen, 1999).

Even though the use of UHS FRC appeared to be highly advantageous as a joint-fill material, UHS FRC or UHPC was not implemented in North America until Rainy Lake Bridge was rehabilitated in 2006. In Canada, the Ministry of Transportation of Ontario (MTO) is responsible for maintaining thousands of bridge structures in the province of Ontario.

Structures located in MTO's Northwestern Region are of special importance to MTO. The Northwestern Region is a remote region relative to the populous southern Ontario and construction or rehabilitation of structures in this location can be problematic. The need for high quality bridges requiring little maintenance, in addition to the need to maintain the important transportation network in the area, has led to ABC practices being frequently implemented for the construction or rehabilitation of bridge structures.

As a result, Lafarge Canada collaborated with MTO to construct the Rainy Lake Bridge structure using precast concrete panels jointed with Lafarge's proprietary UHPC material. This innovative proprietary material was developed in France by Bouygues SA in partnership with Lafarge and Rhodia during the years in which UHPC was gaining popularity in Europe, and is a reactive powder concrete (RPC) presently marketed as Ductal®.

In the summer of 2006, work on the Rainy Lake Bridge in Ontario, Canada was started and completed. This was the first structure in North America to implement the use of UHPC as joint fill for full-depth precast high performance concrete (HPC) panels. This structure was a simple span utilizing half-width panels jointed with Ductal® JS1000 transverse and longitudinal joints (Perry et al., 2007).

Since joints must be capable of transmitting all potential forces between the panels, the UHPC joint detail becomes of significant importance. Traditional CIP concrete joints can be upwards of 600 mm wide and often suffer from durability issues; to combat this, two highly durable materials – UHPC and fibre reinforced polymer (FRP) reinforcing bars – were used

in the transverse joints. While decreasing the width of the transverse joints is desired, enough lap length must be provided to fully develop the strength of the reinforcing bars. MTO retained EBA Consultants to perform pull-out tests on FRP bars in UHPC to determine the appropriate lap lengths required in the joint to ensure the required development of the FRP reinforcement (Perry et al., 2007).

MTO concluded that by using concrete deck panels reinforced with FRP and jointed using UHPC, the size and complexity of the joints is reduced, the continuity and speed of construction are improved, and the structure ultimately demonstrates improved durability, lower maintenance requirements and extended service life. The innovative precast deck panel system using UHPC allowed the Rainy Lake Bridge to be rapidly constructed and opened to traffic within 48 hours of the joint closure pour. Due to Rainy Lake's success, MTO has become one of the largest users of this system having implemented UHPC joints on close to 50 applications to date.

After the successful implementation of UHPC joints for full-depth precast deck panels at Rainy Lake Bridge, the New York State Department of Transportation (NYSDOT) recognized the potential of this innovative bridge deck system to rapidly construct and rehabilitate bridges. However, NYSDOT felt that further research was warranted. Therefore, NYSDOT partnered with the Iowa Department of Transportation (IDOT) and the Federal Highway Administration (FHWA). A major research program was developed under the Structural Concrete Research Program as part of Transportation Pooled Fund Project No.

TPF-5(217), leading to the publication of FHWA-HRT-11-023 in November 2010 (Graybeal, 2010).

FHWA-HRT-11-023 reports on a research project conducted to investigate the performance of UHPC joints for precast bridge components, namely full-depth precast concrete panels and precast concrete side-by-side deck bulb tees (Graybeal, 2010). The research program consisted of four phases (Perry and Royce, 2010):

- Phase 1: Prototype and test panels with UHPC joint fill in a laboratory;
- Phase 2: The use of UHPC joint fill in side-by-side deck bulb-tees;
- Phase 3: The use of UHPC joint fill in full-depth precast deck panels on a single span two-lane rural bridge; and,
- Phase 4: The use of UHPC joint fill in full-depth precast deck panels on a large scale structure.

Phase 1 of the research project consisted of the testing of six different joint details. Four of the tested details were transverse UHPC joints for full-depth precast concrete deck panels. These four joints varied in rebar type (epoxy coated, galvanized and black) and detailing (straight, hooked and headed). The other two joint details were for longitudinal UHPC joints for side-by-side deck bulb-tees (Graybeal, 2010).

The six details were tested initially under cyclic loading with at least 2 million cycles to a load just under the cracking strength of the specimen followed by 5 million cycles to a load exceeding the cracking strength of the specimen. The specimens were then statically loaded

to failure. All testing was performed with the joint under ponded water to determine the water-tightness of the joint throughout the loading stages (Graybeal, 2010).

It was observed that all joint types tested surpassed the expectations of a CIP monolithically poured deck. The cyclic response of the specimens demonstrated favorable cracking behavior with no interface debonding. The static loading to failure progressed through cracking, rebar yielding and eventual concrete crushing. This research project also demonstrated that the discrete reinforcement in the transverse and longitudinal joints was not susceptible to debonding within the joint. Finally, the water-tightness of the joint was verified and it was concluded that the UHPC joints tested were not likely to leak under cyclic loading or static overloading (Graybeal, 2010).

Phase 3 and 4 are of particular interest however no report containing results and conclusions pertaining to these phases of the research project have been found at this time.

2.4.5 Use of UHPC Joints in Negative Bending

Recently, the TRB has developed project R04, Innovative Designs for Rapid Renewal, as part of the Second Strategic Highway Research Program (SHRP2). The goal of SHRP2 is to develop a set of standard ABC details and methods to use nationwide. Being leaders in UHPC research and construction, IDOT was asked to develop a demonstration bridge showcasing various ABC components being studied. This led to the design and construction of the Highway 6 Bridge over Keg Creek. This structure is especially interesting as it is the first bridge to implement a full-depth transverse joint over the pier cap carrying the live-load

negative moment between adjacent spans (Hartwell, 2011). Researchers at Iowa State University conducted research on this negative moment transverse UHPC joint and provided recommendations for the construction of the actual joint used on the demonstration bridge over Keg Creek (Hartwell, 2011).

Iowa State University developed a research program focused on the laboratory testing of UHPC full-depth deck joints over the pier, in the negative moment region, to quantify the cracking and ultimate strengths of the joint. The abrasion resistance and constructability of the joints were also examined. Finally, recommendations were provided for the demonstration structure constructed in 2011 under the SHRP2 and Highways for Life (HFL) Program in Iowa (Hartwell, 2011).

To examine the structural performance of the negative moment joint, a full-scale test was conducted using two precast bridge deck modules. Each module consisted of a precast panel supported on two 6,096 mm long W760 x 147 steel girders. The panels were 2,235 mm wide by 216 mm thick. The two modules were then tied together using Ductal® UHPC. The deck modules were tested upside down to induce a negative moment across the joint (Hartwell, 2011).

Fatigue testing was performed with one million cycles of simulated AASHTO HS20 loading. The test specimen had a significant number of gauges mounted to it that allowed researchers to monitor stresses and strains throughout the full profile of the system providing an indication of the composite behavior of the system (Hartwell, 2011). It was determined that

the proposed joint designed for the negative moment region performed poorly under loading less than the cracking strength of the specimen. Significant debonding of the UHPC was observed. Therefore, design engineers developed a joint retrofit that served to post-tension the joint inducing compressive forces to prevent the debonding of the UHPC.

The joint was retested with the externally applied post-tensioning tendon using the same test setup. The retrofit demonstrated improved performance of the negative moment region joint and was ultimately implemented on the demonstration structure in Iowa over Keg Creek (Hartwell, 2011).

2.5 Ultra-High Performance Concrete Material Characterization

Ultra-high performance concrete, or reactive-powder concrete as it was originally termed when first patented by a French construction company in 1994, is generally characterized by a significantly high compressive strength and very low porosity – approximately 170-225 MPa and 2-6% respectively (Ahlborn et al., 2008) – when compared to normal-strength concrete (NSC) and even high-strength concrete (HSC) (Kosmatka et al. , 2011).

Today, the term UHPC can be seen applied to many products; however, it is generally accepted that UHPC will have the following properties: a compressive strength exceeding 150 MPa, internal fiber reinforcement to develop a degree of ductility, a high binder content, a low water content, and carefully graded and sourced aggregates. In addition, a high-range water-reducing admixture (HRWRA) combined with the concept of particle packing is utilized to achieve desirable rheological properties (Ahlborn et al., 2008).

2.5.1 UHPC Constituents and Mix Design

The proportions of the UHPC constituents are determined to optimize the granular mixture in an attempt to achieve a highly homogeneous and dense matrix (Kosmatka et al. , 2011). Constituent particle sizes typically range from 0.02 to 300 μm. The largest constituent by size is generally steel or synthetic fibers (approximately 0.2 mm in diameter by 12.7 mm long), followed by fine sand (150-600 μm), cement powder (approximately 15 μm), and finally ground quartz, the smallest sized constituent (approximately 10 μm). Silica fume (0.2 μm) is also incorporated into the mix and fits in the voids between the cement powder and ground quartz (Graybeal, 2006).

Due to the high binder content and low water content, a HRWRA (typically a polycarboxylate superplasticizer) is required to achieve sufficient rheological properties for placement and finishing (Graybeal, 2006). Since HRWRAs generally act as a retarding agent delaying the UHPC set time, an accelerating agent is frequently used to speed up the setting process; this is especially critical in situations in which the bridge is required to be open to traffic as soon as possible following placement of the UHPC joints.

Table 2-1 provides a comparison between high-performance concrete and two documented UHPC mixes used in industry projects. As the definition of HPC is very broad, the HPC mix presented in Table 2-1 was selected due to its potential use in a similar joint application; UHPC1 was the mix used on the Sherbrooke Footbridge, Quebec (the world's first RPC structure) and UHPC2 is the mix currently sold by Lafarge North America under the product

name Ductal® JS1000 (the exact nature of the mix is not disclosed as Ductal® is a proprietary product).

Table 2-1–Typical Proportions for HPC and UHPC

Constituent (kg/m^3)	**Mix**		
	HPC[1]	**UHPC 1[2]**	**UHPC 2[3]**
Portland Cement	513	710	712
Coarse Aggregate	1080	-	-
Fine Aggregate	685	-	-
Fine Sand (Silica Sand)	-	1010	1020
Ground Quartz	-	210	211
Silica Fume	43	230	231
Water	130	200	109
Steel Fibers	-	190	156
HRWRA	15.7 (L/m^3)	19 (L/m^3)	30.7 (kg/m^3)
Accelerator	-	-	30.0
Water/Cementitious Materials*	0.24	0.21	0.12

Note: All proportions in kg/m^3 unless indicated otherwise
[1]Typical HPC mix – Two Union Square, Seattle, 1988 (Kosmatka et al. , 2011)
[2]Early UHPC mix – Sherbrooke Footbridge, Quebec, 1997 (Blais and Couture, 1999)
[3]Typical current UHPC mix – Ductal® JS1000, Lafarge Ductal North America (Graybeal, 2006)
*w/cm ratio consists of Portland cement and silica fume constituents

It can be seen in Table 2-1 that UHPC2 has a higher Portland cement and silica fume content as well as a lower water content compared to HPC. When sourcing the cement powder, it is desirable to obtain cement with high proportions of tricalcium aluminate (CA_3) and tricalcium silicate (CS_3) in addition to a low Blaine fineness; higher CA_3 and CS_3 proportions aids in increasing the early age strength (important for accelerated bridge construction) and a low Blaine fineness aids in reducing the water demand of the mix (Ahlborn et al., 2008). Also, it is important to note that there is no coarse aggregate in UHPC and that the fine aggregate portion is further divided into fine silica sand and ground quartz flour. The overall fineness of the mix constituents plays a significant role in providing a densely packed and homogenous matrix as previously discussed. Given the dramatic differences between HPC

and UHPC mix designs, it is of interest to compare certain mechanical and durability properties of these concretes. Table 2-2 provides a comparison of selected material properties for typical NSC, HPC and UHPC mixes.

Table 2-2–Comparison of Selected NSC, HPC, and UHPC Properties

Property	NSC	HPC	UHPC
Compressive Strength (MPa)	20-40	40-95	170-225
Porosity	20-25%	10-15%	2-6%
Modulus of Rupture [1st Crack] (MPa)	2.8-4.1	5.5-8.3	16.6-22.1
Ultimate Flexural Strength (MPa)	-	-	21-62
Shrinkage	-	(40-80)x10^{-5} Post Cure	< 1 x10^{-5} Post cure and No Autogenous Shrinkage Post Cure
Ductility	-	-	250 Times Greater Than NSC
Freeze/Thaw Resistance	10% Durable	90% Durable	100% Durable
Chloride Penetration (Coulombs Passing)	> 2000	500-2000	<100

Note: Table adapted from MDOT Research Report RC-1525 (Ahlborn et al., 2008) and based on various research programs published between 1997 and 2006

As can be seen in Table 2-2, UHPC appears to out-perform both NSC and HPC in every category. One interesting feature of UHPC is its high ultimate flexural strength. Achieving flexural strengths of 40 MPa in UHPC is not uncommon and the overall structural behaviour tends to vary from conventional reinforced concrete; as a result, design codes have been written specifically for designing UHPC structures (AFGC, 2012).

2.5.2 Important Properties of UHPC as a Joint Fill Material

While UHPC has been used in many joint applications, its use has been limited to a few very progressive departments of transportation. There are several concerns that infrastructure

owners frequently cite prior to specifying UHPC as a joint-fill material. In particular, owners are concerned with the shrinkage cracking of UHPC as any cracking in the joint will lead to water leakage and significant durability concerns.

While many joint applications in the past have relied on longitudinal post-tensioning to ensure the joint remains in compression throughout the service life of the structure as discussed in Sub-section 2.4.2, UHPC has shown the potential to provide a post-tensioning free joint while maintaining acceptable service conditions; thus, flexural strength of UHPC is also of interest, especially in areas of high negative moments as is the case in deck regions over interior substructures on a continuous bridge.

Finally, the freeze/thaw and chloride penetrability of UHPC is commonly of concern to owners, especially in cold climates where the use of deicing salts to keep roads free of ice is common practice. As an owner, to properly evaluate these concerns when specifying a joint-fill material, it is important to define the curing method to be used since research has shown that UHPC properties can vary drastically depending on the curing regime used.

2.6 Code Provisions for Designing PPCP Bridge Deck Systems

In the United States, bridge designs are typically governed by AASHTO LRFD Bridge Design Specifications (AASHTO, 2007). In Canada, all provinces and territories except the province of Manitoba require bridge structures be designed according to CAN/CSA S6-06 Canadian Highway Bridge Design Code (CAN/CSA, 2006). In Manitoba, structures owned by the City of Winnipeg are designed according to CAN/CSA S6-06 while structures owned

by Manitoba Infrastructure and Transportation are principally designed according to AASHTO LRFD specifications. This section presents the specifications related to PPCP deck systems prescribed by these two main North American bridge codes. Additional full-depth deck panel guidelines prepared by the Precast Concrete Institute (PCI) Northeast Bridge Technical Committee are also discussed.

2.6.1 CAN/CSA S6-06 Canadian Highway Bridge Design Code

Concrete slabs supported on girders, stringers or floor beams of concrete or steel are covered under Section *8.18 Special Provisions for Deck Slabs* of the Canadian Highway Bridge Design Code (CAN/CSA, 2006). Clause *8.18.1 Design Methods* describes two options to design a concrete bridge deck. If the requirements of Clause *8.18.4 Empirical Design Method* are met, deck slabs do not need to be analyzed except for negative transverse moments due to loads on the deck-slab overhang or barrier walls and for longitudinal moments in continuous span bridges. If the criteria for the empirical design method are not met, flexural design methods may be used to design the concrete deck.

Full-depth precast panels are specifically addressed in Clause *8.18.4.4 Full-Depth Precast Panels*. For the empirical design method to apply, the following criteria must be met: "*the panels cover the full width of the bridge; the depth of the panels is not less than 190 mm; at their transverse joints, the panels are joined together by grouted shear keys and are longitudinally post-tensioned with a minimum effective prestress of 1.7 MPa; the grout used in the shear keys has a minimum strength of 35 MPa at 24 h*" among others.

Aside from the limited specifications provided in Clause 8.18.4.4, the Canadian Highway Bridge Design Code does not address precast concrete bridge decks in significant detail. The commentary associated with Clause 8.18.4.4 indicates that the effective longitudinal prestress of 1.7 MPa across the joint is based on AASHTO LRFD (1994). A state-of-the-art report published in 1995 discussed addressing the installation and field performance of the joints. The commentary concludes by indicating that the "*type of grout mortars can have a significant effect on the performance of grouted joints*" (CAN/CSA, 2006).

2.6.2 AASHTO LRFD Bridge Design Specifications

Precast concrete bridge deck panels are discussed briefly in Section *9 Decks and Deck Systems* of the AASHTO LRFD specifications. More specifically, Sub-section *9.7.5 Precast Deck Slabs on Girders* addresses this type of system. Clause *9.7.5.1 General* indicates "*both reinforced and prestressed concrete slab panels may be used. The depth of the slab, excluding any provision for grinding, grooving, and sacrificial surface, shall not be less than 175 mm*".

Clause *9.7.5.2 Transversely Joined Precast Decks* indicates "*flexurally discontinuous decks made from precast panels and joined together by shear keys may be used. The design of the shear key and the grout used in the key shall be approved by the owner*". From this clause, it is evident that there does not exist detailed specifications in AASHTO LRFD governing the design of the joint and the type of material used. The fact that it is up to the owner to approve the joint system inherently increases the risk from an owner's perspective. As such, owners may be reluctant to implement precast deck systems. This also explains the reason that

departments of transportation (DOTs) prefer to conduct local research prior to implementing a system for the first time locally, even if similar research and field applications already exist elsewhere.

The commentary associated with Clause 9.7.5.2 states that the joints are susceptible to cracking due to wheel loads, warping, and environmental effects; this leads to leaking of the joints and a decreased ability to transfer shear between the panels. The commentary states that this construction system isn't recommended for structures constructed in a region where the deck may be exposed to salts.

Sub-section *9.7.6 Deck Slabs in Segmental Construction* further discusses joints but does not appear to be relevant to full-depth precast concrete bridge deck panels. This sub-section applies to the "*top slabs of post-tensioned girders whose cross-sections consist of single or multi-cell boxes*". However, material in this sub-section relates to precast panel joints. Clause *9.7.6.2 Joints in Decks* states that joints in the deck may be dry joints, epoxied match-cast joints or cast-in-place joints. However the use of dry joints should be limited to areas in which deicing salts are not applied. Clause 9.7.6.2 also states that when cast-in-place joints are used, the strength of the concrete shall not be less than that of the precast member and that the joint shall permit the development of any reinforcement within it but shall not be any less than 300 mm.

Clause *9.7.5.3 Longitudinally Post-Tensioned Precast Decks* indicates "*precast components may be placed on beams and joined together by longitudinal post-tensioning. The minimum*

average effective prestress shall not be less than 1.7 MPa". In addition, "*the block outs at the coupling of the post-tensioning ducts shall be filled with a nonshrink grout having a minimum compressive strength of 35 MPa at 24 hours*". The shear pockets are also to be filled with the same grout material after the completion of the post-tensioning.

The commentary associated with Clause 9.7.5.3 indicates that systems in which the deck is made flexurally continuous by longitudinal post-tensioning are preferred as they behave monolithically and are expected to require less long-term maintenance. The deck haunches should be cast at the same time as the shear pockets after the completion of post-tensioning to allow movement of the panels relative to the girders during post-tensioning. Finally, the commentary indicates that there are many joint options available but that research suggests that a "V" shaped joint would be the easiest to form and fill.

2.6.3 PCI Full Depth Deck Panel Guidelines for Deck Replacement or Construction

The Precast Concrete Institute Northeast Regional Bridge Technical Committee has established guidelines on the use of full-depth deck panels for ABC projects. This document was prepared in response to needs determined by northeast transportation agencies and prestressed concrete producers. PCI indicates that these guidelines have been developed to promote a greater uniformity among users of precast bridge deck systems including owners, engineers and producers. These guidelines are not meant to supersede the AASHTO LRFD specifications or DOT design standards.

Sub-section *2.6 Grout for Transverse Shear Keys, Shear Connector Pockets, and Beam Haunches* states that grout used for these applications should be non-shrink, flowable, have a moderate strength (35 MPa) and have low permeability. The guidelines also indicate that field-mixed grouts should not be used and that pre-qualified pre-bagged grouts are recommended. It is advised that transportation agencies have prequalified grouts that may be used as fill-materials.

Sub-section *3.1 General under Section 3 Design Requirements* indicates that the design of full-depth deck panels should follow the requirements prescribed in the AASHTO LRFD specifications. Specifically, AASHTO LRFD Sub-section *9.7.5 Precast Deck Slabs on Girders* should govern the design of the transverse shear keys and post-tensioning systems as previously discussed.

Sub-section *3.11 Composite Deck Design* indicates that the full-depth deck panels should be made composite with the supporting members. The commentary associated with Sub-Section 3.11 suggests that the effectiveness of using welded shear stud clusters on steel girders has been verified by several research projects. Additionally, an embedded steel plate with welded shear stud clusters can also be used for concrete girders as the effectiveness of this shear system has also been verified by research. Ultimately, the AASHTO LRFD provisions for horizontal shear design are appropriate for precast deck panel systems and should be followed.

Interestingly, the PCI Guidelines recommend that discrete shear pocket spacings be kept at a maximum of 600 mm on center where possible. The commentary addresses the fact that research has been conducted demonstrating that pocket spacing can be increased to 1200 mm without losing composite action of the system; however, a confinement pocket such as a steel tube or confinement reinforcement would have to be provided. Additionally, it is suggested that limiting the pocket spacing would limit the required shear studs to a reasonable number as a larger spacing would require an increased number of shear studs to adequately transfer the horizontal shear.

Chapter 3

Research Program

3.1 Introduction

In order to accomplish the research objectives outlined in Chapter 1, a research program was developed by the researchers at the University of Manitoba (UofM) in collaboration with professionals at MIT and Stantec Consulting. This experimental research program consisted of the construction, static testing, and fatigue testing of two full-scale bridge deck specimens at the UofM W.R. McQuade Heavy Structures Laboratory (herein referred to as the Structures Lab). A detailed description of the research program is presented herein.

3.2 Bridge Deck Details

The following sub-sections describe the details of the two full-scale bridge deck specimens that were constructed and tested in the Structures Lab. In particular, the test specimen naming convention and details specific to the steel plate girders, PPCPs, deck haunches, shear pockets and transverse joints are presented in the following sub-sections.

3.2.1 Test Specimen Naming Convention

This research program consists of the testing of two full-scale bridge deck specimens. Test Specimen #1, the first to be constructed and tested, is referred to as TS1; Test Specimen #2, the second to be constructed and tested, is referred to as TS2. Each test specimen was constructed using three PPCPs. These panels are referred to as the west, center, and east panels using north as the orienting direction. Therefore, TS1 was

constructed from panels W1, C1, and E1 while TS2 was constructed from panels W2, C2, and E2. This naming convention is shown in Figure 3-1. Naming conventions for the instrumentation used for each test will be presented in their respective sub-sections.

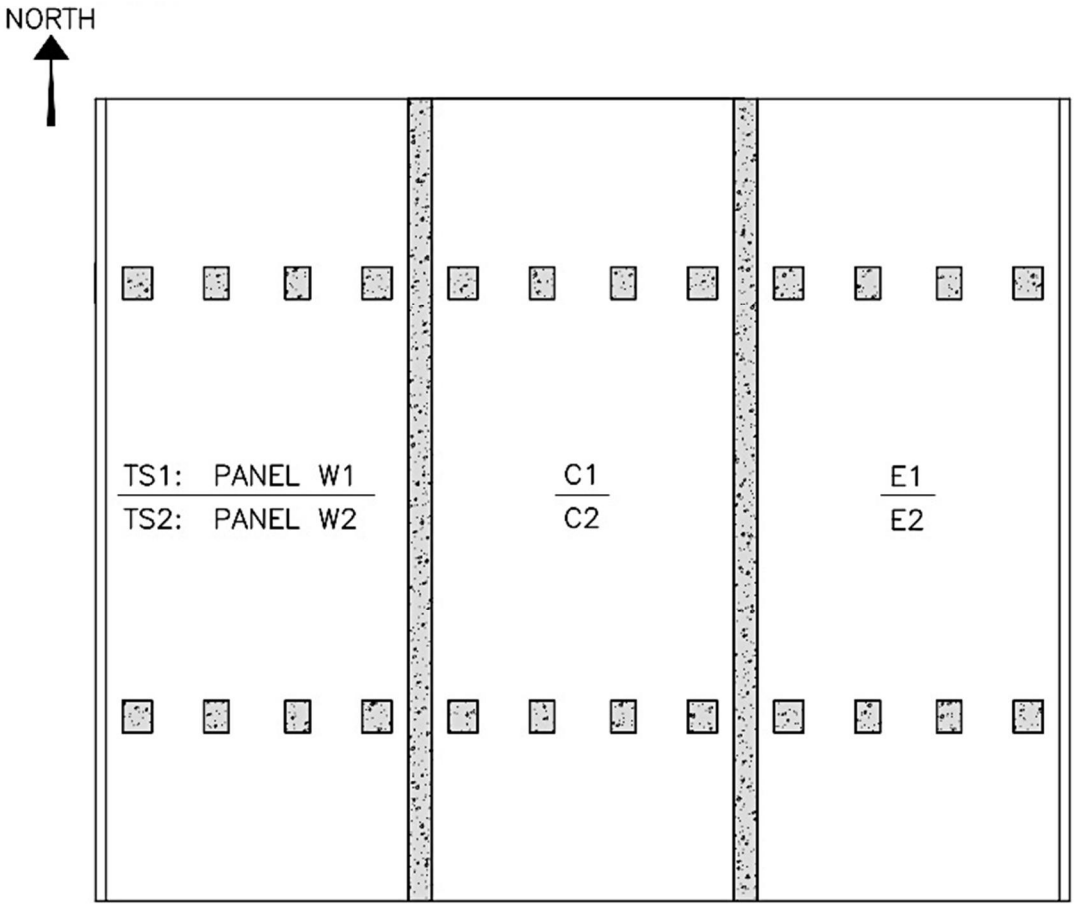

Figure 3-1 – Naming Convention for Test Specimens (Plan View)

3.2.2 Steel Plate Girders

It was chosen early in the research project to build full-scale test specimens using girders representative of the steel-plate girder bridges commonly found in Manitoba and across North America. Therefore, MIT provided four steel plate girders and accompanying end diaphragms through an in-kind material contribution for this research project. Each test specimen was constructed using two steel plate girders spaced at 3251 mm c.t.c; this

girder spacing was chosen to match that of the Red River Bridge introduced in Chapter 1. The girders were 7411 mm in length and 1538 mm in depth with a 9.5 mm thick web. Top and bottom flanges were 375 mm in width and 19 mm in thickness. The girders were fabricated using CAN/CSA 40.21 Grade 350AT Category 3 structural steel. Each test specimen had two end diaphragms consisting of back-to-back 89 x 64 x 8 mm thick steel angles for top, bottom and diagonal members connected by a 550 x 513 x 16 mm thick gusset plate. A plan drawing of the girder system is shown in Figure 3-2 and end-diaphragm details are presented in Figure 3-3. A photograph of the girders and end-diaphragms during construction is shown in Figure 3-4.

It should be noted that due to the fact the donated girders were originally designed to serve a different purpose, the girders did not have a complete set of shear and bearing stiffeners. For example, the TS2 girders were originally designed to be the exterior girders for the intended structure and therefore only had web stiffeners on one side of the web. Ultimately, a number of web stiffeners were installed on the girders to ensure sufficient structural capacity required to safely perform the necessary tests for this research program.

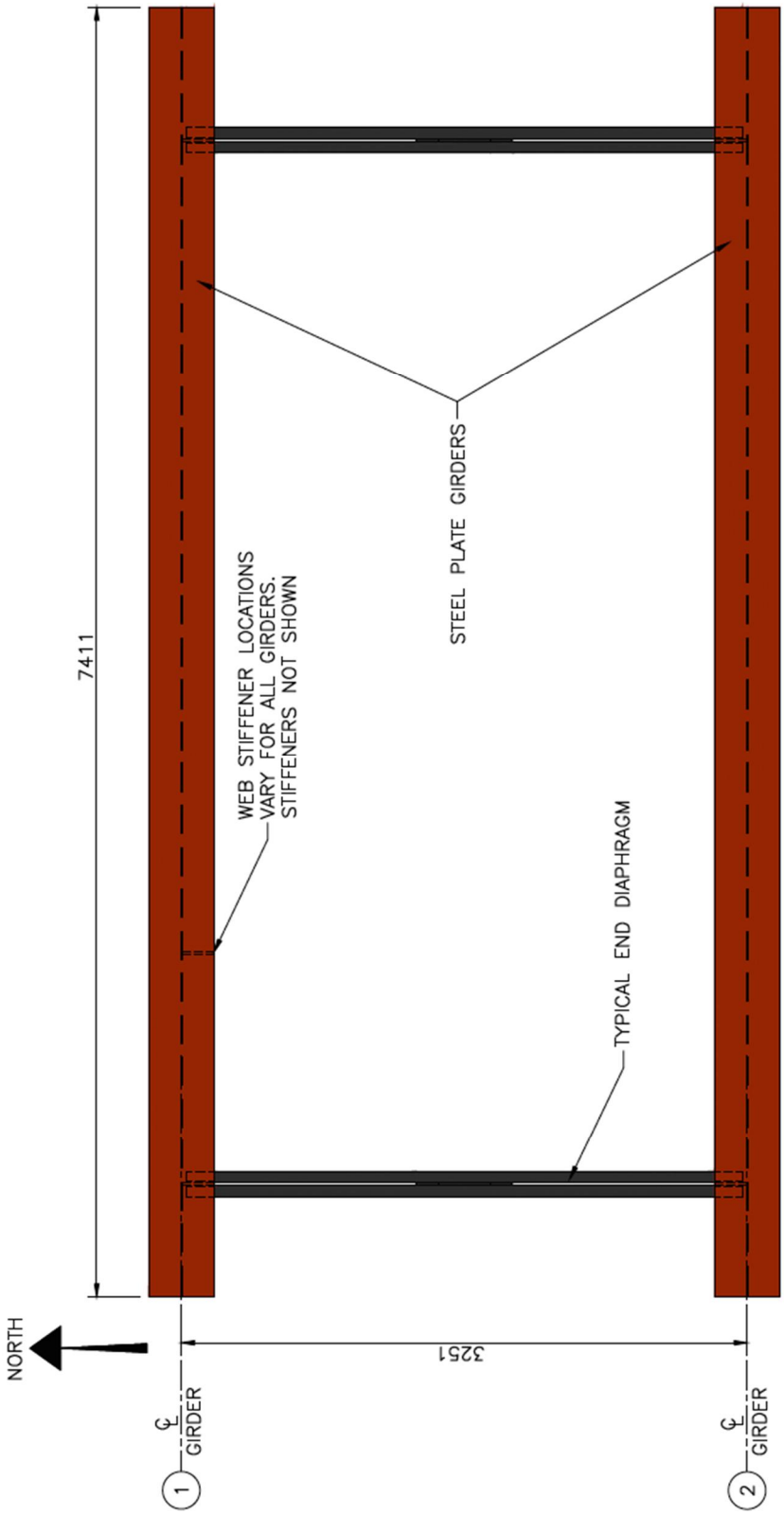

Figure 3-2 – Typical Girder Details (Plan View)

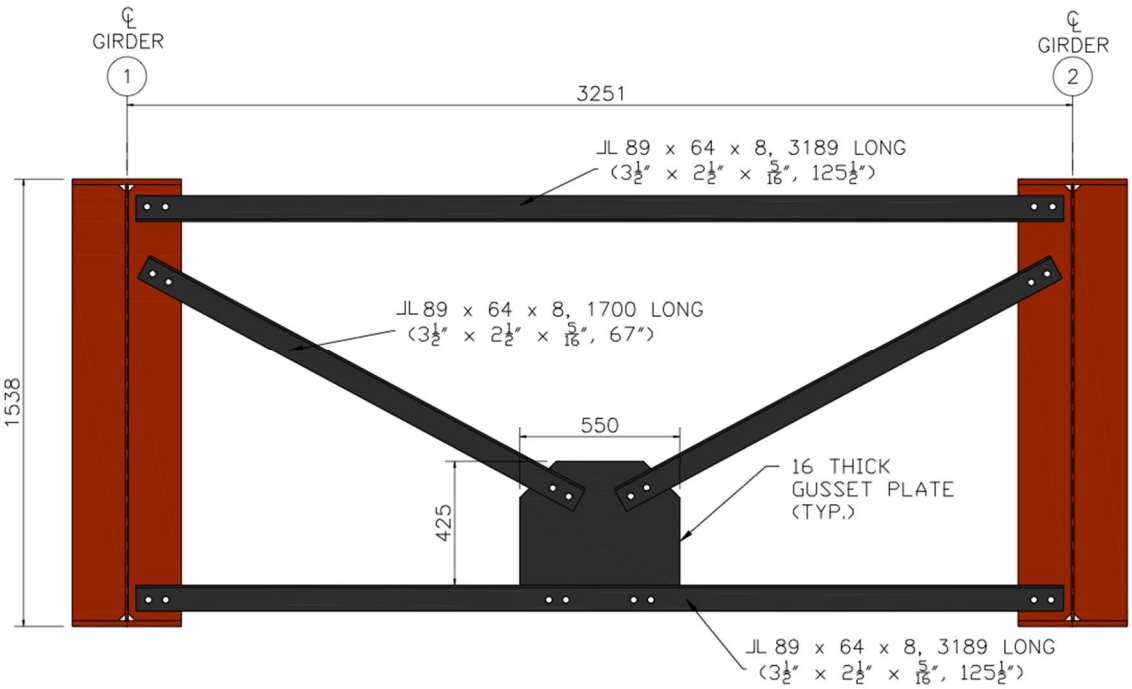

Figure 3-3 – Typical End-Diaphragm Details

Figure 3-4 – Steel Plate Girders and End-Diaphragm Installation (TS1) [Typical]

3.2.3 Precast Prestressed Concrete Deck Panels

The bridge deck for each of the two test specimens was constructed using three full-depth and full-width PPCPs. It should be noted that these PPCPs were based upon those used for the rehabilitation of the Red River Bridge near Morris, MB and were designed by Stantec Consulting; therefore, the PPCPs used for the test specimens have similar reinforcing and prestressing steel layouts, shear pocket and transverse joint details, length, and thickness to those used on the rehabilitation. The panels differ from those used for the rehabilitation only in width due to space restrictions in the Structures Lab. The test panels were 250 mm thick, 2415 mm in length by 6007 mm in width, providing a 1377 mm wide cantilever on each side of the test specimen measured with respect to the girder centerline, as shown in Figure 3-5.

Each test specimen contained two transverse joints 176 mm in width between adjacent panels measured at top of joint. The geometry of the transverse joints is discussed in detail in Sub-Section 3.2.6. Each PPCP contained two sets of four full-depth shear pockets spaced longitudinally at 610 mm c.t.c. These shear pockets varied in size depending upon the presence of a leveling bolt within the pocket. The shear pockets are discussed in detail in Sub-Section 3.2.5. Both the transverse joint and shear pocket faces had an exposed aggregate finish to increase the mechanical bond between the PPCP and the joint-fill material; the PPCP tops were broom finished. The six panels utilized for the project were fabricated and transported to the Structures Lab by Armtec of Winnipeg, MB. All six panels were provided by MIT as an in-kind material contribution.

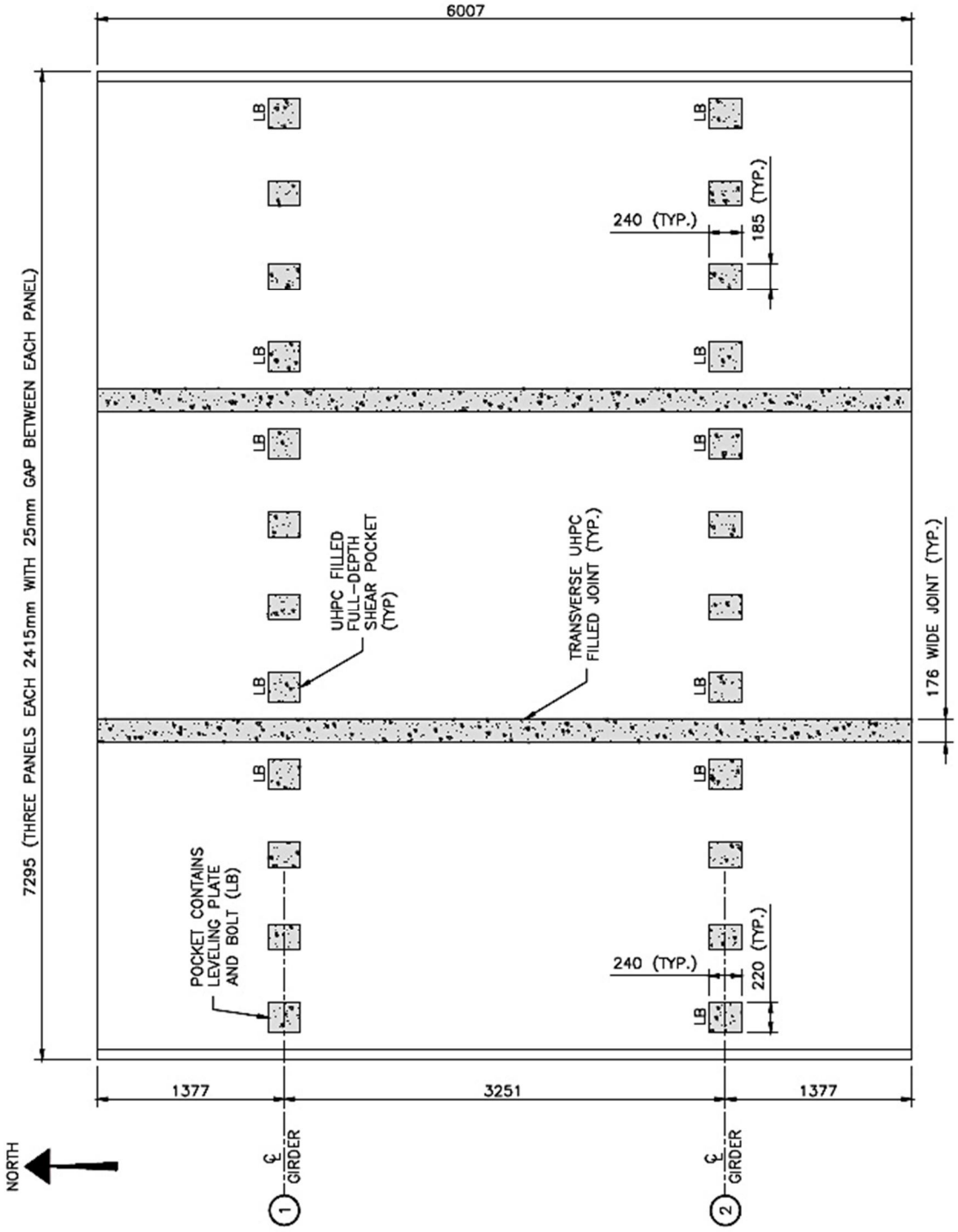

Figure 3-5 – Typical PPCP Dimensions and Details (Plan View)

3.2.3.1 Reinforcement Details

As previously described, the reinforcement for the test panels was based on the reinforcement of the Red River Bridge Rehabilitation PPCPs. The test panels contained top and bottom mats of deformed reinforcing bars in addition to six prestressing strands concentrically placed within the panel. The prestressing strands were typical 13 mm diameter uncoated 7-wire low relaxation (f_{pu} = 1860 MPa) strands (E_s = 194 MPa). To achieve the necessary development length within the UHPC joint, the top longitudinal 15M bars protruding out of the panels were hooked. The reinforcing and prestressing steel details are shown in Figures 3-6 and 3-7 respectively.

During fabrication, both the top and bottom reinforcing mats were prefabricated outside the steel formwork. The bottom mat was placed inside the form by crane followed by the placement of the six prestressing strands. The top reinforcing steel mat was then installed after which the strands were stressed to 95 kN, approximately 52% of their ultimate strength, in the order shown in Figure 3-7. Stressing began with Strand #1, proceeding numerically and ending with Strand #6. The load in the prestressing strands was monitored through the use of a load cell and a portable data acquisition system (DAQ). Finally, the lifting anchors, leveling plates, and leveling bolts were installed prior to concrete casting. Figures 3-8 through 3-10 depict the preparation of the PPCPs prior to concrete casting.

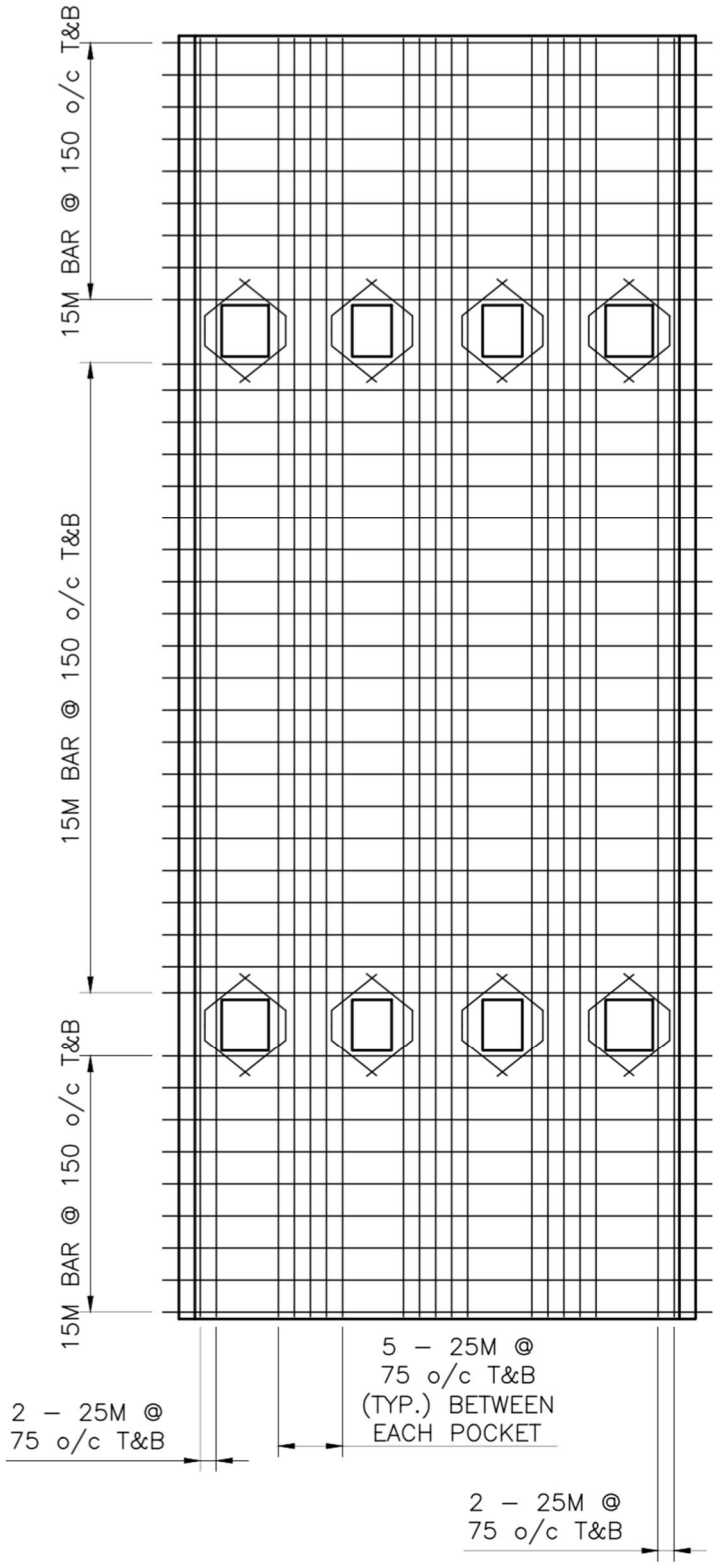

Figure 3-6 – Typical PPCP Steel Reinforcement Layout (Plan View)

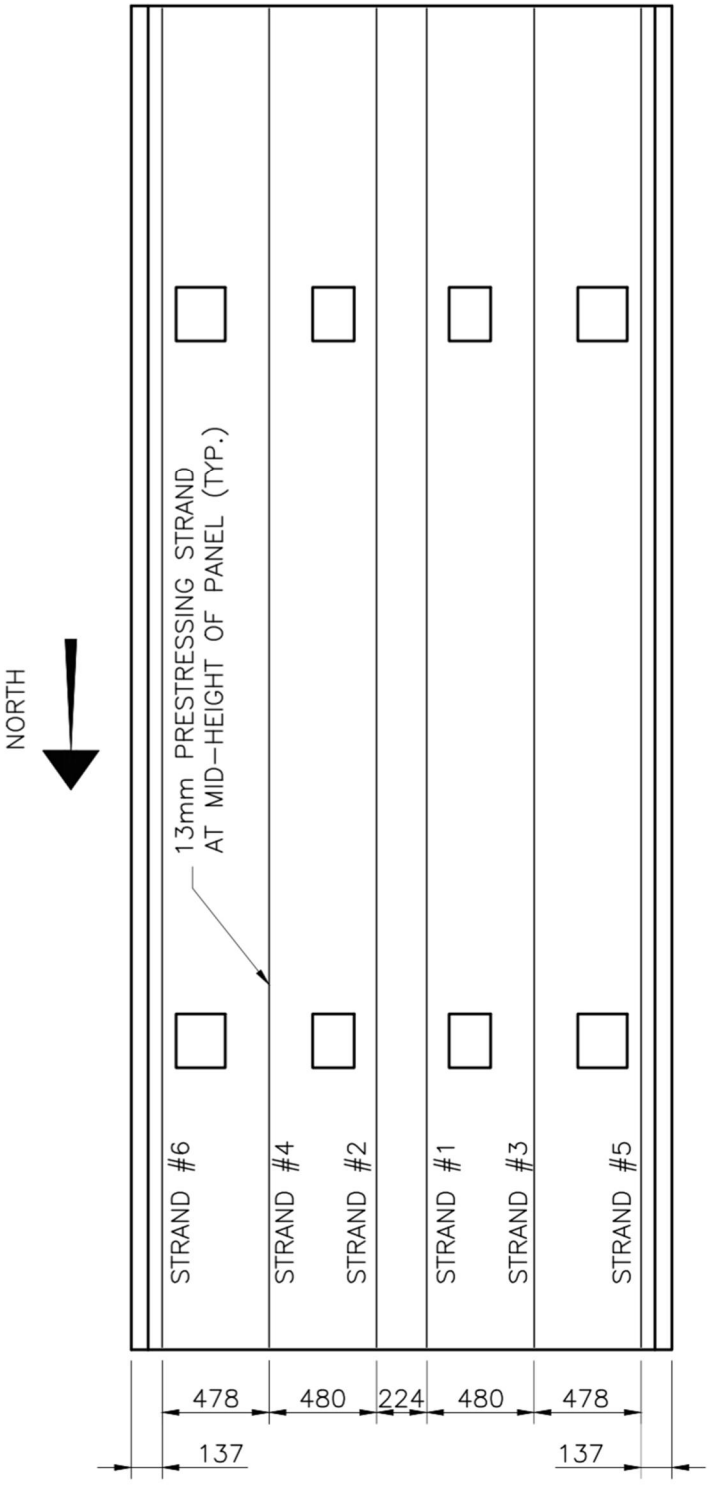

Figure 3-7 – Typical PPCP Prestressing Steel Layout (Plan View)

Figure 3-8 – Steel PPCP Formwork

Figure 3-9 – Placement of Top Reinforcing Steel Mat

Figure 3-10 – Stressing of Strands

3.2.3.2 Concrete Details

The PPCPs were cast using concrete batched onsite at the Armtec plant. The concrete was batched at the batch plant, placed into a concrete mixer, transported to the prestressing plant, and finally transferred into a hopper suspended from an overhead crane before being placed into the steel panel forms. Each panel required approximately 3.4 cubic meters of concrete. The slump flow and plastic air content for each concrete batch were verified by the precaster prior to casting of the PPCPs. The concrete mix design and the specified concrete properties for the mix used in casting the PPCPs are presented in Table 3-1 and Table 3-2 respectively.

After casting, the PPCPs remained within the formwork until the release strength of 35 MPa was achieved. Once the release strength was achieved, the prestressing strands were flame cut and the panels were relocated to continue steam curing, effectively freeing the steel forms to allow fabrication of the next set of panels. Figures 3-11 and 3-12 depict the typical casting of the PPCPs. Table 3-3 provides the date each panel was cast.

Table 3-1 – PPCP Concrete Mix Design

Constituent Material (per m^3)	Quantity
Normal Portland (Type 10) GU (Bulk)	430 kg
Flyash Type CL (Bulk)	60 kg
14 mm Granular Stone (Bulk)	900 kg
Common Concrete Sand (Bulk)	770 kg
Silica Fume (Bagged)	22.80 kg
HRWRA - Glenium 7700	2.60 L
MicroAir	0.07 L
Water	153 L

Note: Mix design information was provided by and printed with permission of Armtec Limited Partnership (Armtec)

Table 3-2 – Specified PPCP Concrete Properties

Property	Specified Value
Water/Cementitious Materials Ratio	0.30
Slump Flow	230 +/- 30 mm
Air Content	5-8%
Density	2336 kg/m^3
Release Strength	35 MPa
28 Day Strength	45 MPa
Rapid Chloride Penetrability	< 1500 Coulombs

Note: w/cm ratio consists of Portland cement, flyash, and silica fume constituents

Figure 3-11 – Casting of PPCP Using Crane Hoisted Hopper

Figure 3-12 – Broom Finishing of PPCP

Table 3-3 – Casting Dates for Test Panels

Panel	Date Cast (2014)
W1	Wednesday, January 15
W2	Wednesday, January 15
E1	Friday, January 17
E2	Friday, January 17
C1	Tuesday, January 21
C2	Tuesday, January 21

3.2.4 Haunches

In conventional CIP bridge deck construction, deck haunches are typically formed using plywood prior to placement of the deck reinforcing steel. Due to the nature of precast bridge deck panel systems, it is not practical to form the deck haunches in this manner. Therefore, adjustable haunch forms are frequently used. The test specimens haunches were formed using ethylene-vinyl acetate (EVA) foam measuring 75 mm in depth and 50 mm in width. This formwork was attached to the topside of the girder flanges prior to placement of the panels as shown in Figure 3-13. Any suitable construction adhesive can be used to adhere the foam to the girders. The adhesive used in this case was Titebond® All Weather Subfloor Adhesive.

Figure 3-13 – EVA Foam Haunch Formwork (TS1) [Typical]

After the foam was attached to the topside of the top girder flanges, the panels were placed atop the girders. The leveling bolts, shown in Figure 3-14, located in the four corner shear pockets of each PPCP were used to attain the desired deck profile and haunch thickness. In practice, the leveling bolts are used to lower, raise, or angle the PPCPs atop the girders to achieve the desired deck profile. As long as the foam haunch formwork is initially deeper than the final haunch height desired, the foam compresses between the girder flange and underside of the PPCP effectively acting as a form for the haunch-fill material; this is depicted in Figure 3-15. The test specimen final haunch depth was 50 mm. The haunches were ultimately filled with UHPC during casting of the shear pockets.

Figure 3-14 – Typical Leveling Plate and Bolt (Head of Bolt Cut Off Prior to UHPC Casting)

Figure 3-15 – EVA Foam Haunch Formwork Compressed from 75 mm to 50 mm After Panel Placement

3.2.5 Full-Depth Shear Pockets

To achieve composite action between the PPCPs and the steel plate girders, eight full-depth shear pockets were used per panel. These shear pockets varied in size depending on the presence of leveling hardware. As previously shown in Figure 3-5, corner pockets containing leveling hardware were 240 mm in width and 220 mm in length; interior pockets not containing leveling hardware were 240 mm in width and 185 mm in length. Regardless of size, all shear pockets contained six 19 mm diameter shear studs, 178 mm in length. These studs were spaced at 65 mm in the longitudinal direction and 70 mm in the transverse direction.

For new construction of precast panel bridge deck systems on steel girders, the shear studs can either be welded on during girder fabrication or welded in place after placement of the panels. Site welding of the shear studs after panel placement is usually performed using a shear stud gun shown in Figure 3-16, as conventional welding techniques may not be feasible in the tightly spaced pockets.

Figure 3-16 – Shear Stud Gun with Shear Stud and Ceramic Ferrule Loaded and Ready for Use

TS1 had the shear studs installed using a stud gun after placement of the PPCPs, as shown in Figure 3-17. Alternatively, TS2 had the shear studs pre-installed on the steel plate girders using a stud gun as shown in Figure 3-18; this was done to minimize welding equipment rental costs, as all shear studs were installed within one equipment rental period. The two girders for TS2, now with the shear studs installed, were stored until they were later required. The shear pockets were ultimately filled with UHPC during casting of the haunches and transverse joints.

Figure 3-17 – Shear Studs Installed in Pockets Using Shear Stud Gun After PPCP Placement (TS1)

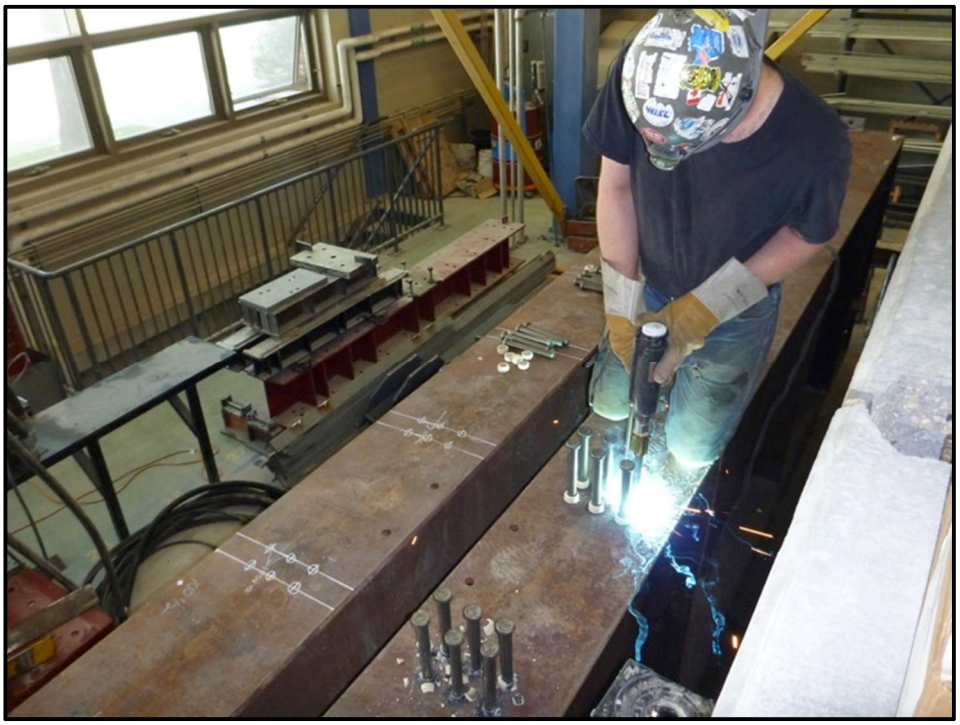

Figure 3-18 – Shear Studs Installed on Girders Using Shear Stud Gun Prior to PPCP Placement (TS2)

It is important to note that the researchers had a difficult time with the placement of the TS2 panels on the girders with the preinstalled studs due to the system geometry. The studs were pre-welded correctly into the appropriate positions but the panels could not be lowered vertically into place. Due to the protruding hooked bars, the panel had to be lowered offset from the adjacent panel to clear the bars and then slid longitudinally to obtain the desired joint width. This resulted in conflicts between the preinstalled shear studs and the underside of the panel as shown in Figure 3-19.

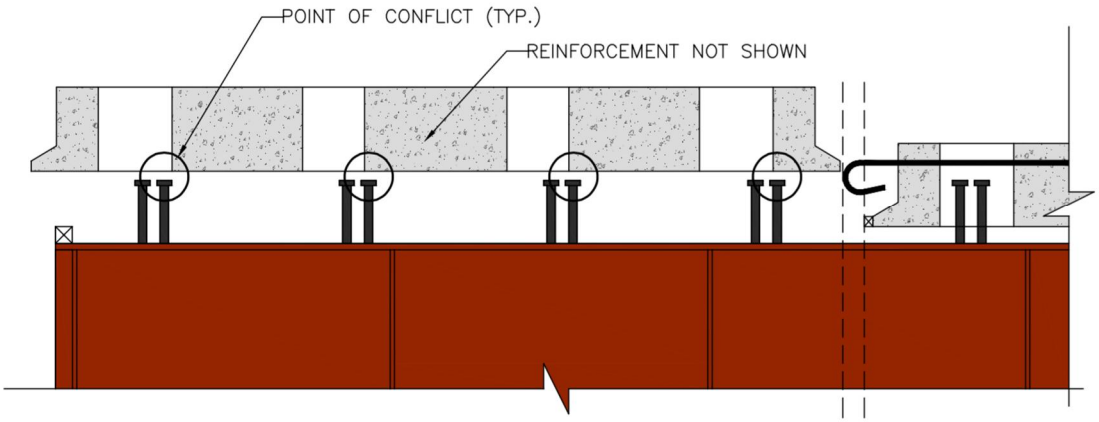

Figure 3-19 – Stud/Panel Conflict During TS2 Panel Placement

To solve this issue, the panels had to be steeply raked, or tilted, to try to clear the shear studs as shown in Figure 3-20. Ultimately, the researchers managed to place the panels but unfortunately caused minor cosmetic damage. The damage was limited to spalling of the inside faces of several shear pockets and breakage of the joint bottom lip in several locations as shown in Figures 3-21 and 3-22 respectively. Overall, the researchers do not believe that this damage affected the research results.

Figure 3-20 – Placement of TS2 Panels Utilizing Steep Tilt

Figure 3-21 – Damage to Inside Face of TS2 Shear Pockets (Panel C2) During Placement

Figure 3-22 – Damage to Bottom Lip of Joint (East Joint of TS2 – Panel E2) During Placement

3.2.6 Transverse Joints

The transverse panel edge geometry (joint geometry) was consistent with that recently used on similar bridges by MTO in Ontario, Canada. As can be seen in Figure 3-23, the transverse joint was 176 mm wide at the top of the panels and narrowed to 25 mm wide at the base of the panels. The transverse joint was sealed along the bottom edge using a 38 mm thick piece of EVA foam compressed to 25 mm during panel installation.

After placement of the panels, additional reinforcing steel was placed within the joints. A total of four 25M bars were placed transversely; two within the hooked bars protruding from the panel edges as shown in Figure 3-24 and two laid on top. The hooked bars within the joint were instrumented with electrical strain gauges (ESGs) as is discussed in

detail in Sub-section 3.4.3. The transverse joints were ultimately filled with UHPC during casting of the haunches and shear pockets.

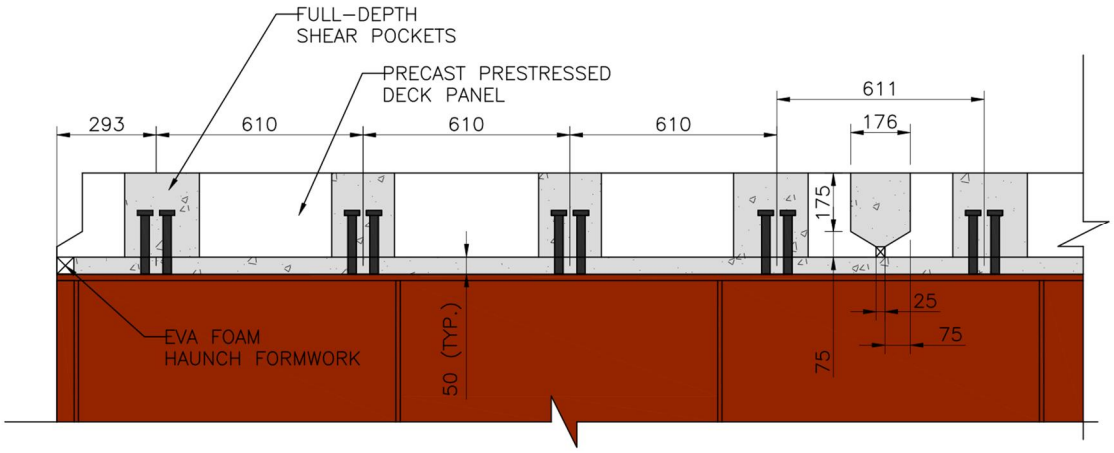

Figure 3-23 – Typical PPCP Section with Joint Details

Figure 3-24 – Typical Reinforcing Steel within Transverse Joint (Two 25M Bars Across Top of Hooked Bars Not Shown)

3.2.7 Haunch, Shear Pocket and Joint-Fill Material

The haunches, shear pockets and transverse joints were all filled using UHPC available for purchase in the North American market. Specifically, Lafarge Ductal® JS1000 Premix Grey was used (see Appendix A for Product Data Sheet). The UHPC was provided as a pre-bagged material consisting of three parts: 50 lb (23 kg) bags of Ductal® JS1000 Premix Grey (pre-bagged dry powder materials); Dramix OL 13/.20 steel fibers measuring 13 mm in length with a nominal diameter of 21 mm (tensile strength of 3000 MPa); and CHRYSO Fluid Premia 150 (an ASTM C-494 Type A and F HRWRA). A Lafarge Ductal® Ryan mixer was rented from Lafarge and used for mixing of the UHPC materials. The UHPC mixing followed the supplier's recommended practice A Lafarge Ductal® representative was present during the mixing of the UHPC for both specimens.

All UHPC for TS1 and TS2 was mixed and cast on June 17, 2014 and February 4, 2015 respectively. A crane hoisted hopper was used to transfer the UHPC from the mixer to the test specimens. The haunches and shear pockets were first filled followed by the filling of the transverse joints. Once all UHPC was placed, the exposed surfaces were dampened with water and covered with polyethylene sheet. As per instructions given by the Lafarge representative, the UHPC was left covered for two to three days and then allowed to cure in the open laboratory air. At no point were the exposed UHPC surfaces wetted or moist cured after the initial dampening and placement of poly. The following Figures 3-25 through 3-27 depict the mixing, casting and curing process for the test specimens.

Figure 3-25 – Mixing of UHPC

Figure 3-26 – Filling of Transverse Joint

Figure 3-27 – UHPC Joint and Shear Pockets Covered with Poly

3.3 Testing Scheme

The testing scheme for this research program was comprised of four different tests at unique locations. Two tests were performed on TS1 and two tests were performed on TS2 as shown in Figures 3-28 and 3-29. Specifically, a static monotonic test to failure was performed on Panel C1 (Test #1) followed by a partial fatigue test on Panel W1 (Test #2) of TS1. A fatigue test was then performed on Panel W2 (Test #3) followed by a final monotonic static test to failure on Panel E2 (Test #4) of TS2.

The test location on Panel C1 was centered on the panel while all the other test locations were adjacent a transverse joint. The location of the testing apparatus in relation to the joints was dependent on the anchor points of the Structures Lab strong floor below.

Therefore, the edge of the loading plate was approximately 25 mm away from the edge of the transverse joint for Tests 2-4. All tests were performed with the loading apparatus acting upwards on the test specimens – loading plate in contact with the deck soffit – to induce negative bending moments in the specimens.

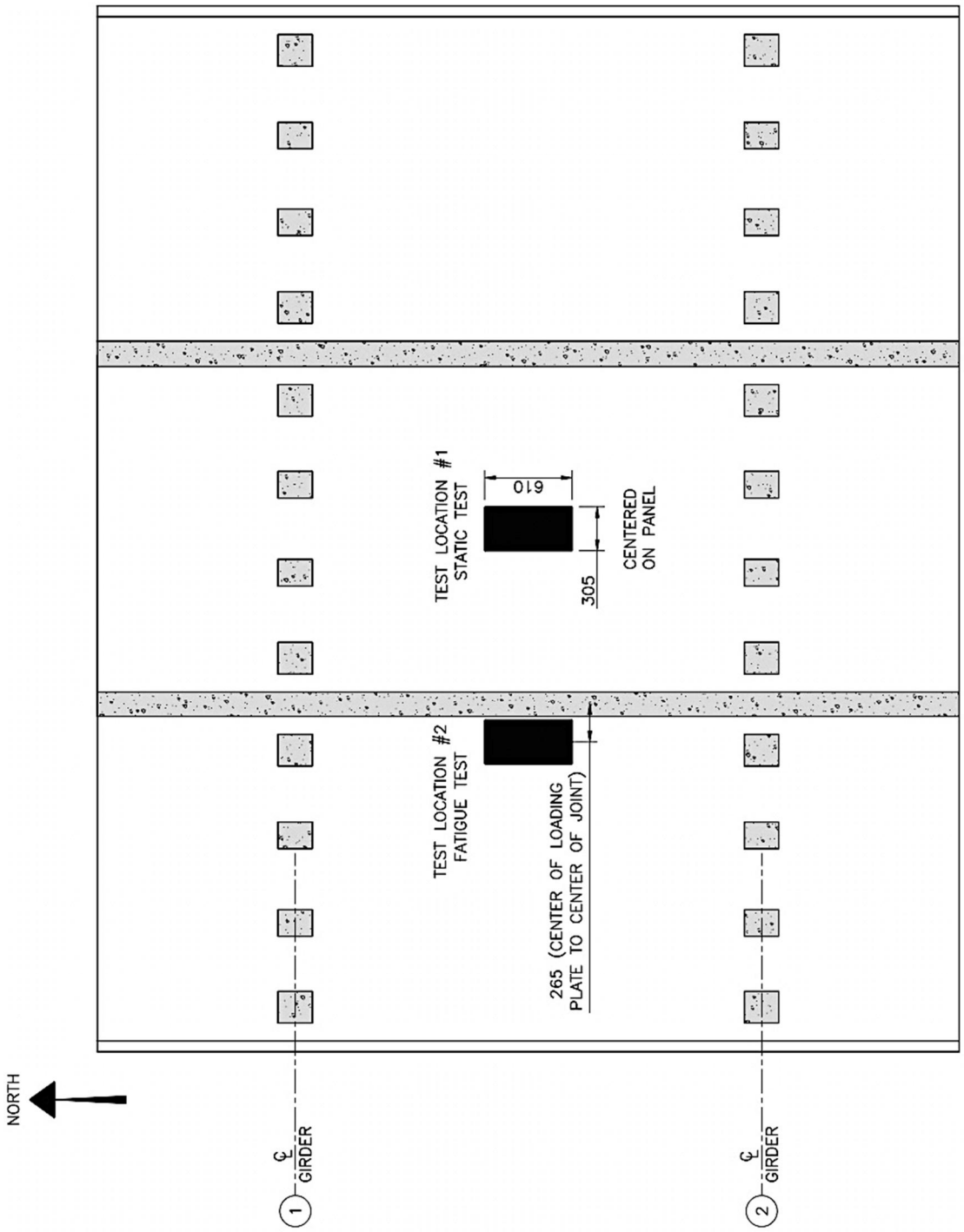

Figure 3-28 – Testing Locations for TS1

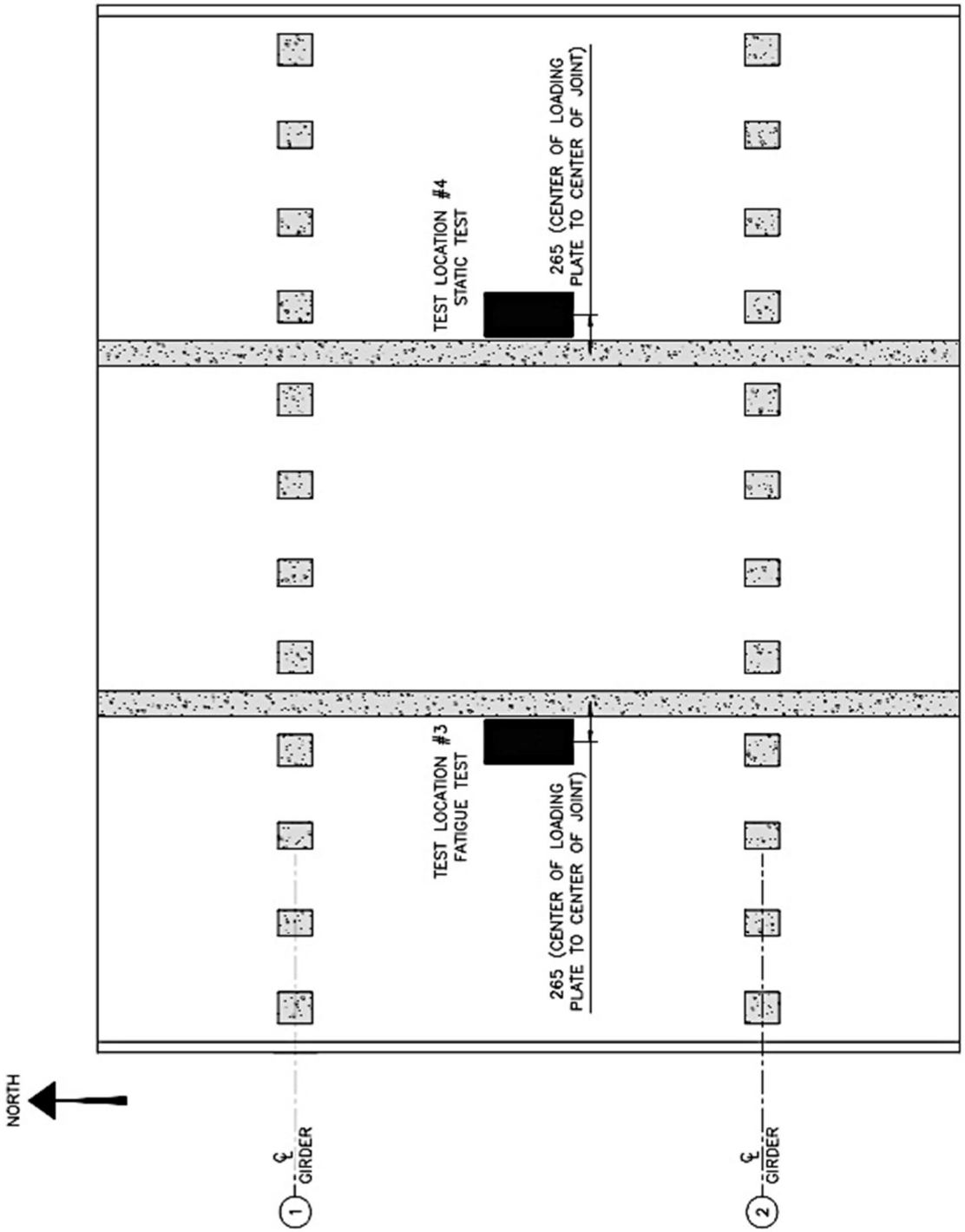

Figure 3-29 – Testing Locations for TS2

3.4 Test Set-up

The following Sub-sections detail the preparatory work completed to undertake the testing program. The superstructure support system, loading apparatuses, and the instrumentation plan including details on the load, displacement, strain and crack measurement devices are presented herein.

3.4.1 Superstructure Support

To accommodate the irregular c.t.c. girder spacing of 3251 mm w.r.t. the Structures Lab strong floor, and to provide the desired span length for the test specimens, four reinforced concrete blocks measuring 1100 x 1100 x 500 mm were constructed to support the superstructure off the strong floor. Two 19 mm thick plywood sheets were used as bearing pads and were placed between the reinforced concrete support blocks and steel girders. In order to avoid any up-lift of the test specimen during Tests 1-4, the superstructure was anchored to the strong floor. This was accomplished by means of four high-strength Dywidag bars passing through the reinforced concrete support blocks and tensioned to the strong floor at each support location. Due to the hole pattern in the strong floor, the Dywidag bars were required to pass through the bottom girder flange on the exterior of the test specimen as shown in Figure 3-30. Dywidag bars coupled with HSS steel tie-downs were utilized on the bottom girder flange on the interior of the test specimen as shown in Figure 3-31.

Figure 3-30 – Test Specimen Tie-downs on Exterior of Girders

Figure 3-31 – Test Specimen Tie-downs on Interior of Girders

3.4.2 Loading Apparatus Details

Two loading apparatus setups were used depending on whether a static or fatigue test was being performed. Due to the limited capacity of the testing equipment available for fatigue testing, a large 5000 kN capacity cylindrical SPX Power Team jack was utilized for the static tests. As shown in Figure 3-32, the loading apparatus for the static tests consisted of a 75 mm thick steel base plate, an HSS and steel plate pedestal, a 5000 kN capacity cylindrical jack, a 5000 kN capacity load cell, a 610 mm by 305 mm load plate and a 610 mm by 305 mm neoprene pad. This assembly was anchored to the strong floor by means of four hand tightened high-strength Dywidag bars.

Figure 3-32 – Loading Apparatus for Static Tests (Tests #1 and #4)

As shown in Figure 3-33, the loading apparatus for the fatigue tests consisted of a 75 mm thick steel base plate, a 1000 kN capacity MTS servo-hydraulic actuator equipped with a swivel base, a 1000 kN capacity load-cell, a 1000 kN capacity compression head, a 610 mm by 305 mm load plate and a 610 mm by 305 mm neoprene pad. Additionally, steel chains equipped with clevises and turn-buckles were used to level the actuator and stabilize it during testing. This assembly was anchored to the strong floor by means of four tensioned high-strength Dywidag bars.

Figure 3-33 – Loading Apparatus for Fatigue Tests (Tests #2 and #3)

3.4.3 Instrumentation Details

Extensive instrumentation was incorporated into the test set-up to monitor the: strain in the reinforcing steel and shear studs within the PPCPs and UHPC joints, concrete strain in the vicinity of the loading point, deflections, and crack widths during testing. All instrumentation was attached to a DAQ system for data collection. A detailed description of the instrumentation scheme is presented herein.

3.4.3.1 Load Measurement

During testing, the applied load was measured by means of a load cell attached to either a cylindrical jack (for static tests) or a servo-hydraulic actuator (for fatigue tests). A 5000 kN capacity load cell and a 1000 kN capacity load cell were used for the static and fatigue tests respectively. The load cell was connected to the DAQ, which recorded the load magnitude at a rate of 2 Hz (two readings per second) for static tests and at a rate of 20 Hz (twenty readings per second) for fatigue tests.

3.4.3.2 Displacement Measurement

Linear variable displacement transducers (LVDTs) were used to measure the deflections of the PPCPs during testing. These LVDTs were placed on the topside of the specimens along the longitudinal centerline at various points of interest including: directly above the loading plate, PPCP quarter points, and locations along the longitudinal centerline immediately adjacent the UHPC joints. The detailed LVDT layouts for each test location are presented along with the deflection results in Chapter 4.

The LVDTs measuring the PPCPs deflections were supported from above the test specimens by a uni-strut system; the uni-strut system was supported by steel angles and clamps placed directly over the girder center-lines. The LVDTs were supported in this manner to ensure that the displacement readings being recorded were the true deflections of the PPCPs relative to the supporting steel girders. The uni-strut LVDT support system is shown in Figure 3-34.

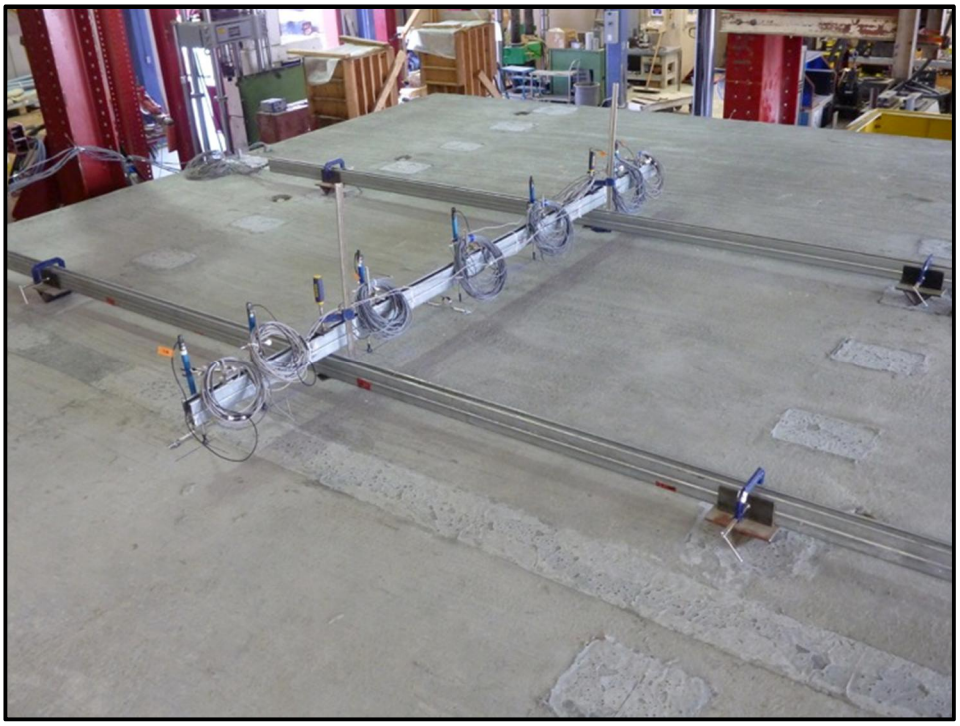

Figure 3-34 – Typical Uni-strut LVDT Rack with LVDTs (Test #1 Setup Shown)

3.4.3.3 Strain Measurement

Various types of electrical strain gauges (ESGs) were used for each test specimen to monitor: strains on the reinforcing steel bars within the PPCPs and within the UHPC joints, strains on the shear studs, and to monitor the compressive concrete strains in the

vicinity of the loading point. All ESGs placed on reinforcing bars or shear studs were installed in the following manner (presented in order of preparation):

- Surface preparation of the steel substrate using a grinder or sander followed by fine grit sandpaper to remove all surface imperfections;
- Cleansing of the substrate surface using Prep Conditioner A with Kimwipes;
- Cleansing of the substrate surface using Prep Neutralizer 5A with Kimwipes;
- Placement of the ESG on the substrate using M-BOND 200 catalyst and adhesive, applying thumb pressure for two minutes (see Figure 3-35);
- Coating of the ESG using M-COAT B Nitrile Rubber Coating;
- Placement of Teflon Tape over nitrile rubber coated ESG;
- Placement of butyl rubber completely covering ESG and the additional coatings; a
- Final wrapping of ESG installation using Scotch Liner Rubbing Splicing tape (see Figure 3-36).

All ESGs placed on concrete were installed in the following manner (presented in order of preparation):

- Surface preparation of the concrete substrate using a grinder or sander followed by fine grit sandpaper to remove all surface imperfections;
- Placement of a thin layer of five minute epoxy over the prepared surface to fill any voids. The layer of epoxy was sanded smooth once cured;
- Placement of the ESG on the substrate using M-BOND 200 catalyst and adhesive, applying thumb pressure for two minutes; and,
- Final coating of the ESG using a protective rubber coating.

Figure 3-35 – ESG Adhered to Reinforcing Bar Prior to Coating (Typical)

Figure 3-36 –ESG Installation With All Protective Coatings In Place (Typical)

Figure 3-37 – ESG Installed on Concrete Prior to Protective Coating

To monitor strains on the hooked 15M joint reinforcing bars (top mat of longitudinal bars) within the PPCPs, 6 mm – 120 Ω ESGs were installed on three hooked bars per panel side. The hooked bars were instrumented with ESGs placed within the panel located approximately 25 mm from the panel edge. The hooked bars protruding from the free ends of the test specimens were not instrumented. The instrumented hooked bars prior to installation within the panel are shown in Figure 3-38.

Strains within the UHPC joints on the same hooked 15M reinforcing bars instrumented within the PPCPs were measured using either 6 mm – 350 Ω ESGs or 6 mm – 120 Ω ESGs depending on the test (due to ESG product availability). These ESGs were placed within the joint, approximately 25 mm from the panel edge. The exact location and

naming convention for the reinforcing steel strain gauges placed on the test specimens is shown in Figures 3-39 to 3-44.

Figure 3-38 – Hooked Bars With Instrumentation (Typical)

The strains on the shear studs were also monitored in one pocket for TS1 and in four pockets for TS2. For TS1, the ESGs were placed on the loose shear studs, which were then welded to the girder using the stud gun shown in Figure 3-16. As a result, the ESGs on TS1 were not all oriented in the same direction as can be seen in the shear stud ESG layout for TS1 shown in Figure 3-45. In addition, while the gauges appeared to have been functional, they were subjected to high heat during the installation of the shear studs with the stud gun which may have potentially damaged the gauges. For TS2, the ESGs were placed on shear studs after they were installed on the girder eliminating the issues encountered with the TS1 gauges. The TS2 shear stud ESG layout is shown in Figure 3-46.

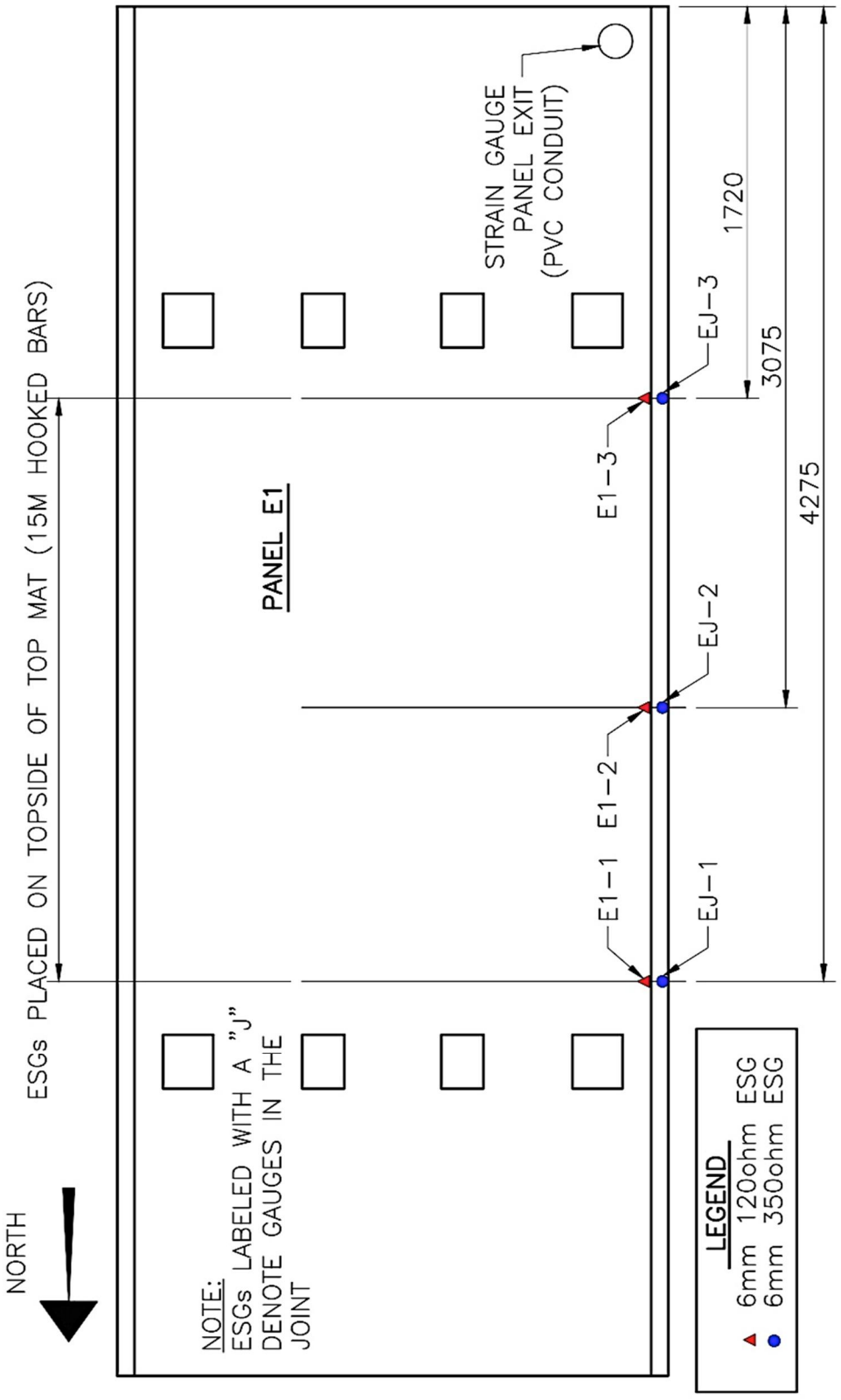

Figure 3-39 – ESG Placement for Panel E1

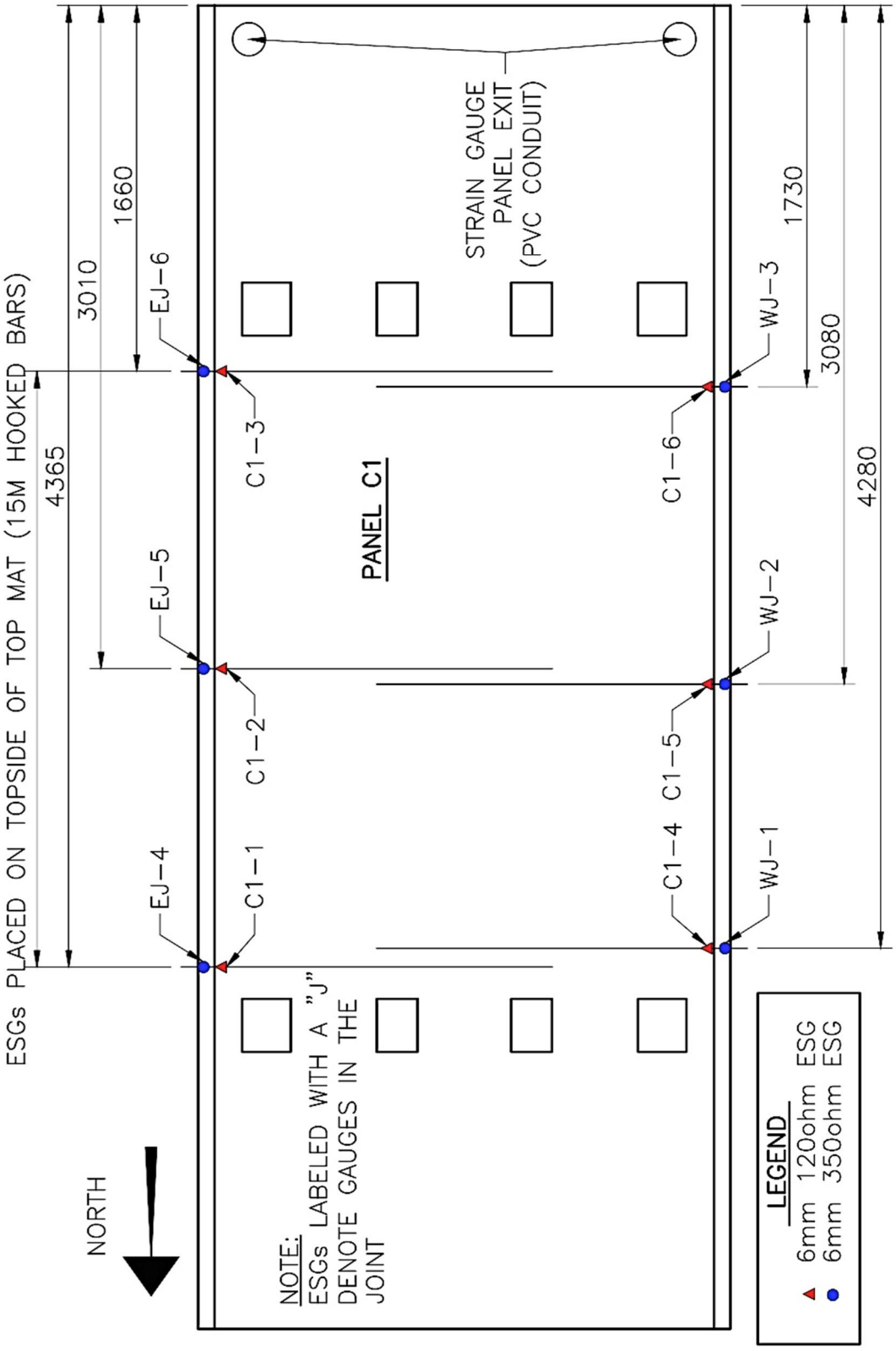

Figure 3-40 – ESG Placement for Panel C1

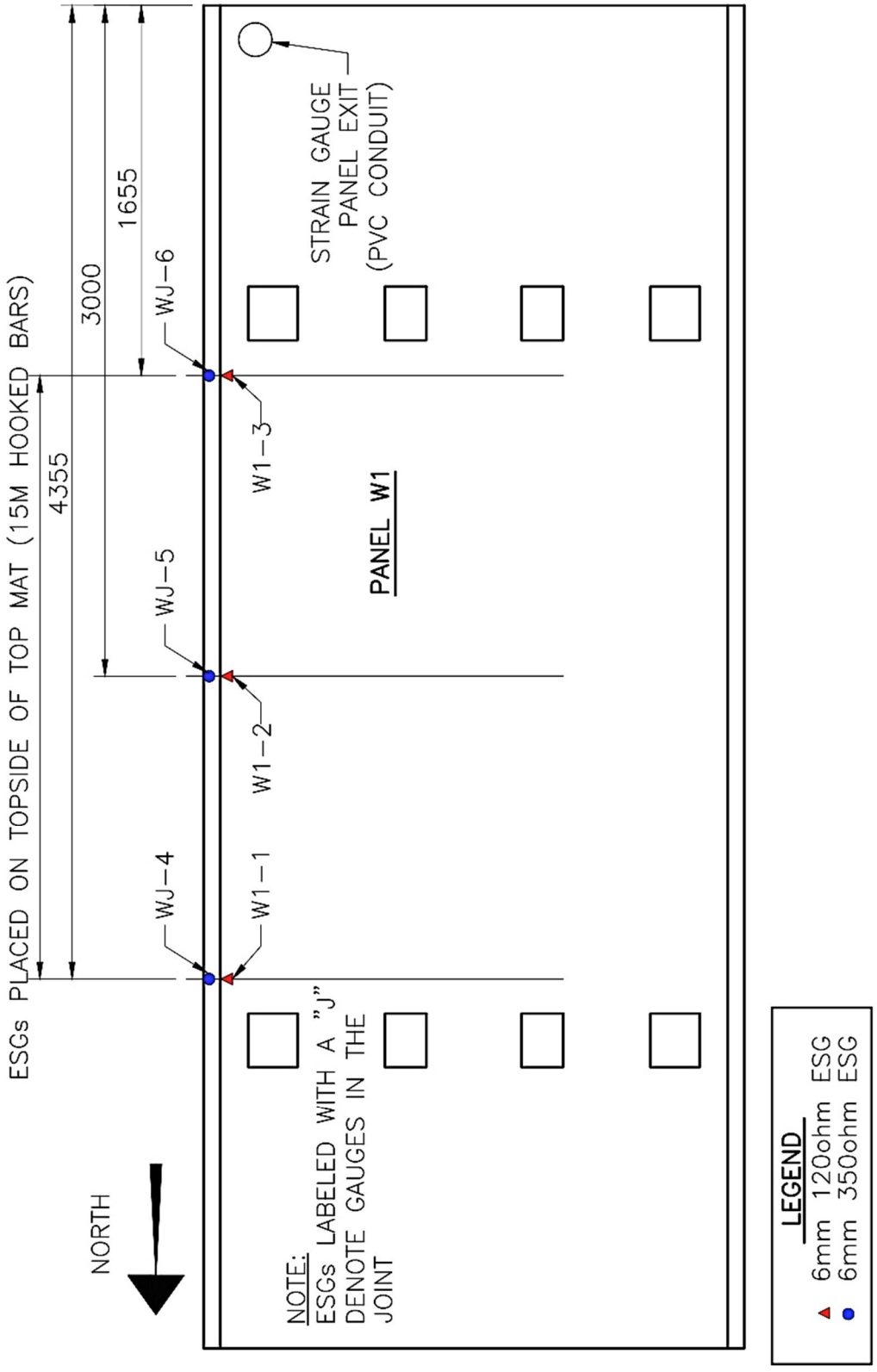

Figure 3-41 – ESG Placement for Panel W1

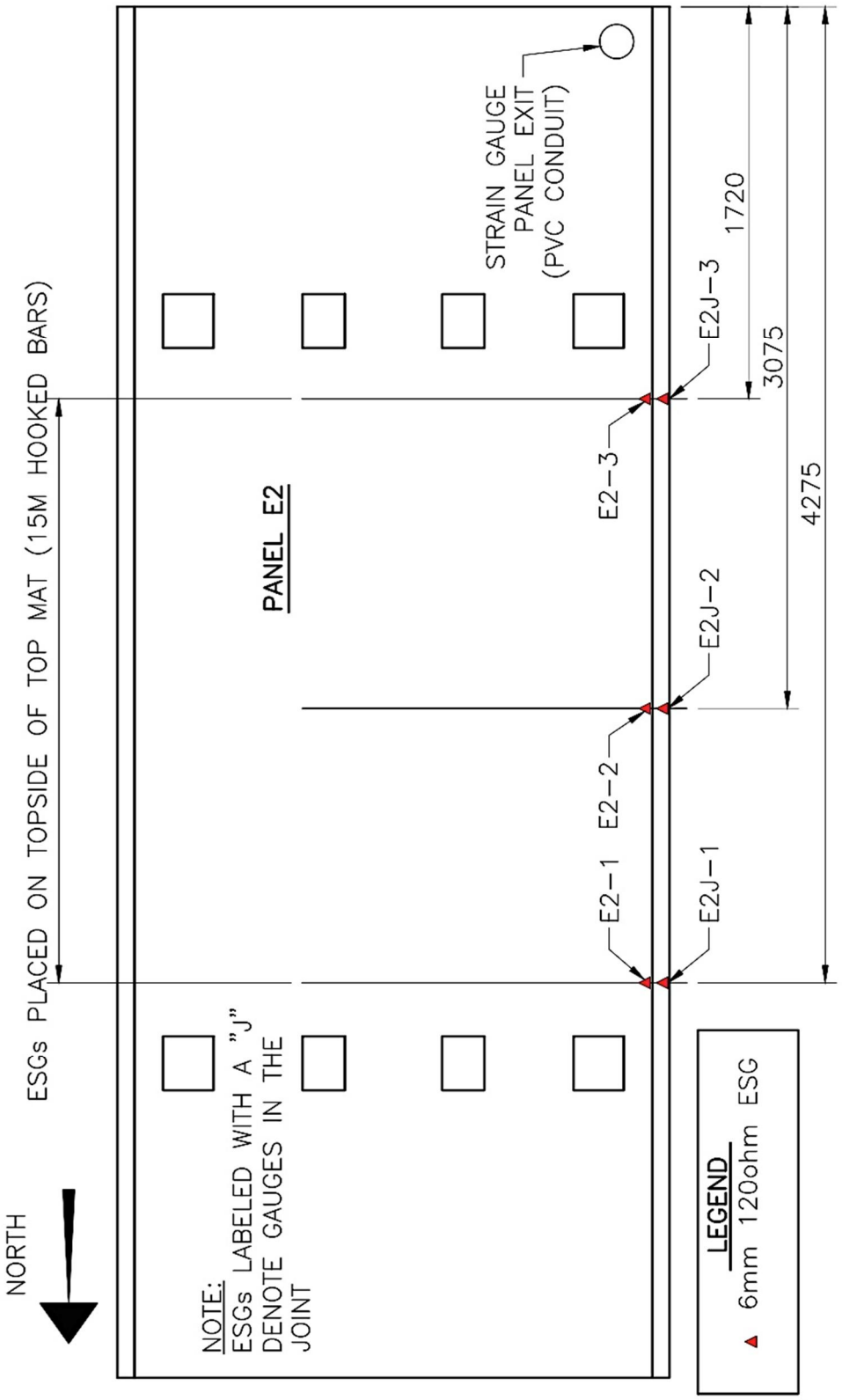

Figure 3-42 – ESG Placement for Panel E2

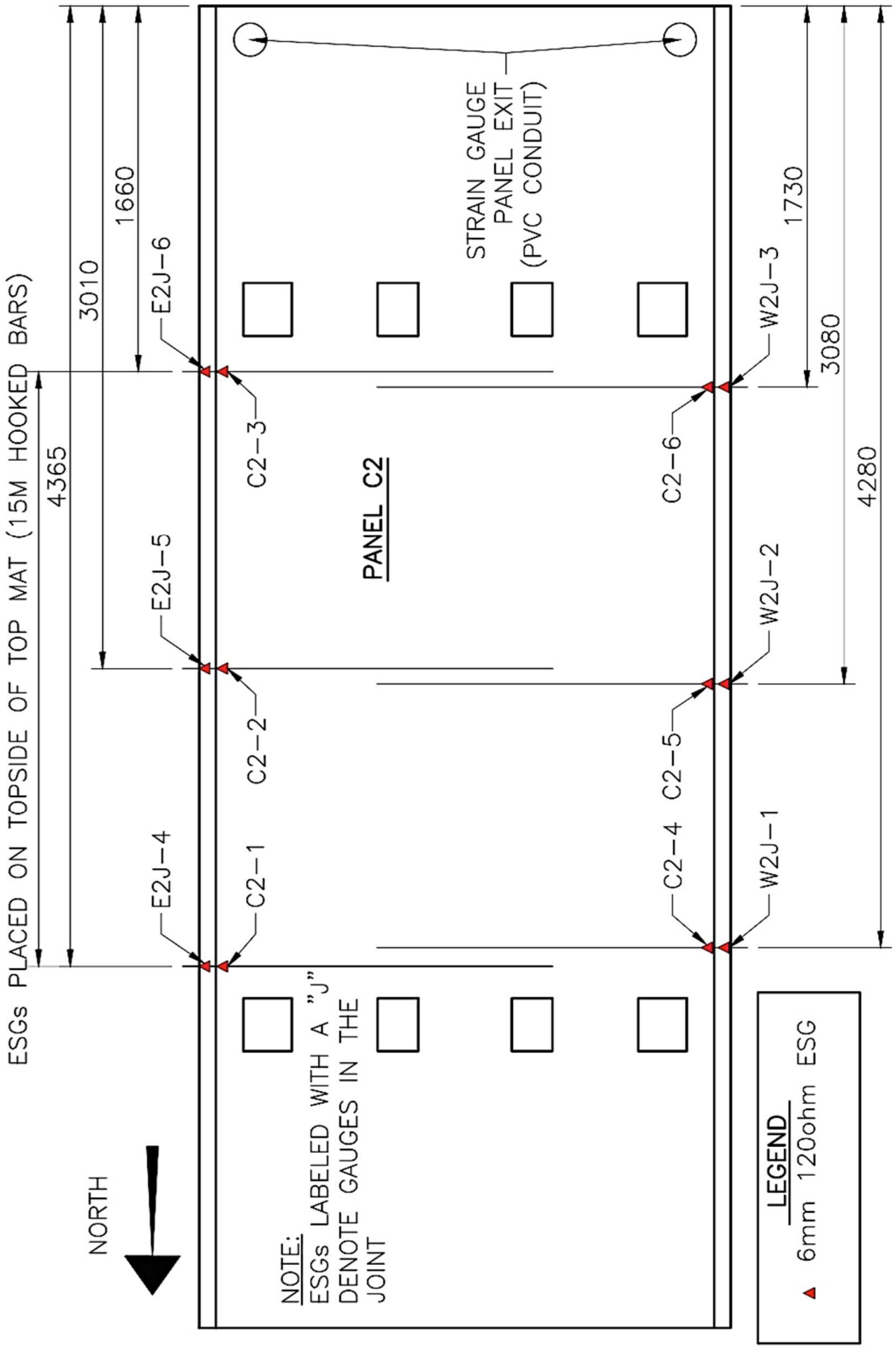

Figure 3-43 – ESG Placement for Panel C2

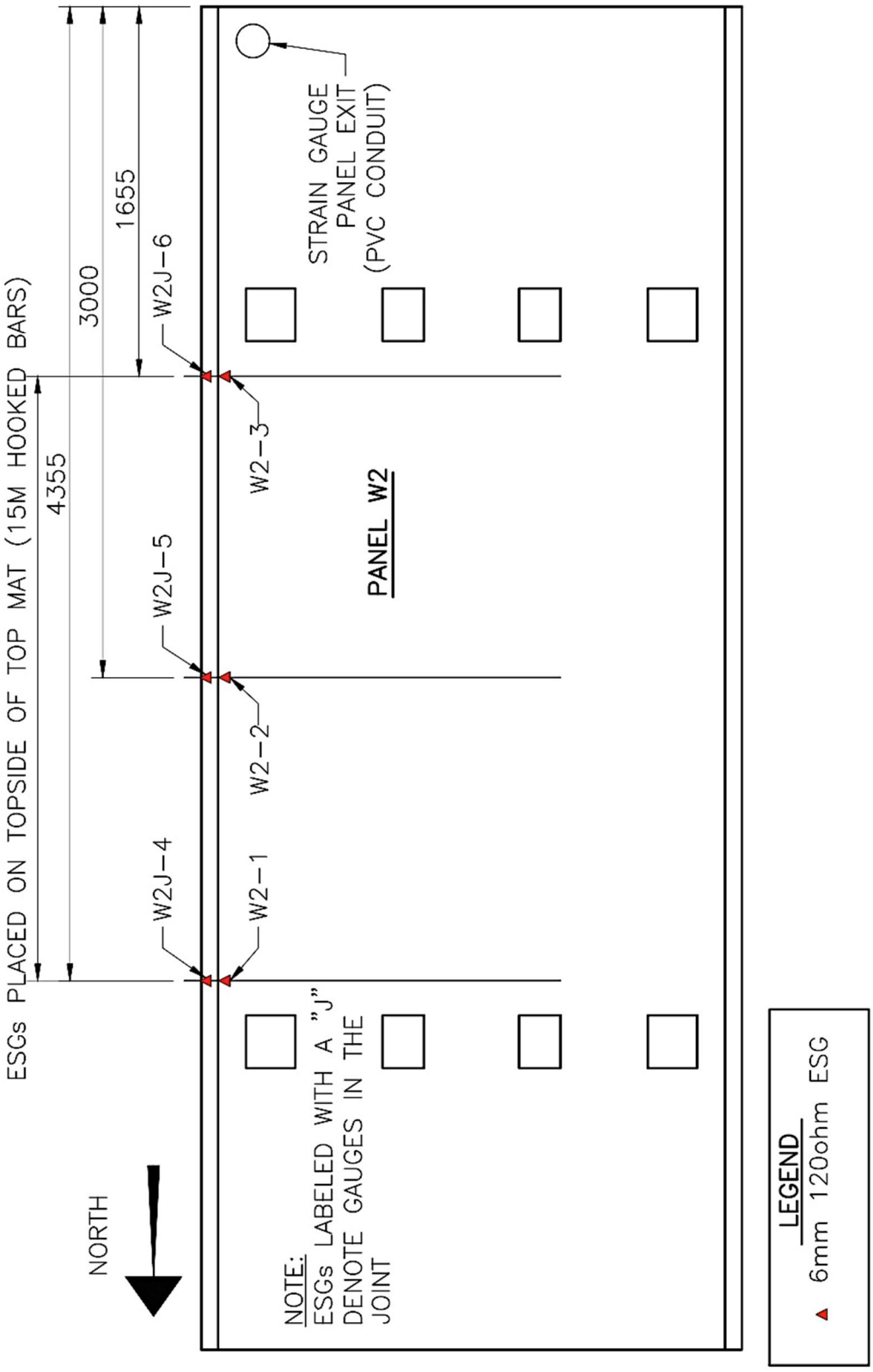

Figure 3-44 – ESG Placement for Panel W2

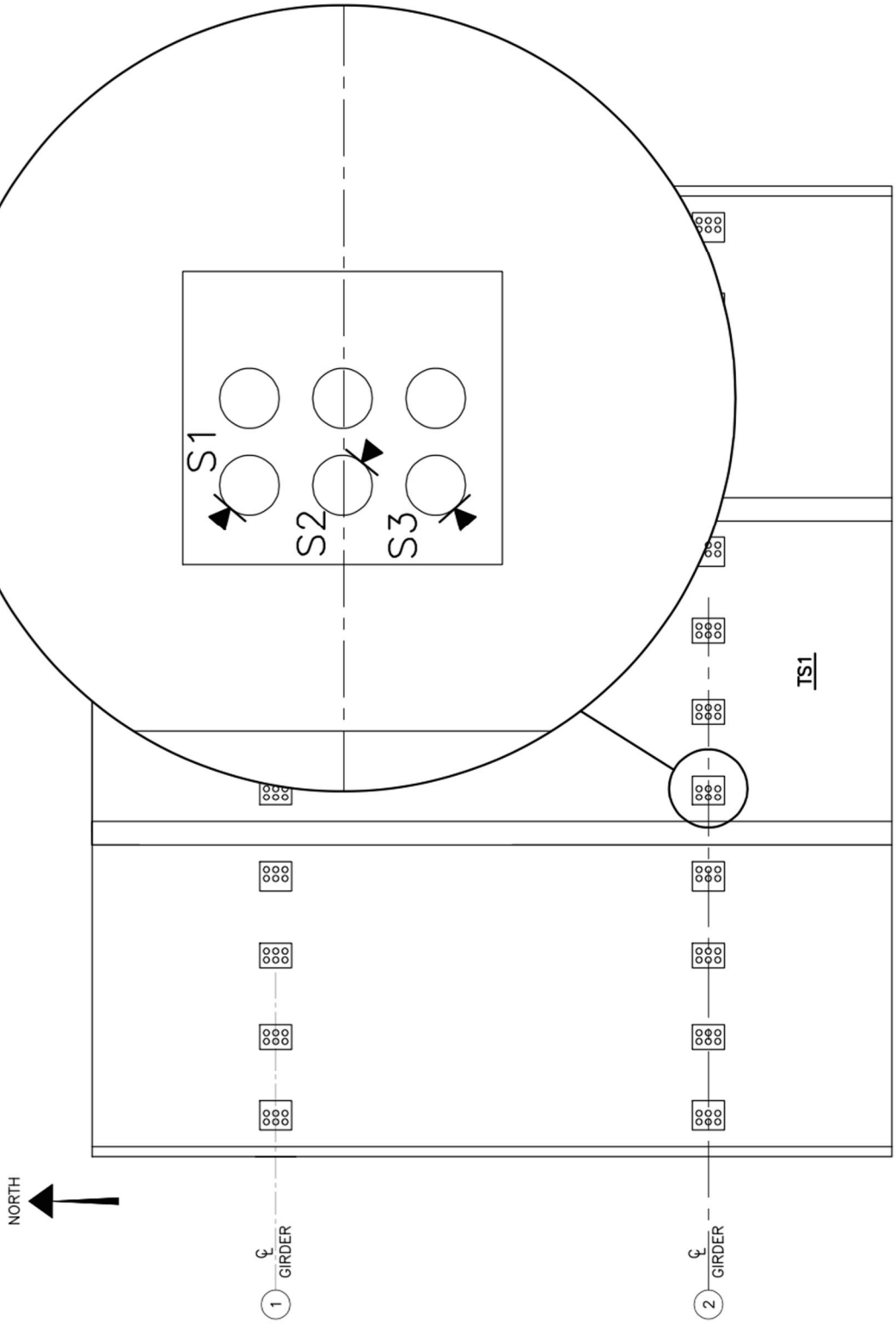

Figure 3-45 – Shear Stud ESG Layout for TS1

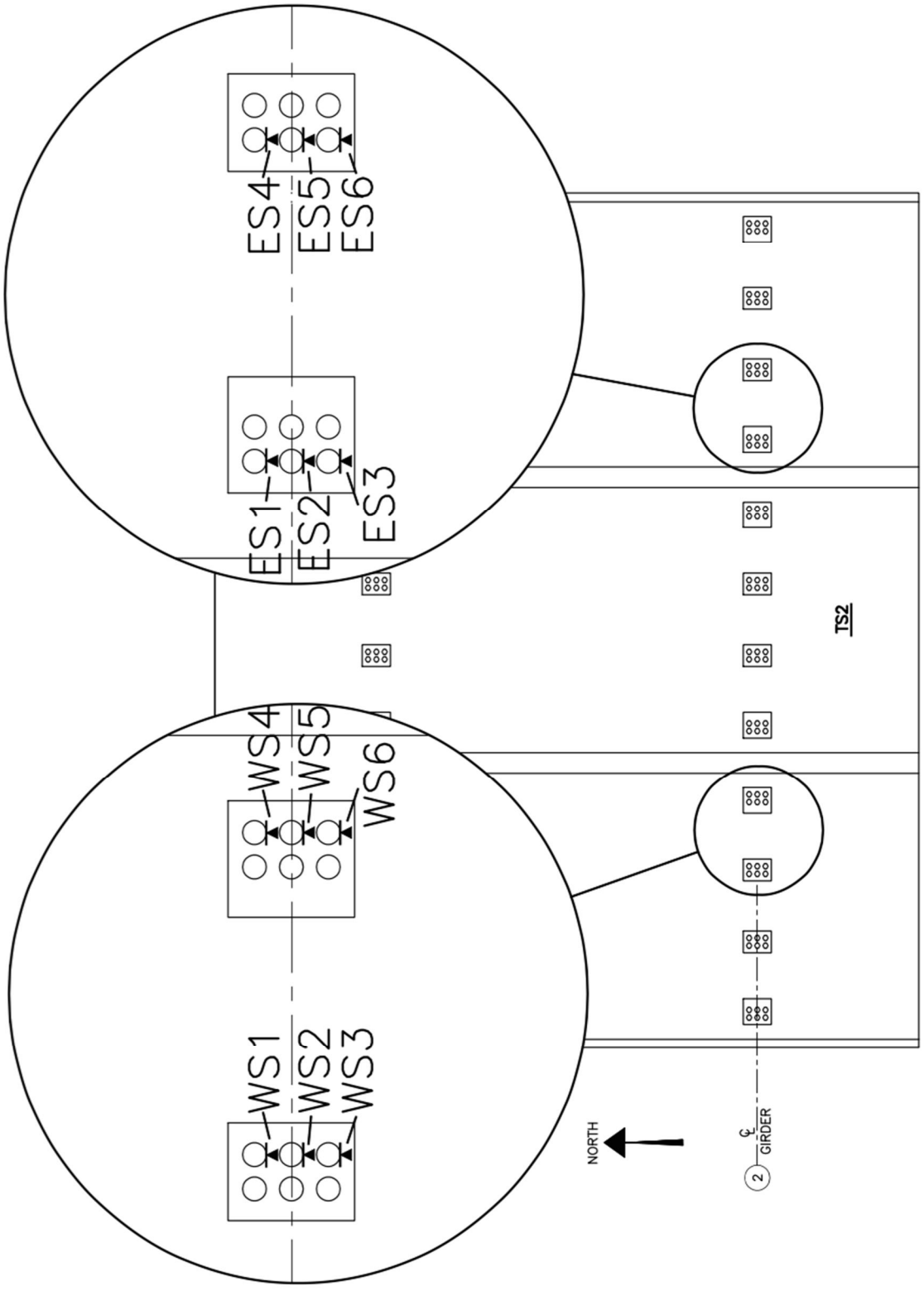

Figure 3-46 – Shear Stud ESG Layout for TS2

3.4.3.4 Crack Measurement

In addition to the strain and deflection monitoring instrumentation, 200 mm pi-gauges were used in a number of locations during each test to monitor crack widths. Specifically, pi-gauges were placed:

- Across the PPCP and UHPC joint interfaces in line with the loading point as shown in Figure 3-47;
- Across a diagonal crack (relative to the longitudinal bridge axis) in the vicinity of the loading point as shown in Figure 3-48; and,
- Across a longitudinal crack overtop the loading point as shown in Figure 3-47.

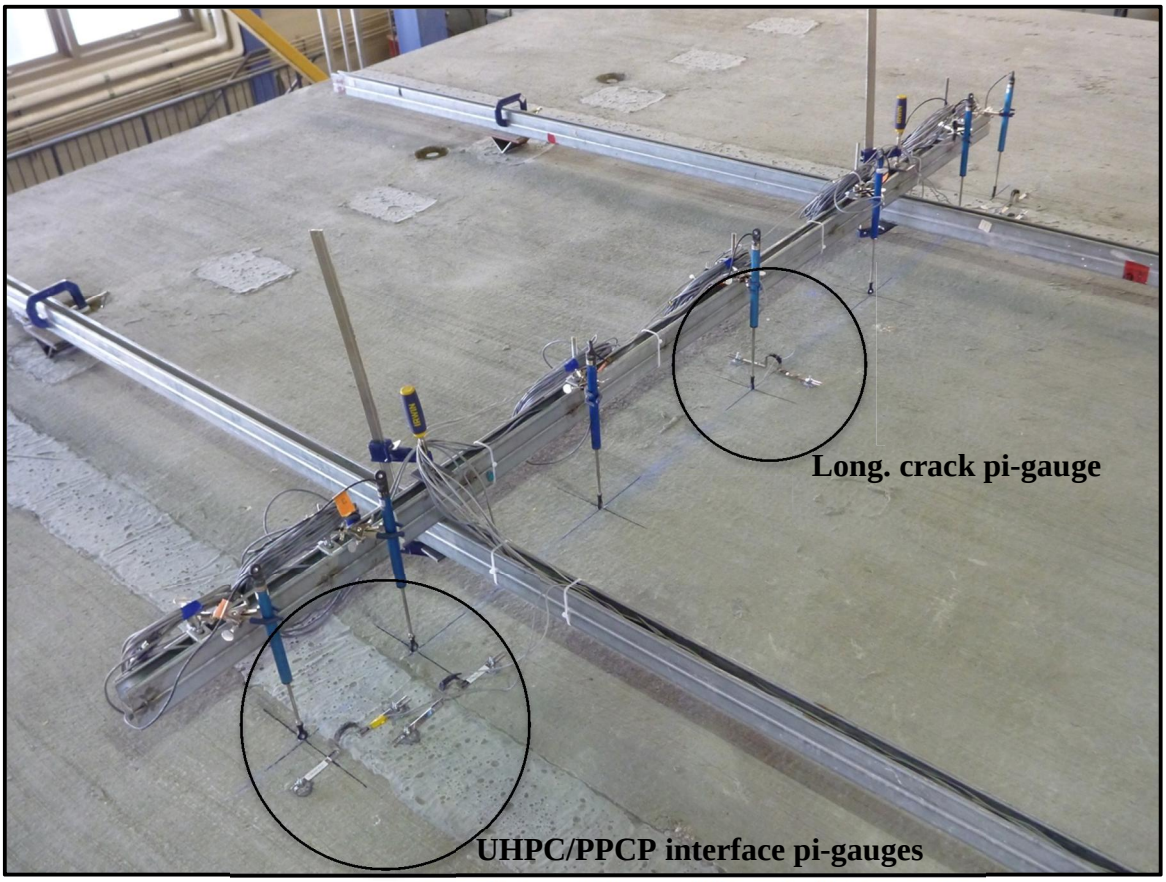

Figure 3-47 – Typical Pi-Gauge Setup (Diagonal Crack Pi-Gauge Not Shown)

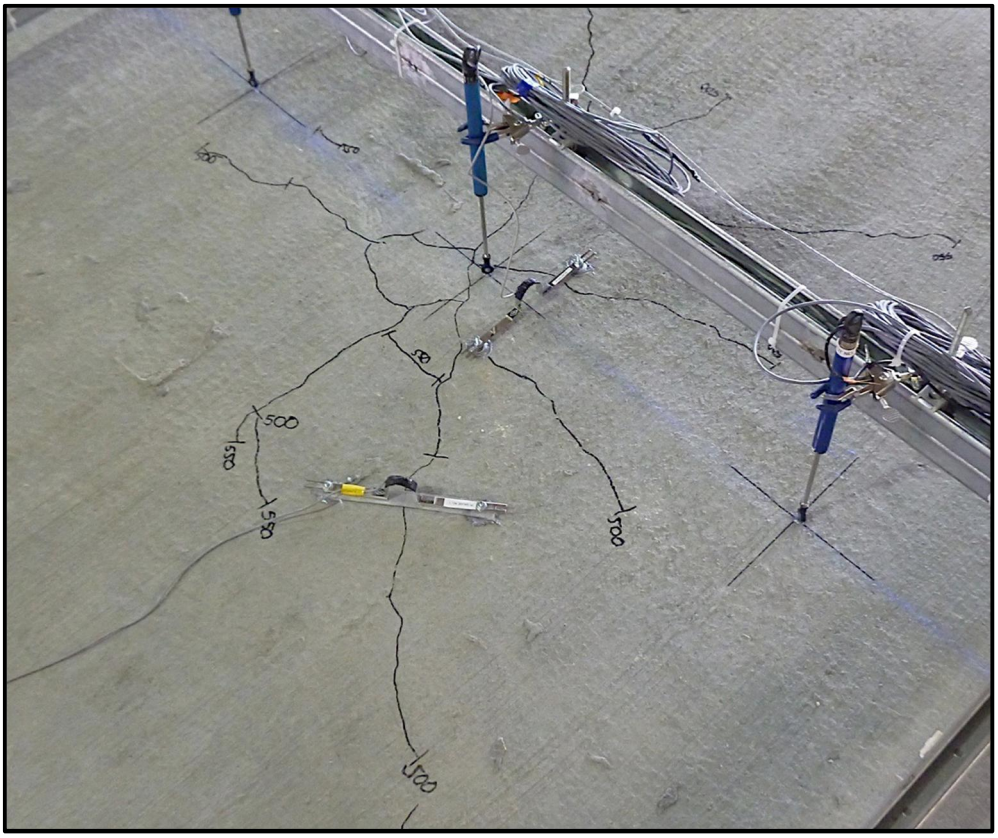

Figure 3-48 – Typical Pi-Gauge Setup With Diagonal Crack Gauge Installed

Chapter 4

Experimental Results and Analysis

4.1 Introduction

The following Chapter contains a summary of the experimental results obtained from the research program followed by an analysis of this data. In particular, results and analysis of various materials tests as well as deflection, strain, and crack width results for each of the full-scale tests conducted are presented herein. This Chapter is divided into seven Sub-sections: Materials Testing, one sub-section for each of the four test locations, Comparison of Test Results, and Yield Line and Punching Shear Analysis of Failure Loads.

4.2 Materials Testing

To quantify various fresh and hardened properties of the construction materials used in this research program, several tests were conducted by the researchers on the materials of interest; specifically, the compressive and splitting-tensile strength of the concrete used for the PPCPs as well as the compressive strength of the UHPC joint-fill material were verified. Additionally, the slump and plastic air content of the PPCP fresh concrete as well as the slump flow of the UHPC were also tested by others. A summary of the results of these material tests is presented herein. Detailed results can be found in Appendix B.

4.2.1. PPCP Materials Testing

The compressive and splitting tensile strengths of the concrete used to fabricate the PPCPs were determined for each panel at various ages throughout the testing program.

ASTM C39/C39M Standard Test Method for Compressive Strength of Cylindrical Concrete Specimens and ASTM C496/C496M Standard Test Method for Splitting Tensile Strength of Cylindrical Concrete Specimens were followed for the compressive strength and splitting tensile strength testing respectively.

A total of twenty 4" x 8" (102 mm x 203 mm) cylinders were cast for each panel. These cylinders were stored alongside the PPCPs until the time of testing. Early age testing of the PPCP cylinders was performed by the precaster to verify that the PPCP release strength was achieved prior to releasing the prestressing force. The remainder of the cylinders were tested by the researchers at the University of Manitoba using the cylinder testing machine shown in Figure 4-1. The summarized test results are provided in Tables 4-1 and 4-2.

Figure 4-1 – University of Manitoba Cylinder Testing Machine

Table 4-1 – Summary of PPCP Average Compressive Strength Test Results

Cylinder Age at Test (Days)	Average PPCP Compressive Strength (MPa)					
	W1	W2	C1	C2	E1	E2
7	80.1	72.9	77.7	76.1	63.3	68.8
28	71.7	82.3	75.2	74.0	81.3	75.1
419-482[1]	101.2	83.5	N/A[2]	89.6	92.8	77.0

Notes:
[1]Naming convention follows Subsection 3.2.1
[2]W1/W2 cylinders tested at 482 days; C2 cylinders tested at 476 days; E1 cylinders tested at 419 days; E2 cylinders tested at 480 days.
[3]Several C1 cylinders misplaced therefore no long-term results obtained.

Table 4-2 – Summary of PPCP Average Splitting Tensile Strength Test Results

Cylinder Age at Test (Days)	Average PPCP Splitting Tensile Strength (MPa)					
	W1	W2	C1	C2	E1	E2
14	5.3	4.7	5.4	4.6	5.7	5.1
28	5.7	6.1	5.3	4.6	5.8	4.9
419-482[1]	5.5	4.9	N/A[2]	5.0	5.4	4.8

Notes:
[1]Naming convention follows Subsection 3.2.1
[2]W1/W2 cylinders tested at 482 days; C2 cylinders tested at 476 days; E1 cylinders tested at 419 days; E2 cylinders tested at 480 days.
[3]Several C1 cylinders misplaced therefore no long-term results obtained.

4.2.2 UHPC Materials Testing

4.2.2.1 Fresh Properties

The UHPC batched for the specimens had an average static flow of 238 mm and an average dynamic flow of 248 mm measured by the UHPC supplier technical representative. Further information is provided in Appendix B.

4.2.2.2 Compressive Strength Testing

A total of twenty 3” x 6” (76 mm x 152 mm) UHPC cylinders were cast along with the joints and shear pockets for each test specimen. The cylinders were cast from the end of a

0.5 m^3 batch. As per the cylinder preparation procedure supplied by the UHPC manufacturer, the cylinders were not rodded as is conventionally done with other concrete mixes. The molds were filled and then sealed with polyethylene film. The poly covering was left in place for approximately three days after which the cylinders were demolded. The cylinders were then left in the open laboratory air to follow the same curing regime as both the specimen joints and pockets.

The UHPC cylinder ends were prepared as per *Ductal Operating Procedure 5.4 Cylinder-End Grinding (SOP-S6-04)* (Lafarge Ductal, 2015). The cylinder end preparation was performed at the Lafarge Quality Control Laboratory at 210 Dawson Road, Winnipeg, MB using a Marui & Co., Ltd. Hi-KENMA grinder. Throughout the grinding process, the appearance and levelness of the cylinder ends and the overall height of the cylinder were monitored. SOP-S6-04 required a final cylinder height of 150 mm +/- 1 mm and a levelness within 0.5° between the center of the cylinder and four random points on the cylinder end as shown in SOP-S6-04.

It should be noted that due to the nature of the material, there were large air pockets on the unmolded (top) ends of many of the cylinders varying in depth between 3 mm to 8 mm. Since the starting cylinder height was 152 mm, it was not possible to meet the cylinder height requirements of 150 mm +/- 1 mm as 3 mm to 8 mm of material had to be ground off to achieve a cylinder end free of air bubbles. In addition, it was not possible to achieve the specified 0.5° of levelness for all cylinders. While it would have been possible to continue grinding the cylinders to achieve a more level end, the overall

cylinder height would have been further reduced. A typical UHPC cylinder end is shown in Figure 4-2; large air pockets are still present even after numerous cycles of grinding.

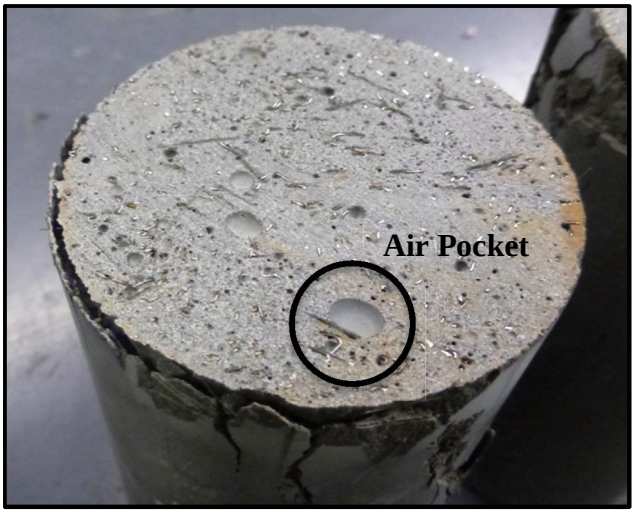

Figure 4-2 – Typical UHPC Cylinder End After Grinding (Shown After Failure)

The cylinders were tested in the cylinder testing machine at the University of Manitoba previously shown in Figure 4-1. As per the recommendation of the FHWA, ASTM C39 with a modified loading rate was followed for the compression testing (Graybeal, 2006). The cylinders were loaded at 1 MPa/s (150 psi/s) to failure. A summary of the UHPC compressive strengths is provided in Table 4-3.

Table 4-3 – Summary of UHPC Average Compressive Strength Test Results

Cylinder Age at Test (Days)	Average Compressive Strength (MPa)	
	TS1	TS2[1]
7	145	-
14	166	-
28	181	-
36	-	172
72	188	-
97	-	188
268	218	-

Notes:
[1]Due to scheduling conflicts, test results for TS2 were not obtained at regular intervals as was the case for TS1.

With the exception of several cylinders tested after 268 days, all UHPC cylinders displayed a similar failure pattern. The cylinders remained mostly intact with the failure surface splitting the cylinder from side to side. The failure surface did not typically progress through the tops or bottoms of the cylinders. This failure mode, consistent with typical failures in other fibre-reinforced concretes varies drastically from that observed in concrete without fibers. Concretes lacking fibers typically fail in an explosive fashion with an hourglass type failure surface. Figure 4-3 depicts the typical UHPC failure pattern.

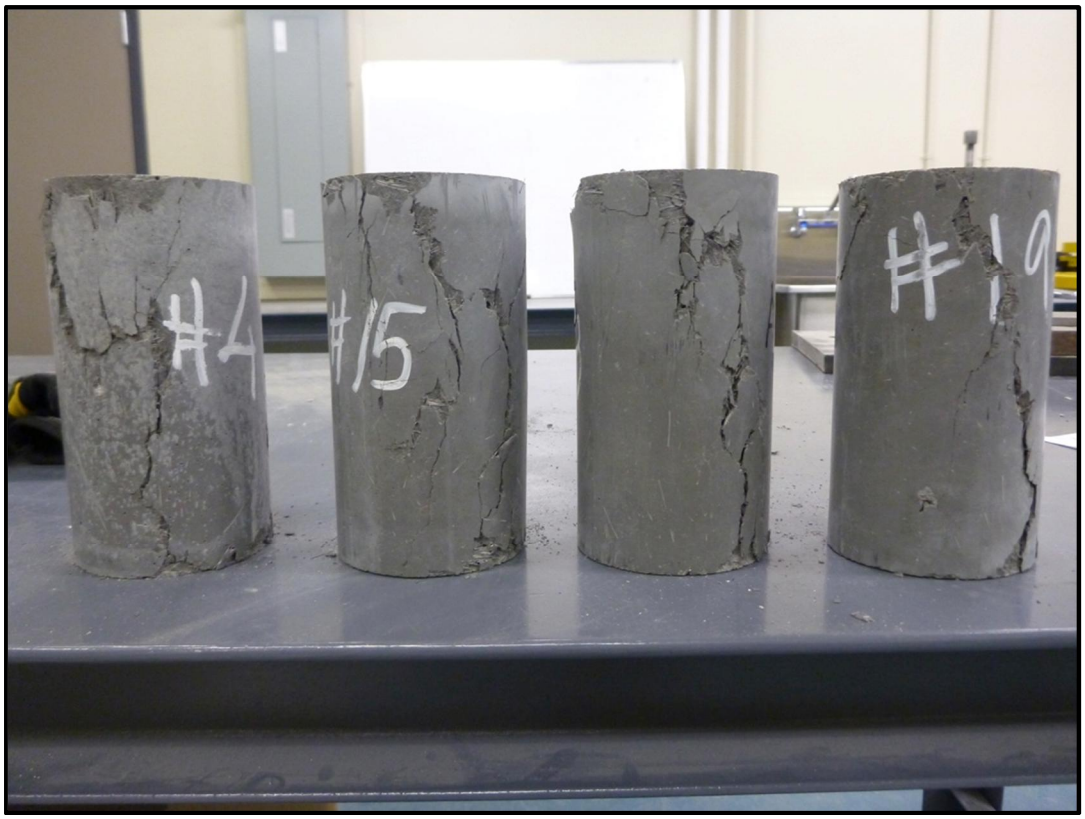

Figure 4-3 – Typical UHPC Failure Pattern

4.3 Static Test on TS1 (Test #1)

The static test to failure of Panel C1 of TS1 was the first test performed as part of this research program. Test #1 was performed on August 15, 2014. The experimental results and analysis of the data for this test is presented herein.

4.3.1 Deflection of Test Specimen #1 (Test #1)

A total of seven LVDTs were implemented above the bridge deck to monitor the deflection of the test specimen during Test #1 as shown in Figure 4-4 and schematically in Figure 4-5. The LVDTs were placed along the longitudinal centerline of TS1 at panel quarter points and within 50 mm of the UHPC joints on either side. The load-deflection curve for the LVDT placed directly above the loading location (LVDT 4) is shown in Figure 4-5. It can be seen that the load-deflection curve is essentially linear until approximately 325 kN is achieved at which point it is assumed that crack initiation occurred. For the purposes of comparison with subsequent tests, the slope of the initial tangent has been found to be approximately 220 kN/mm.

To the naked eye, cracks were not observed on the deck until 500 kN was reached, however, it is likely that cracks began forming earlier as the change in the initial tangent slope around 325 kN suggests. The irregularities in the curve between loads of 500 kN and 1200 kN are due to the pausing of the test to monitor crack growth. The loading was paused at 500, 550, 600, 700, 800, 900, 1000, 1100, and 1200 kN to allow the researchers an opportunity to mark cracks.

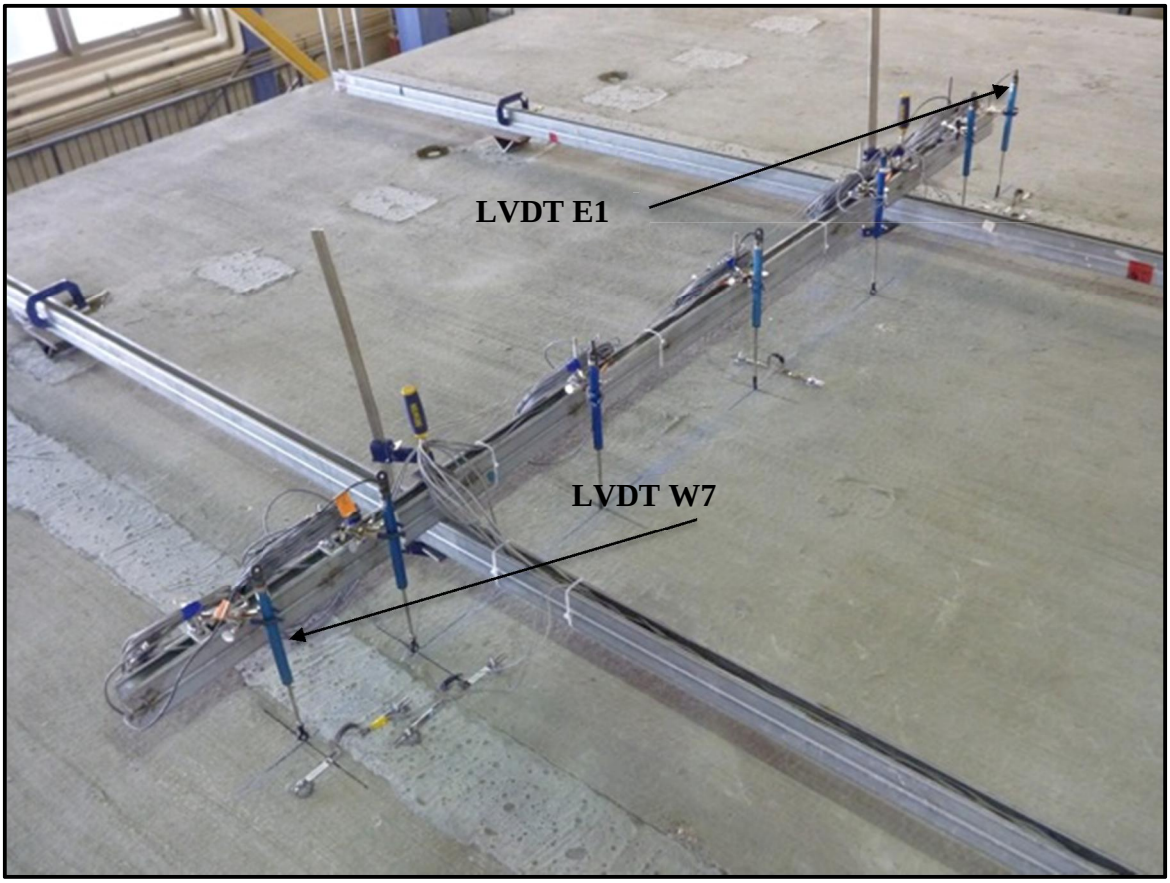

Figure 4-4 – LVDT Set-up (Test #1)

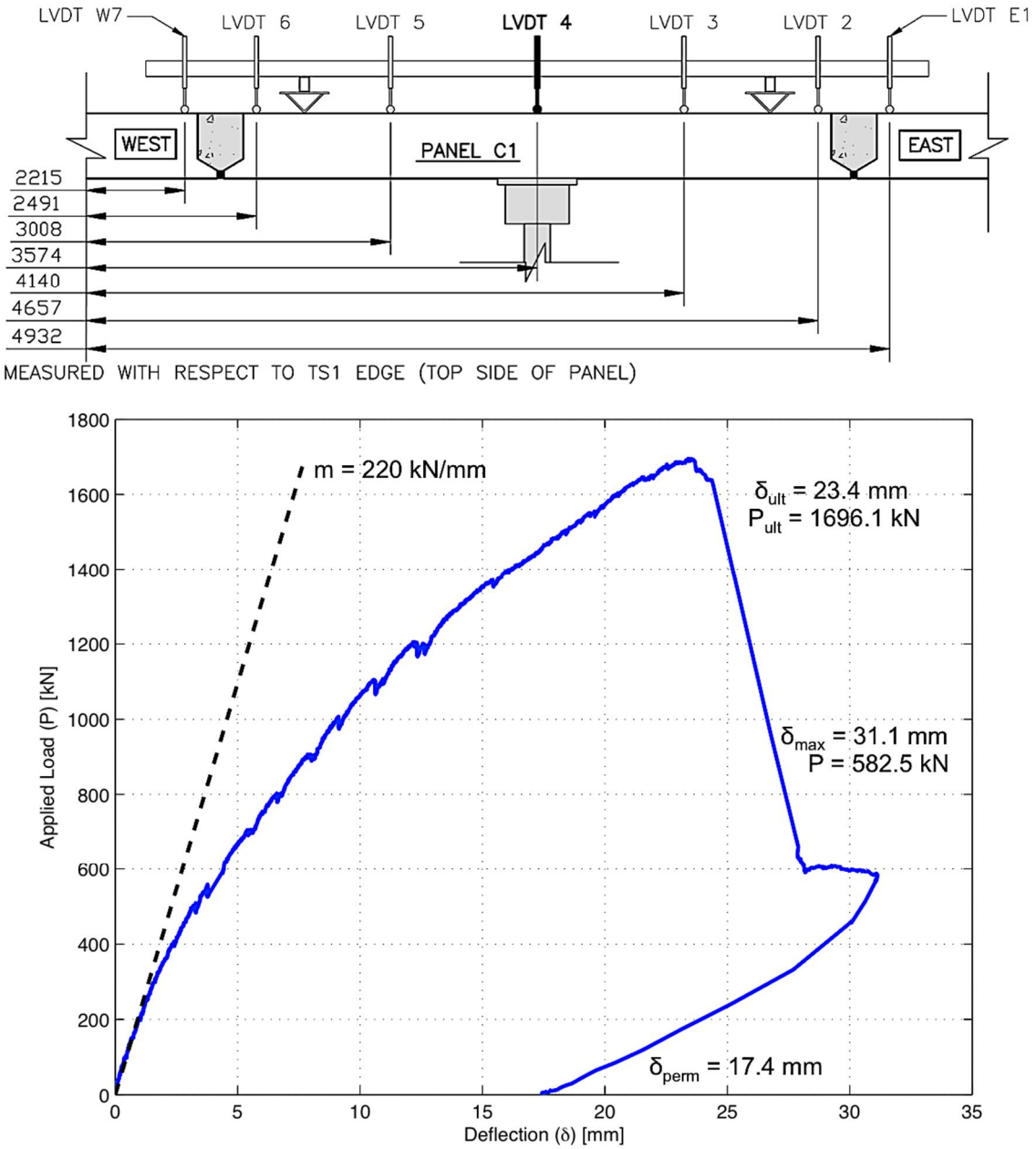

Figure 4-5 – Load-Deflection Curve for LVDT 4 (Loading Point) [Test #1]

From Figure 4-5, it can be seen that the specimen deflection begins to increase at a quicker rate nearing failure and reaches 23.4 mm (δ_{ult}) at an ultimate load of 1696.1 kN (P_{ult}). Failure was marked by a sudden and significant drop in load to approximately 600 kN. The researchers continued to load the deck but it was observed that the specimen

continued deflecting (δ_{max} = 31.1 mm) without any recovery in load carrying capacity; thus the test was terminated and the specimen was unloaded. The specimen was observed to have a permanent deflection of 17.4 mm (δ_{perm}) at the loading location. This permanent deflection corresponds to approximately 74% of the ultimate deflection.

Longitudinal deflection profiles for TS1 are shown in Figure 4-6 at 25%, 50%, 75%, and 100% of P_{ult} and after unloading to capture the permanent deflection profile corresponding to approximate loads of 424, 848, 1272, 1696 and 0 kN respectively. From this figure, it is evident that the deflections up to and including the ultimate load were essentially symmetrical about the loading point. By comparing the slopes of the deflection profiles between two adjacent LVDTs prior to failure, it is also clear that the deflection profiles across either joint were not as steep as the deflection profiles across the PPCP; this suggests that there may have been a transition in curvature across the joint. This observation is further reinforced by the strains observed in the longitudinal reinforcement inline with the loading point across the transverse joint as well as the crack formation across the PPCP and UHPC transverse joint in this location as will be further discussed.

On average, from 25% to 100% of P_{ult}, the LVDTs furthest from the load point (LVDTs E1 and W7) had deflections of 46% that of LVDT 4 (the loading point); LVDTs 2 and 6 had deflections 55% that of LVDT 4; and the closest LVDTs to the load point (LVDTs 4 and 5) had deflections of 78% that of LVDT 4. The permanent deflection profile closely resembles the general deflection trend but has a maximum permanent deflection at the

PPCP quarter point nearest the east joint; this is due to the nature of the punching shear failure in which the east end of Panel C1 appears to have been damaged more than the west end as is suggested by the ultimate crack mapping shown in Figure 4-18.

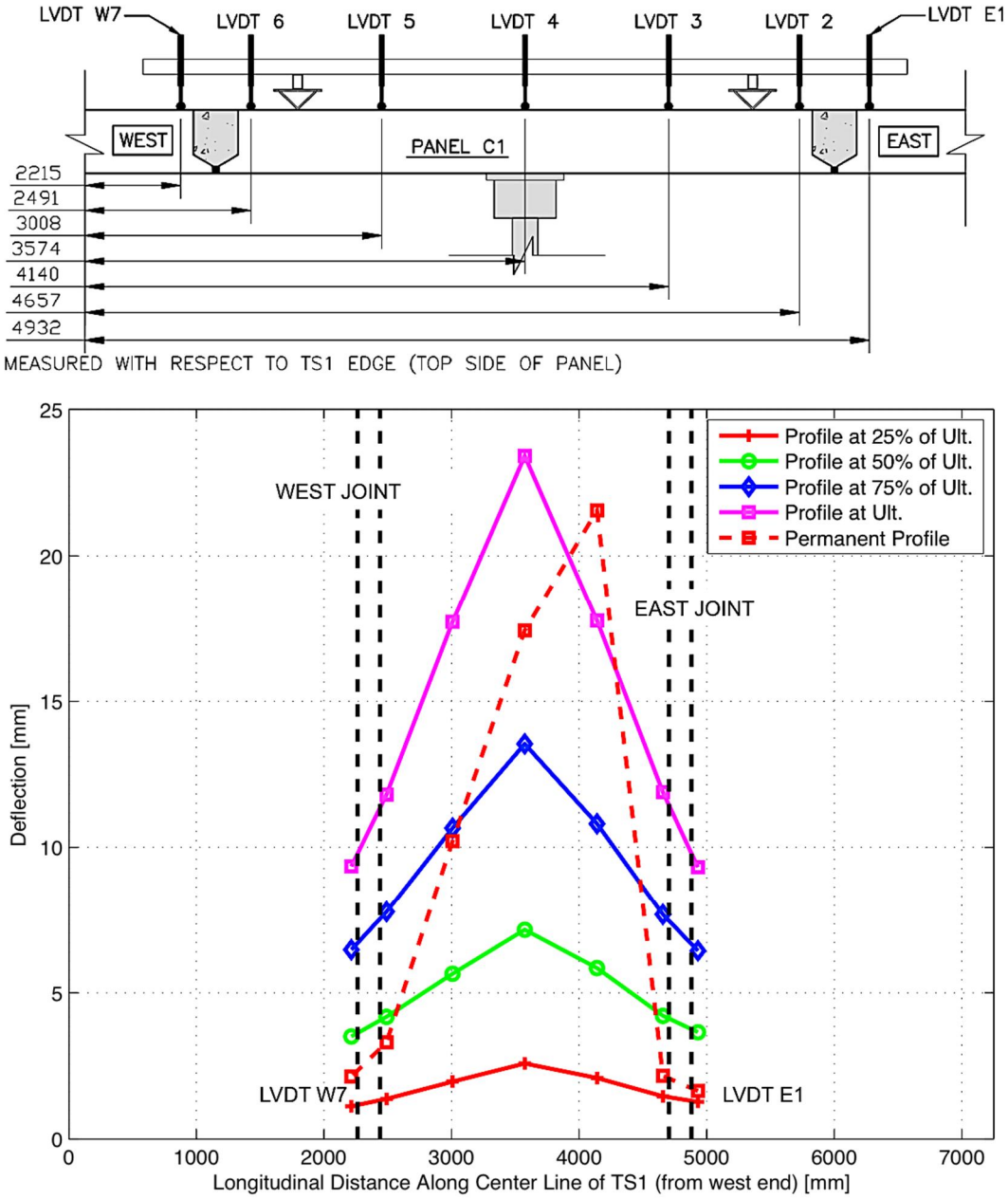

Figure 4-6 – Longitudinal Deflection Profiles (Test #1)

4.3.2 Crack Widths and Strains (Test #1)

4.3.2.1 Crack Widths

Four pi-gauges were used to monitor crack widths at locations of interest (refer to Sub-section 3.4.3.4 for details). Since the test specimens in this research program were loaded to induce negative bending, tensile stresses were expected to develop across the PPCP and UHPC transverse joint interface potentially leading to crack formation across this interface. However, as previously commented in Sub-section 4.3.1, from the deflection profiles, it appears that a point of contra-flexure occurs in the vicinity of the transverse joints inline with the loading point causing the transverse joint to develop compressive stresses across the top of the deck. Figure 4-7 and 4-8 provide the results of the pi-gauges placed across the east and west joints respectively.

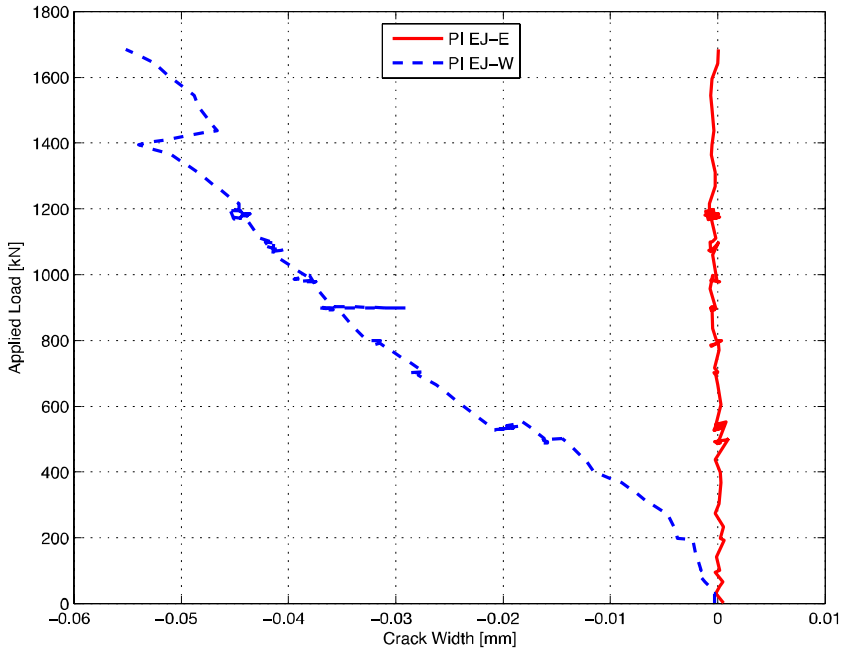

Figure 4-7 – Crack Widths Across the PPCP and UHPC Transverse Joint Interfaces in the East Joint [Test #1]

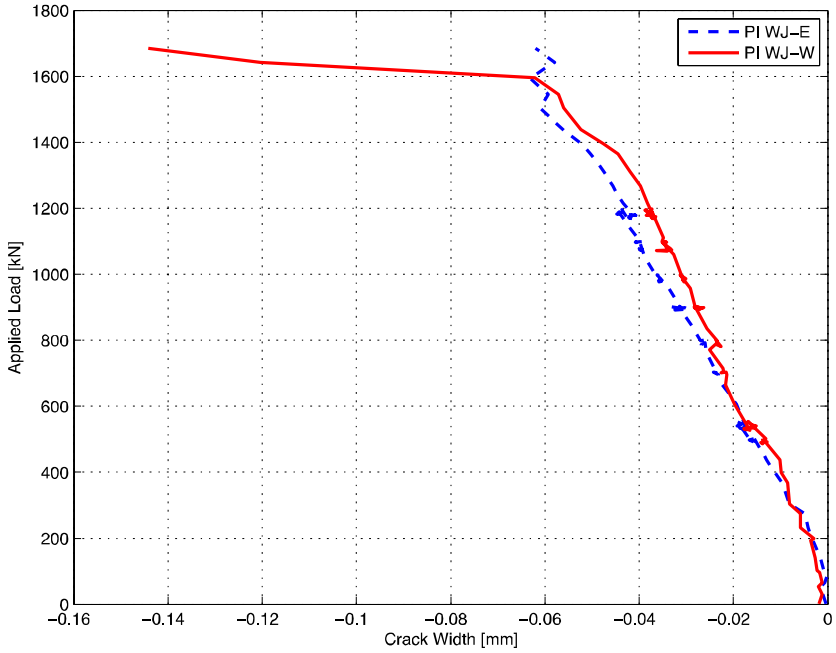

Figure 4-8 – Crack Widths Across the PPCP and UHPC Transverse Joint Interfaces in the West Joint [Test #1]

A positive crack width suggests crack growth while a negative width suggests compression in the region of the pi-gauge application. From Figure 4-7, it was originally suspected that the pi-gauge (PI EJ-E) across the east Panel E1/UHPC interface failed and did not provide meaningful data. However, the data from this gauge was compared with the corresponding gauge used in Test #4 (see Sub-section 4.6.2) and it was determined that the joint crack widths for each test were quite similar. It is unlikely that both the gauges in Test #1 and Test #4 failed; rather, it is concluded that this interface location remained intact as no cracks developed across the interface joint. In addition, it is evident that both the pi-gauges (PI EJ-W and PI WJ-E; Figures 4-7 and 4-8 respectively) on the PPCP and UHPC interfaces nearest the loading point provided similar results. Overall, there were no positive recorded crack widths confirming the possibility that a point of

contra flexure developed in the deck at the joint locations, as previously proposed in Sub-section 4.3.1, resulting in compressive stresses across the top of the joint.

There appears to be three major events seen in pi-gauge results that go hand-in-hand with the strain related results presented in Sub-section 4.3.2.2. Specifically, two spikes in pi-gauge PI EJ-W occurred at approximately 900 kN and 1400 kN (Figure 4-7) and a spike in pi-gauge PI WJ-W occurred at approximately 1600 kN (Figure 4-8). The presence of these three events in the pi-gauge results is addressed during discussion pertaining to the strains in Sub-section 4.3.2.2.

4.3.2.2 Transverse Joint Strains

Strains within the top mat of longitudinal reinforcement across the transverse joints were monitored to access the structural performance of the joint and its ability to transfer stresses from one PPCP to the next. As previously discussed in Sub-section 3.4.3.3, three locations per transverse joint were instrumented: approximately 350mm in from the girder center line on either side, and at the midspan. Figures 4-9 through 4-14 depict the typical strains across the joint at the locations depicted on the top right of each figure.

ESG E1-1 to C1-1 (Strains 350mm in from Girder Center-Lines)

The strain results for ESGs E1-1 to C1-1 are shown in Figure 4-9. This location does not follow the ideal trend observed in the west joint in which the ESG strains decreased with distance away from the loading point. This can be due to two of the events previously identified from the pi-gauge data shown in Figure 4-7. At roughly 900 kN, the strain

recorded by ESG EJ-4 increased rapidly and ended up significantly higher than the other ESGs. Furthermore, both ESG EJ-4 and PI EJ-W are along the west side of the east joint further suggesting that these two events are related. In addition, at roughly 1400 kN, the strain recorded by ESG E1-1 also increased rapidly. It is suspected that cracks may have formed or rapidly widened at these load levels causing a quick increase in strain recorded by these two gauges. Overall the magnitude of the strains recorded for both the east joint locations are very similar.

ESG E1-3 to C1-3 (Strains 350mm in from Girder Center-Lines)

The strain results for ESGs E1-3 to C1-3 are shown in Figure 4-10. Similar to the strain profile from ESG E1-1 to C1-1, there does not appear to be a trend between the observed strain and the distance from the loading point as was observed for the west joint. ESG C1-3 appeared to be reading strain prior to any loading being applied suggesting that the gauge was not properly zeroed or that it may have been defective or improperly applied. In addition, the strain recorded by ESG EJ-6 rapidly increased at approximately 1400 kN which corresponds to the applied load at which point an event was noticed in the pi-gauge results shown in Figure 4-8. Overall, both locations on the east joint have more irregular results than those for the west joint, however this may be explained by the extensive cracking that occurred in the vicinity. Despite the lack of a trend similar to that seen in the west joint, the magnitude of the recorded strains for both the east joint locations are very similar.

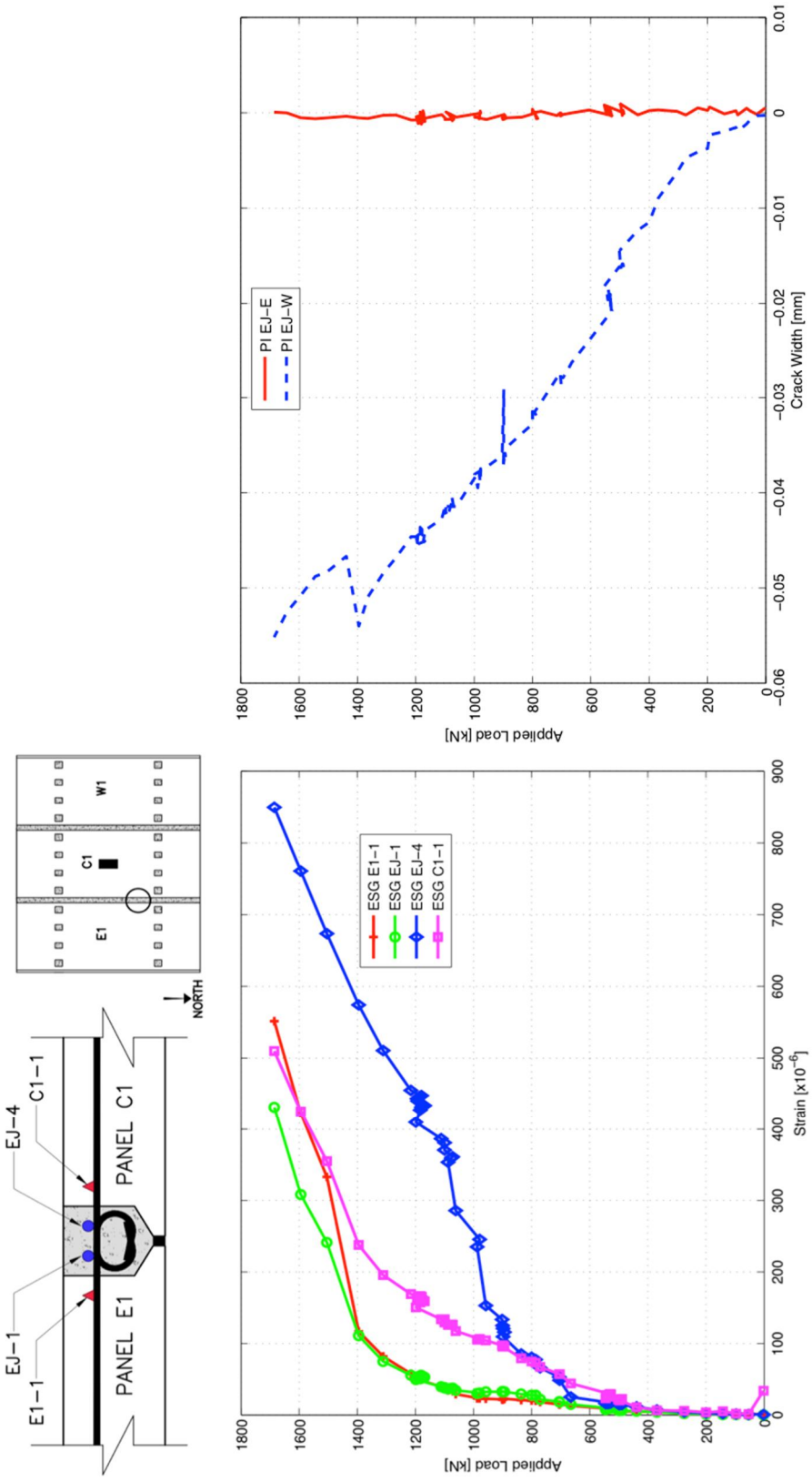

Figure 4-9 – Strains Across East Joint from ESG E1-1 to C1-1 [Test #1]

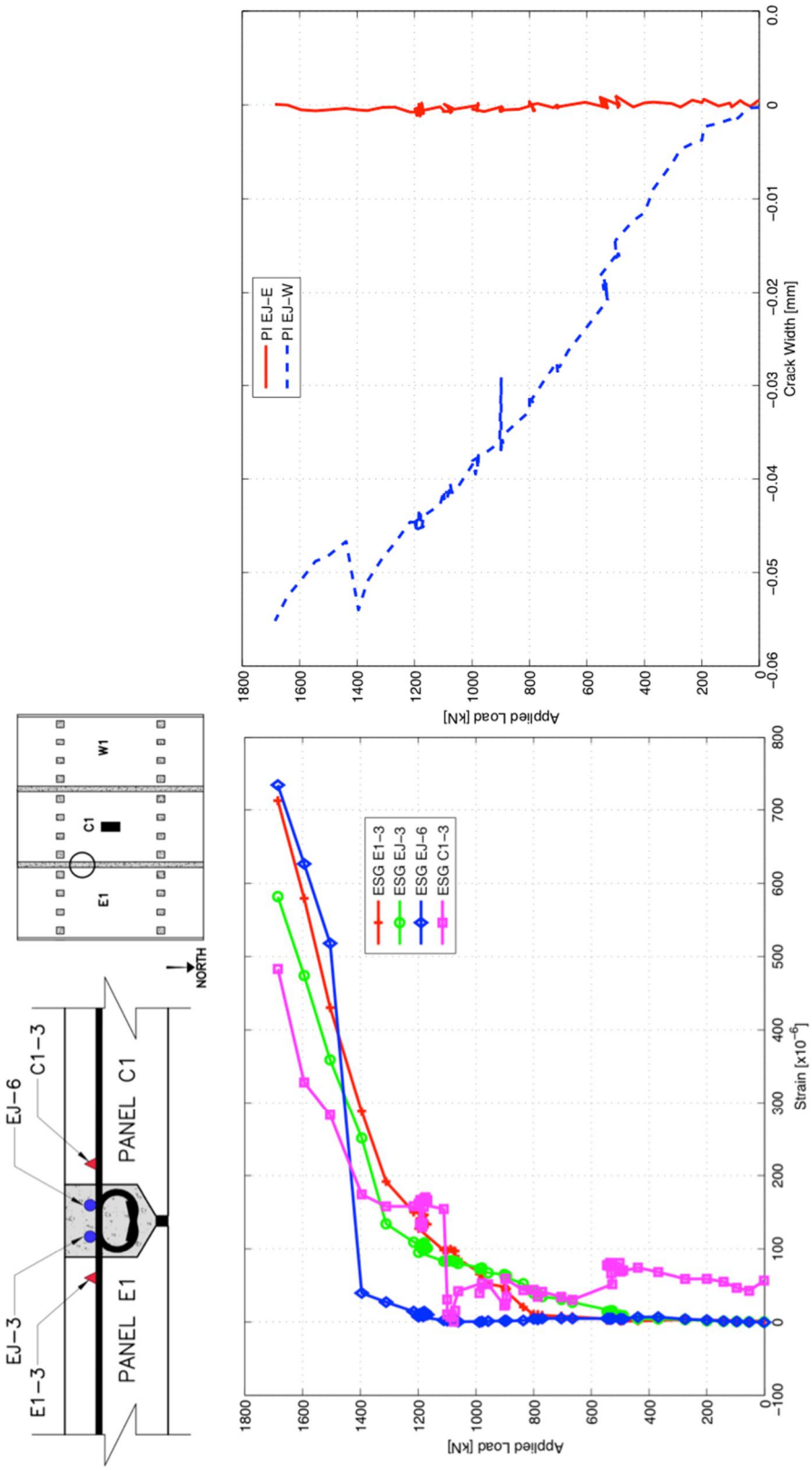

Figure 4-10 – Strains Across East Joint from ESG E1-3 to C1-3 [Test #1]

ESG C1-4 to W1-1 (Strains 350mm in from Girder Center-Lines)

The strain results for ESGs C1-4 to W1-1 are shown in Figure 4-11. Unlike the locations monitored along the east joint, both west joint locations have strains at failure that decrease with increasing distance away from the loading point as can be reasonable expected in a perfect system. Aside from ESG C1-4, which appears to have been damaged, the recorded strains are fairly minimal until approximately 1000 kN suggesting a lack of cracking in the vicinity before this point. Between 1000 kN and the ultimate load, the longitudinal bars began to strain with the most strain occurring in the bar closest to the loading point (ESG WJ-1) and vice-versa. Notwithstanding ESG C1-4, this location exhibited the most ideal strain plot. It should be noted that this location also had the least cracks in the vicinity as can be seen in Figure 4-18. Overall the magnitude of the recorded strains for both the west joint locations are very similar.

ESG C1-6 to W1-3 (Strains 350mm in from Girder Center-Lines)

The strain results for ESGs C1-6 to W1-3 are shown in Figure 4-12. Similar to ESGs C1-1 to W1-4, this location had strains at failure decreasing with increasing distance from the loading point. It should be noted that this trend does not hold true throughout the entire load range however; this may be due to the increased presence of cracks in the area possibly engaging the bars at different points during the test. Recorded strains are again minimal until approximately 1100 kN after which they begin to increase rapidly until failure. Overall the magnitude of the recorded strains for both the west joint locations are very similar.

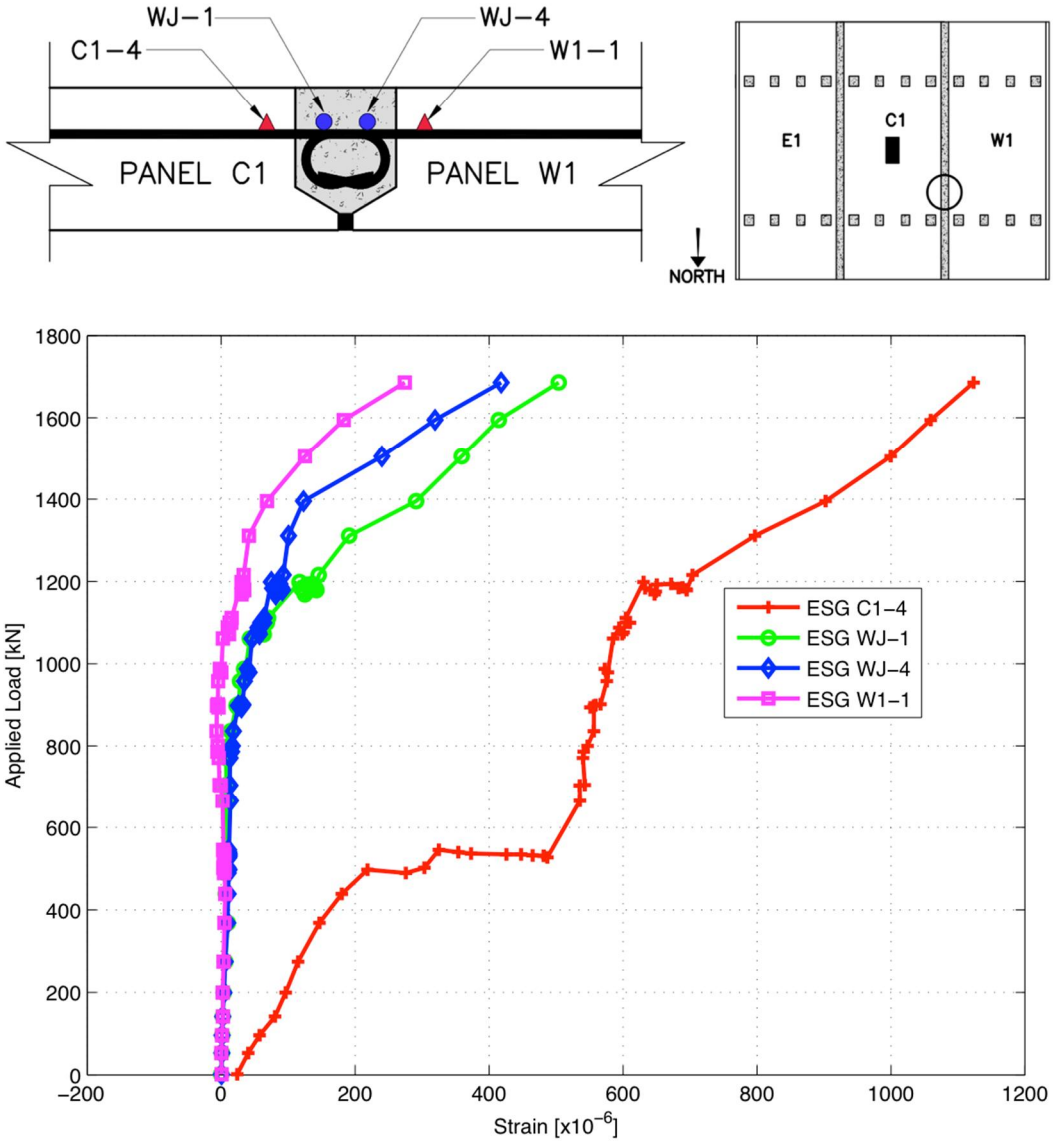

Figure 4-11 – Strains Across West Joint from ESG C1-4 to W1-1 [Test #1]

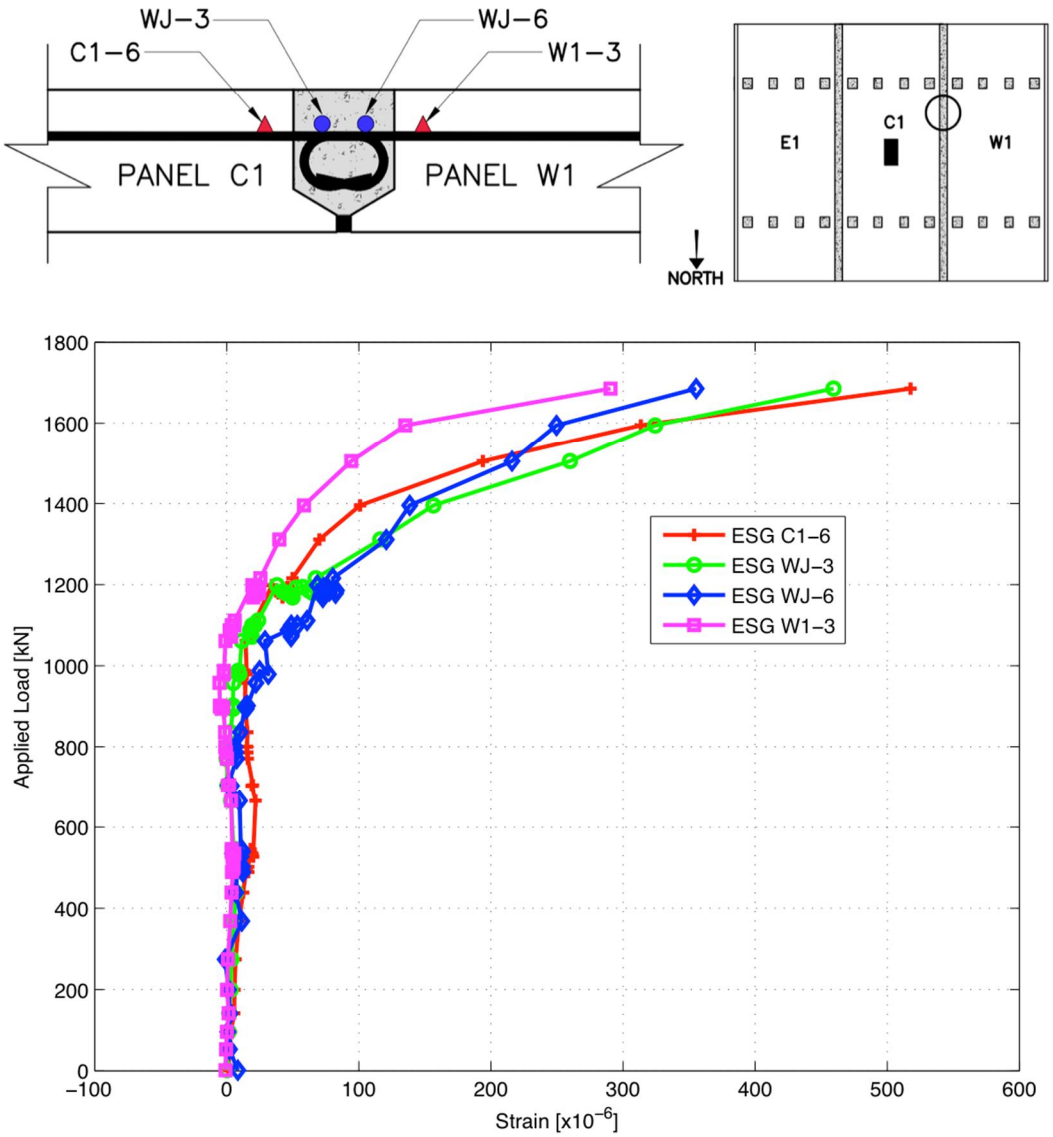

Figure 4-12 – Strains Across West Joint from ESG C1-6 to W1-3 [Test #1]

ESG E1-2 to C1-2 (Strains at Midspan)

The strain results for ESGs E1-2 to C1-2 are shown in Figure 4-13. Unlike the strains shown for the locations nearest the girders (Figures 4-9 to 4-12), the strains across the transverse joint longitudinally in line with the applied load are fundamentally different. The top reinforcement across the joint initially experiences compressive strains which continue to increase until a load of approximately 1400 kN. This trend agrees with the pi-gauge data for the east joint (Figure 4-7) which suggested that the joint appeared to be under compressive strains as it was likely in a point of inflection as previously discussed (Figure 4-6). At this point, the strain readings from the ESGs on the longitudinal bar furthest from the applied load (ESGs E1-2 and EJ-2) suddenly transition to tensile strains. This correlates with the event occurring at approximately 1400 kN in the pi gauge data for the east joint.

It is suspected that cracks may have initiated along the PPCP and UHPC joint interface furthest away from the loading point inducing tension in ESGs E1-2 and EJ-2. While the crack mapping revealed minimal cracking of the UHPC joint fill material overall, any cracks that were observed were of a very small width and barely visible to the naked eye. In addition, the finishing of the UHPC joint at the interface did not easily allow for identification of the interface and in some instances, it appears as if the vertical interface has been slightly covered by UHPC. Therefore, it is likely that interface cracks may have developed that went unseen to the researchers during testing.

ESG C1-5 to W1-2 (Strains at Midspan)

The strain results for ESGs C1-5 to W1-2 are shown in Figure 4-14. The strains at this location behaved very similarly to that across the east joint in line with the loading point. All gauges initially read compressive strains before the two gauges furthest away from the loading point rapidly transitioned to tensile strains at approximately 1600 kN. Once again, this transition point corresponds to the event observed in the pi-gauge data for the west joint (Figure 4-8). As with the same location on the east joint, it is believed that interface cracking may have intercepted the instrumented longitudinal bar inducing tensile strains near failure. It should be noted that the tensile strains measured in line with the loading point across both the east and west joints near failure are of a similar magnitude to that recorded in the other joint locations.

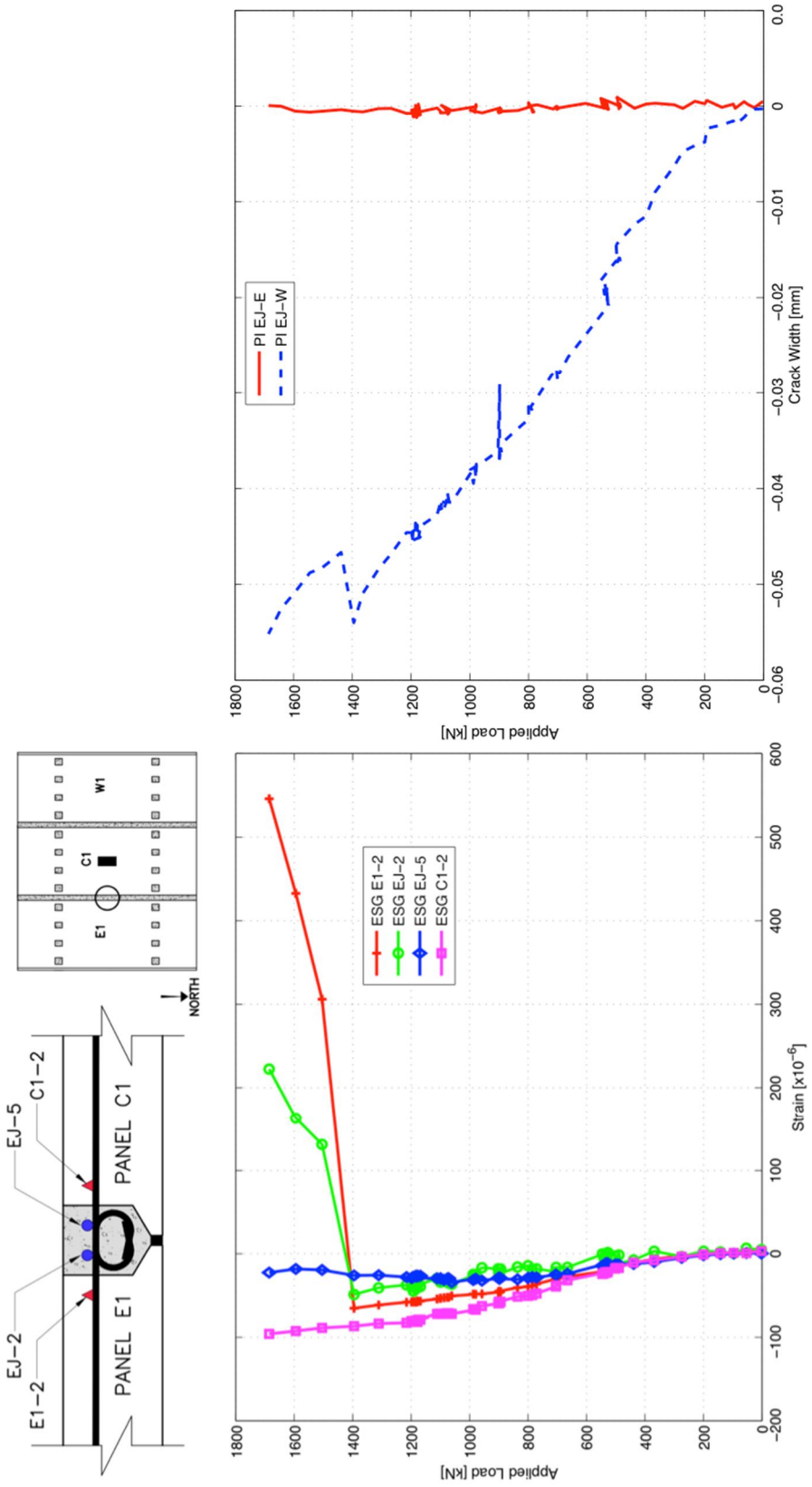

Figure 4-13 – Strains Across West Joint from ESG C1-2 to E1-2 [Test #1]

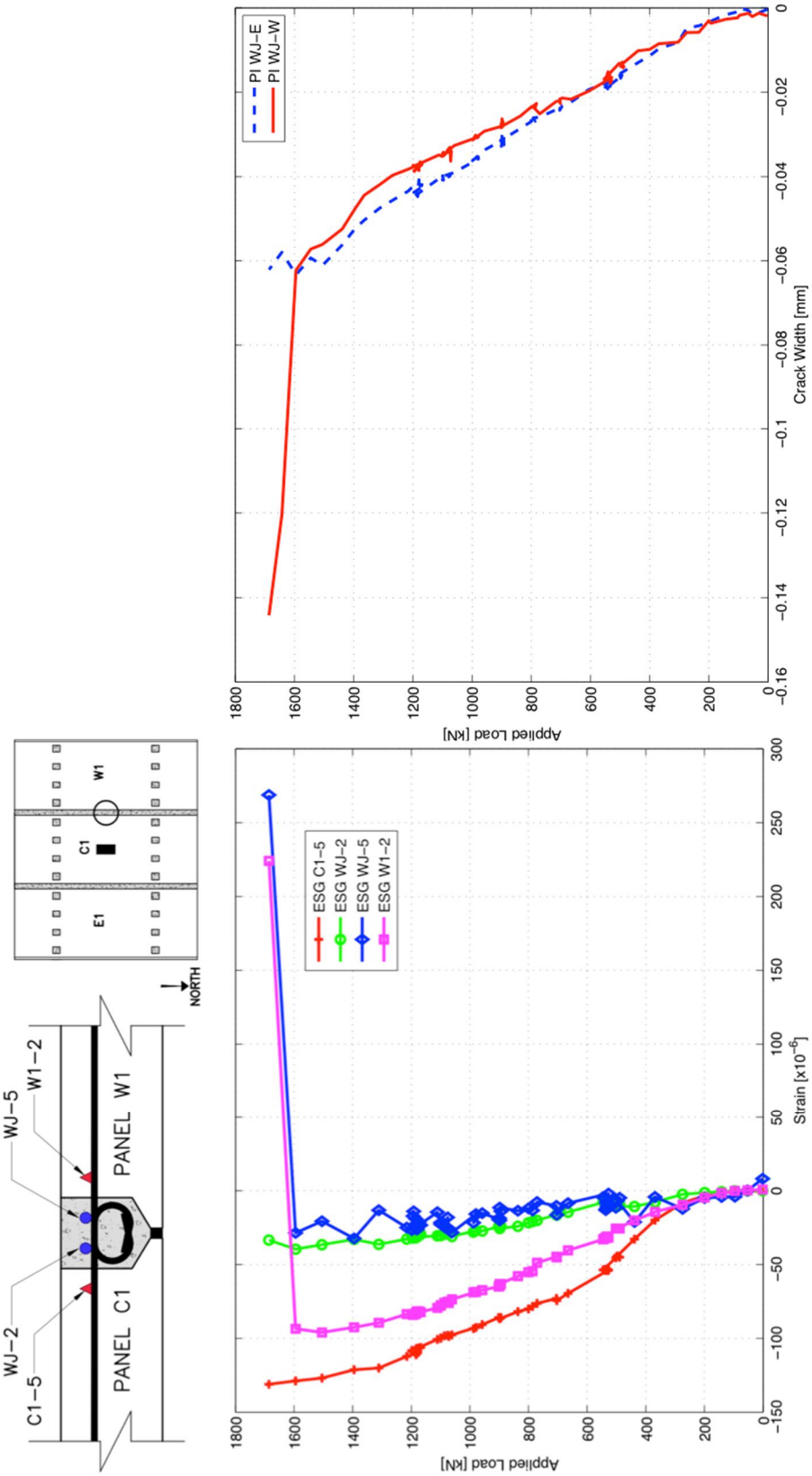

Figure 4-14 – Strains Across West Joint from ESG C1-5 to W1-2 [Test #1]

4.3.2.3 Crack Progression and Mapping

Cracks were mapped by the researchers at the onset of cracking (visually observed to occur at 500 kN), 550, 600, 700, 800, 900, 1000, 1100, 1200 kN and post failure. Cracks were not mapped past 1200 kN during the test due to safety reasons. The visual crack mapping results are presented herein. Figures 4-15 to 4-17 depict the progression of crack formation from 500 kN to 1200 kN.

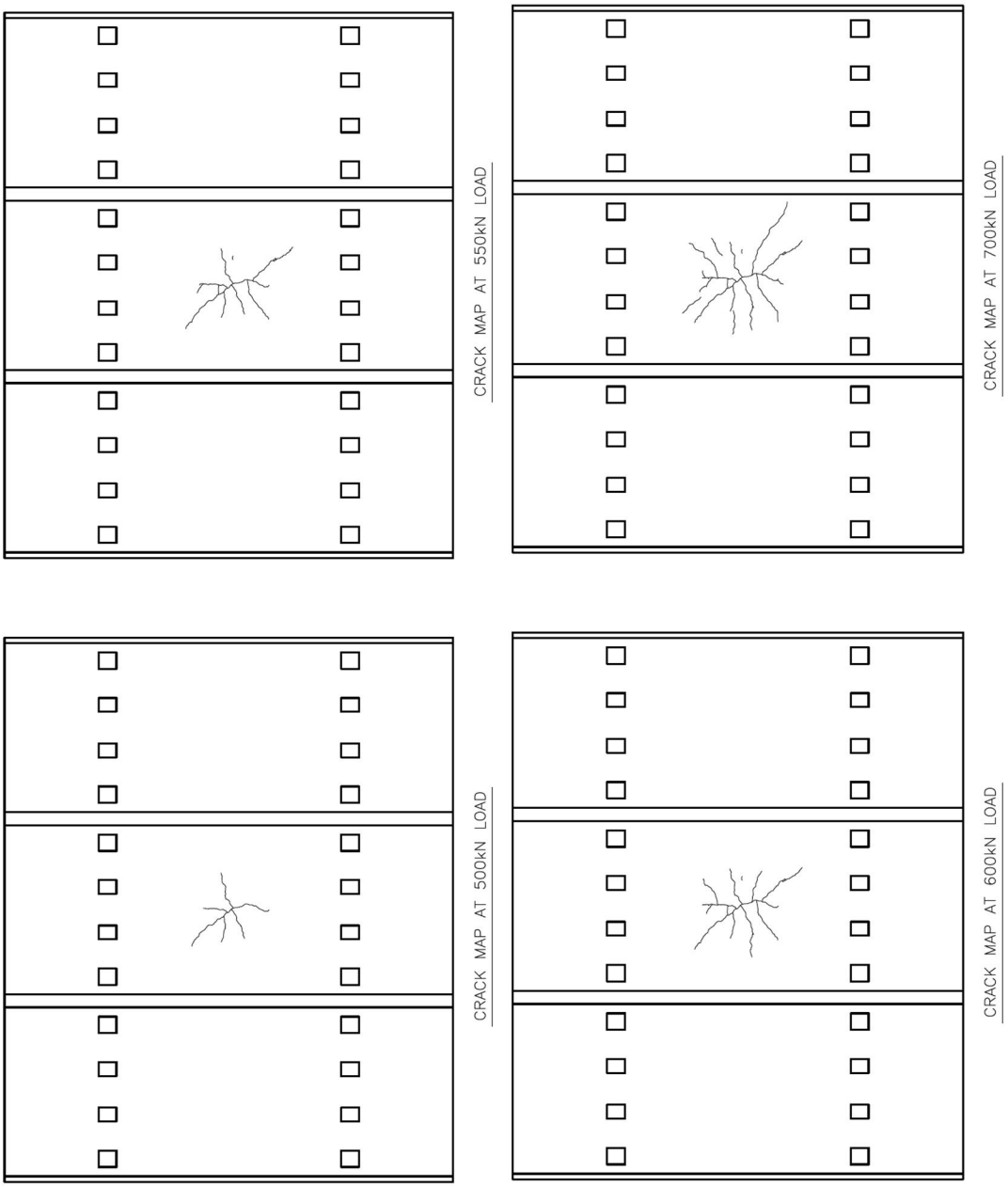

Figure 4-15 – Crack Progression from 500 kN to 700 kN (Test #1)

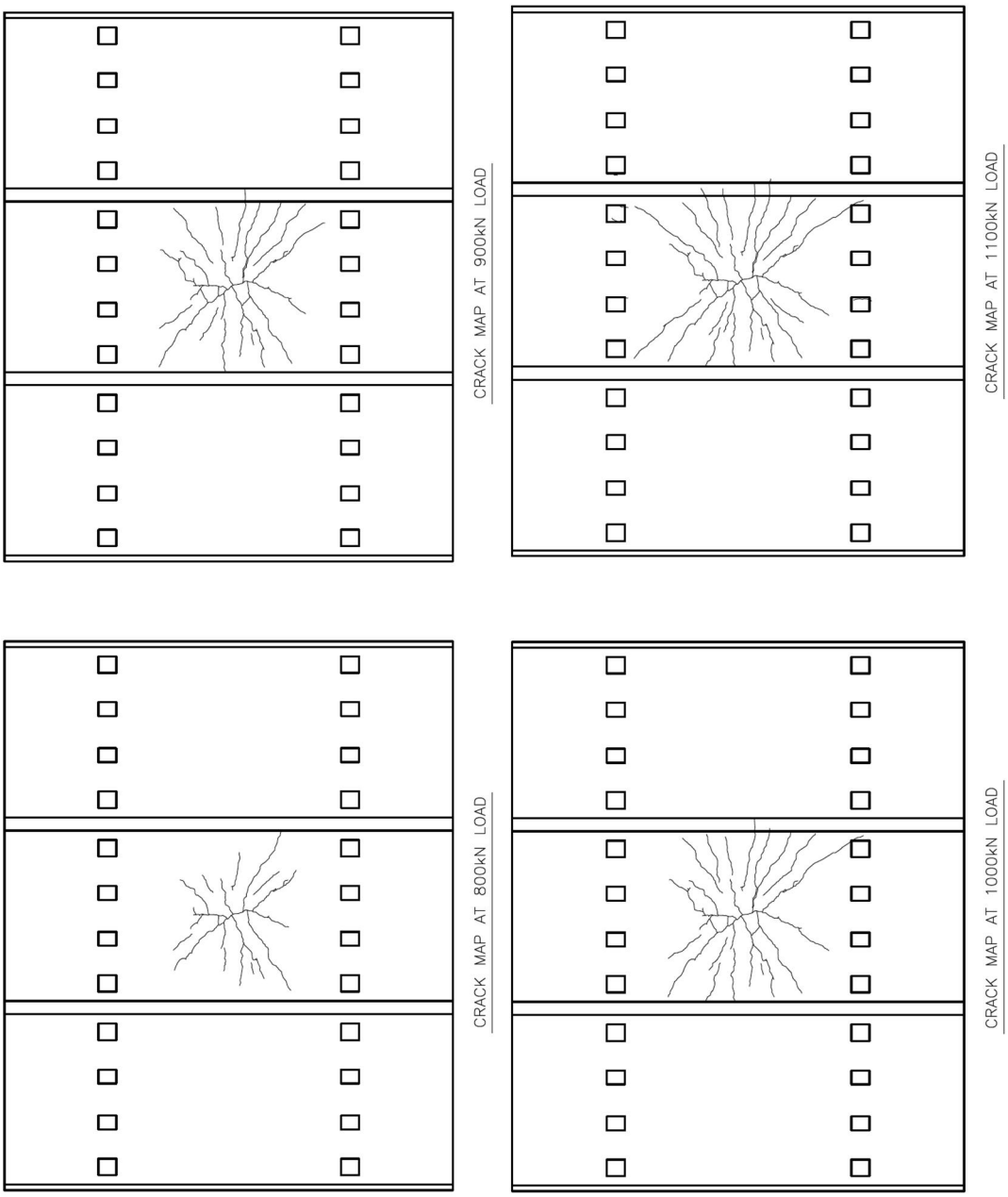

Figure 4-16 – Crack Progression from 800 kN to 1100 kN (Test #1)

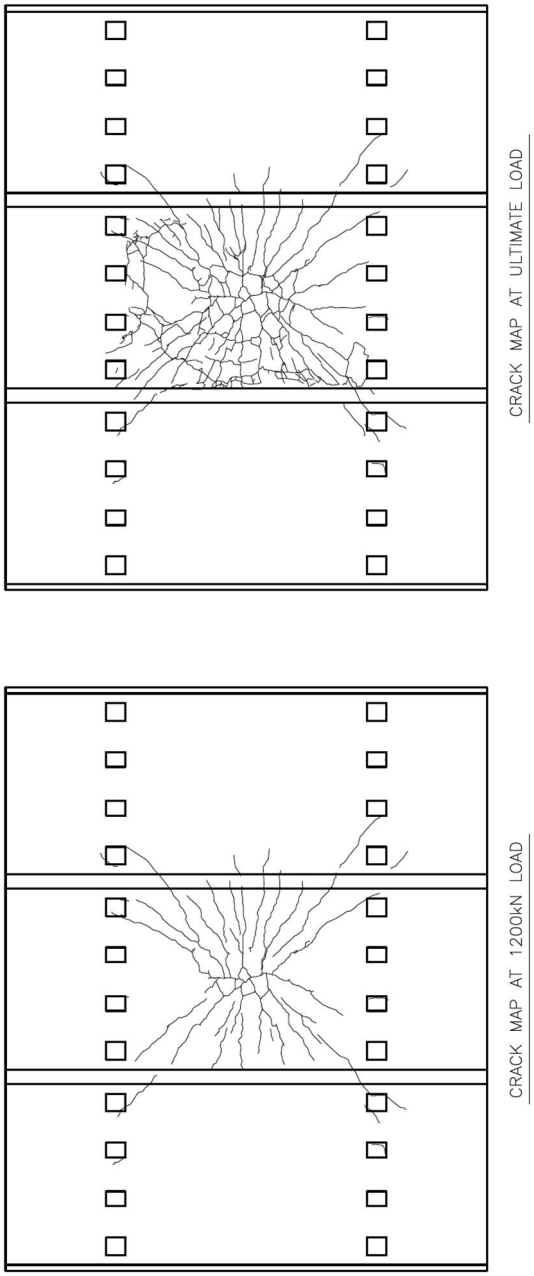

Figure 4-17 – Crack Progression from 1200 kN to Failure (Test #1)

Following unloading of the deck after the completion of Test #1, the specimen was once again minimally loaded to force existing cracks to slightly open allowing a crack map post failure to be obtained. The post failure crack map is shown in Figure 4-18.

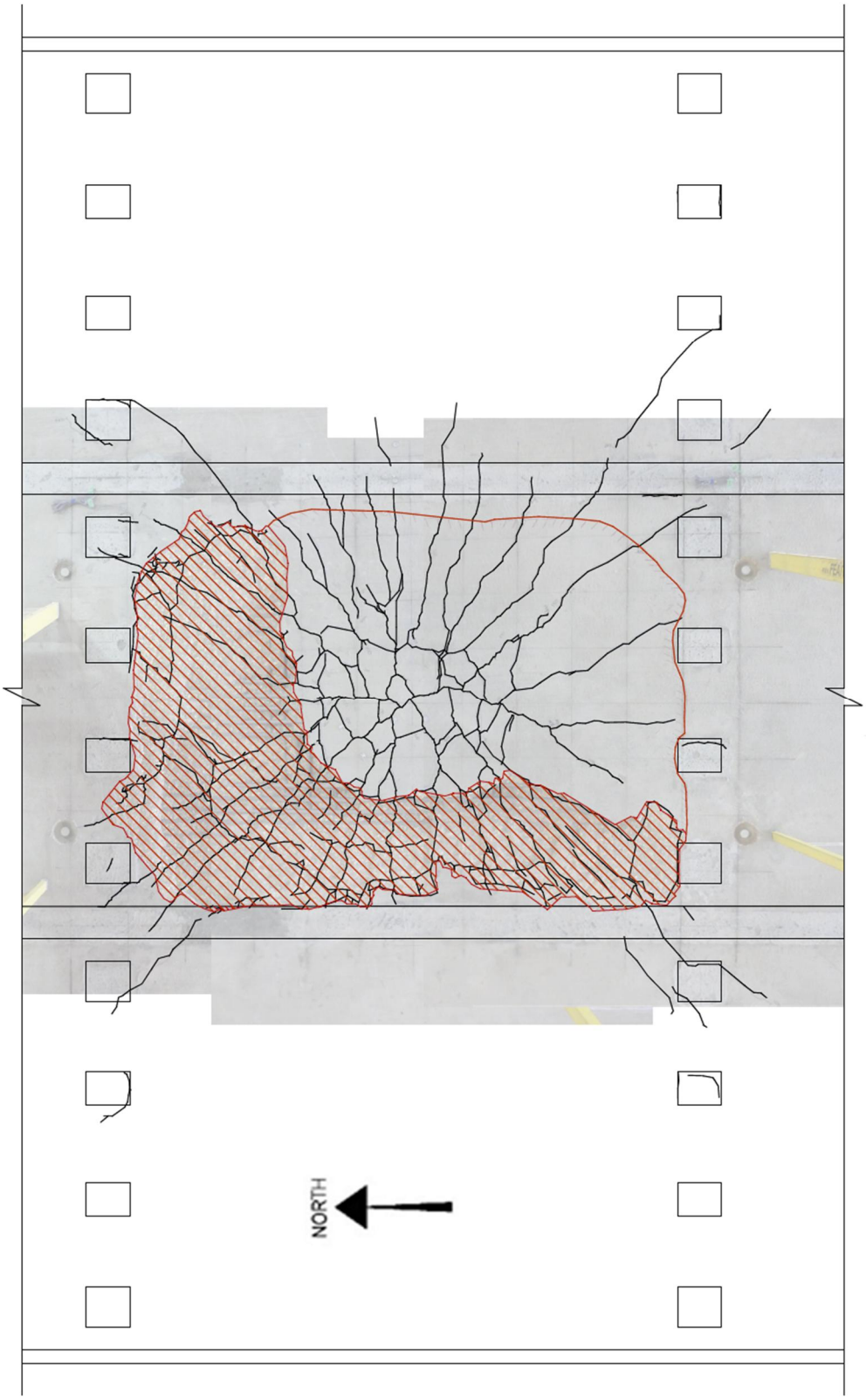

Figure 4-18 – Crack Mapping at Failure (Test #1)

It should be noted that the entire portion of the deck contained within the red boundary in Figure 4-18 is no longer intact due to delamination caused by punching shear. The hatched portion of the deck represents delaminated concrete that was easily removed by hand effectively exposing the reinforcing steel within; the non-hatched portion of the deck is delaminated concrete held in place by the reinforcing steel (identified by finding the limits of the hollow sounding concrete when hit with a ballpeen hammer). Overall, this crack pattern is very typical of a punching shear failure for a traditional CIP deck.

4.4 Fatigue Test on TS1 – West Joint (Test #2)

The second test performed as part of this research program was the cyclic fatigue testing of Panel W1 (TS1) along the west transverse joint between October 8 and October 30, 2014. Test #2 consisted of approximately 575,000 fatigue cycles and was mainly performed by the researchers to ensure the adequacy of the test setup and instrumentation system. Since TS1 was previously failed during Test #1 with cracks extending through the west transverse joint, the effect of the Test #1 failure and cracking on the results of Test #2 are difficult to determine; therefore, the experimental results will not be discussed in detail and it is important to note that the results provided herein may have been affected by the failure of TS1 during Test #1. The loading scheme for Test #2 followed that presented in Sub-section 3.3.

4.4.1 Deflection of Test Specimen #1 (Test #2)

A total of six LVDTs were implemented above the bridge deck to monitor the deflection of the test specimen during Test #2 as shown in Figure 4-19 and schematically in Figure

4-20. The LVDTs were placed along the longitudinal centerline of TS1 at panel quarter points and within 50 mm of the UHPC joints on either side. The load-deflection curves at log cycles (1, 10, 100, 1000 cycles…) and at the final cycle (574,854) for the LVDT placed directly above the loading point (LVDT 4) are shown in Figure 4-20.

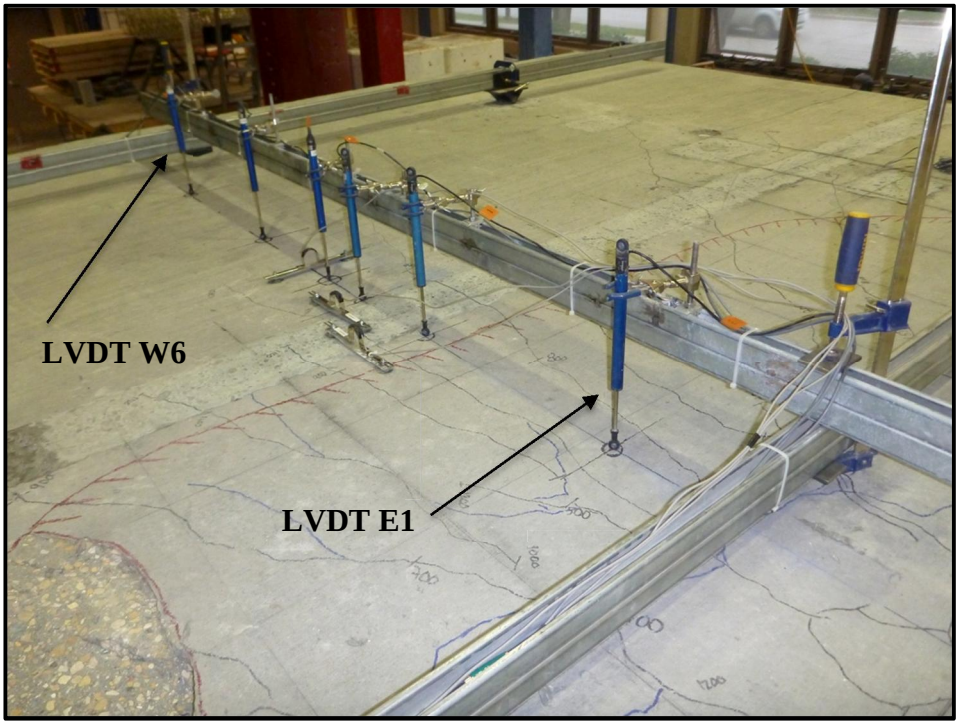

Figure 4-19 – LVDT Set-up (Test #2)

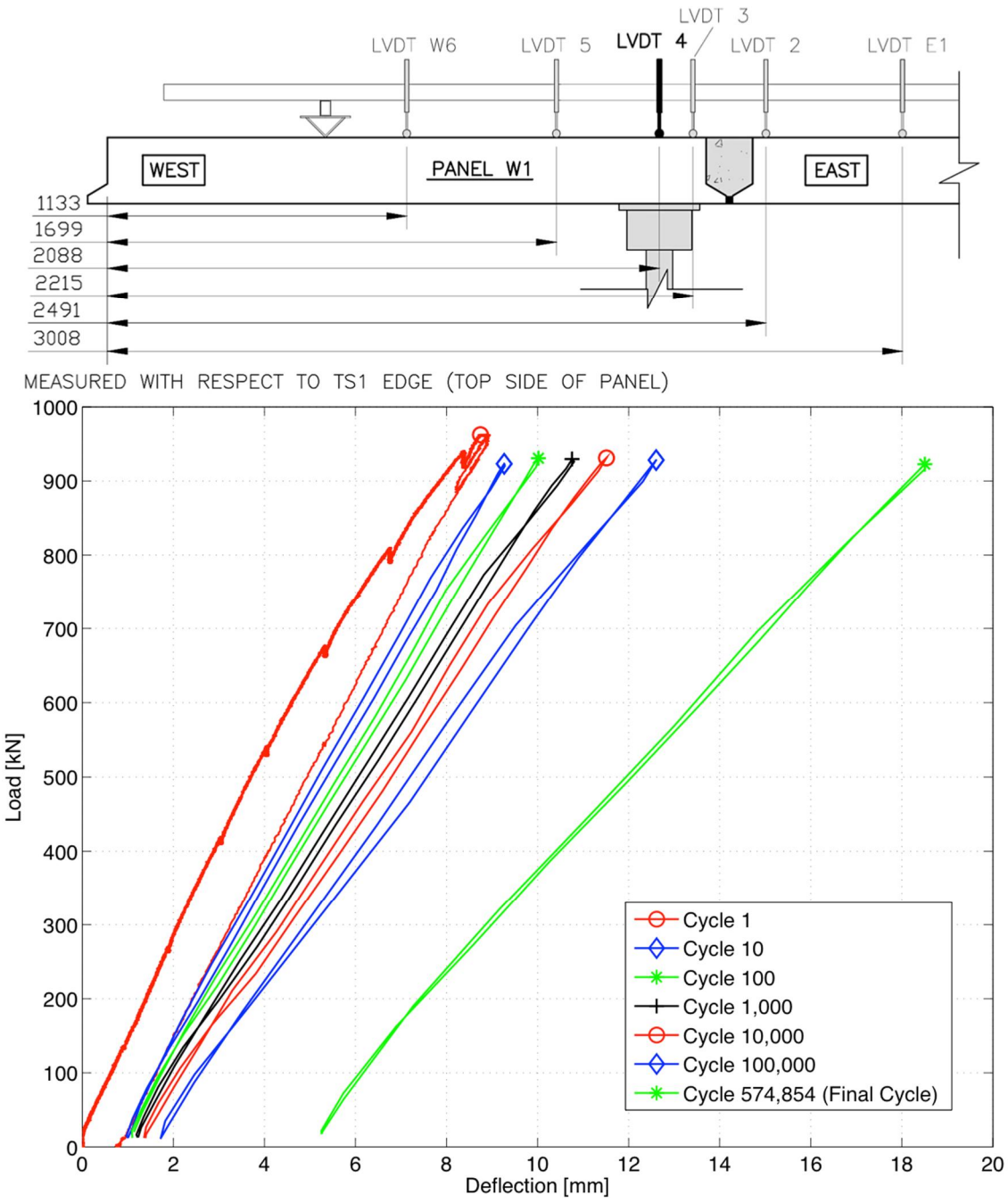

Figure 4-20 – Load-Deflection Curves at Log Number Cycles for LVDT 4 (Loading Point) [Test #2]

Two important characteristics of the system can be observed in Figure 4-20, namely: the specimen's stiffness degradation in fatigue and the energy absorption of the system providing an indication of its current stage in the overall fatigue life.

It can be seen that the area within the first cycle loop is substantially greater than for the subsequent cycles; this area relates to the irreversible energy absorbed by the system through crack formation. Since cracks are mainly formed during the first cycle, subsequent cycles have much less area under the loops as the system stabilizes and minimal energy is absorbed by crack propagation. Typically, as the system approaches failure, the slope of the load-deflection curve will begin decreasing rapidly and the area under the loops will begin increasing drastically as substantial energy is absorbed for crack propagation and ultimately failure. Due to the minor change in load-deflection curve slope as well as the minimal area under the cyclic loop, it can be concluded that this specimen was far from failure at the time the test was terminated.

4.4.2 TS1 Shear Stud Failure (Test #2)

Once the researchers were satisfied that the proposed test method and set-up performed adequately, Test #2 was stopped and the specimen was demolished and removed from the lab. During the demolition, damage to the shear studs resulting from the fatigue test was observed in the two full-depth pockets along either girder closest to the west joint in panel W1. Figures 4-21 depicts undamaged shear studs from a pocket far from the loading point while Figures 4-22 and 4-23 depict the damaged shear studs from the pocket inline with the loading point. It should be noted that these pictures are after removal of the deck panels by cutting along the haunch with a concrete saw. Due to the conical depression in the top girder flange, shown clearly in Figure 4-23, it appears as though the shear studs failed due to fatigue along the girder flange and weld material interface.

Figure 4-21 – Undamaged Shear Stud Cluster Far From Loading Point (Test #2)

Figure 4-22 – Damaged Shear Studs In-Line with Loading Point (Test #2)

Figure 4-23 – Close-up of Damaged Shear Stud Weld (Test #2)

Upon discovery of the shear stud failures, the researchers opted to instrument a number of shear studs with ESGs to monitor their behaviour and to try to pinpoint instances and reasons for failure. The instrumentation of the shear studs was previously discussed in Sub-section 3.4.3.3. Further discussion of the shear stud failures is provided in during discussion of Test #3 results in Sub-section 4.5.4.

4.5 Fatigue Test on TS2 – West Joint (Test #3)

The third test performed as part of this research program was the cyclic fatigue testing of Panel W2 (TS2) along the west transverse joint between March 3 and April 7, 2015. Test #3 consisted of 1,219,620 fatigue cycles prior to failure of the shear stud clusters in Panel W2 and subsequent lifting of Panel W2 off the girder. The experimental results for Test #3 are presented in the following subsections.

4.5.1 Deflection of Test Specimen #2 (Test #3)

A total of six LVDTs were implemented above the bridge deck, in a similar manner to that used for Test #2 (Figure 4-19), to monitor the deflection of the test specimen during Test #2. The LVDT layout is shown schematically in Figure 4-24. The LVDTs were placed along the longitudinal centerline of TS2 at panel quarter points and within 50 mm of the UHPC joints on either side. The load-deflection curves at log cycles (1, 10, 100, 1000… cycles) and at the final cycle (1,219,620) for the LVDT placed directly above the loading point (LVDT 4) are shown in Figure 4-24.

Similarly to Test #2, it can be seen that the area within the first cycle loop is substantially greater than for the subsequent cycles. While the slopes of the curves do decrease throughout the test, the reduction in stiffness is very minor. Due to the fact that the area within the final curve at failure is minimal and the overall system stiffness is minimally reduced from Cycle 1, it can be concluded that the system did not go through its true fatigue life to fatigue failure. Rather, as will be described in Sub-section 4.5.3, the system failed prematurely due to the fatigue failure of the shear studs within the shear pockets. This resulted in Panel W2 being lifted up and off the girders prompting the researchers to stop the test. Unfortunately, it is not possible to determine or even simply approximate how many cycles the system would have gone through before reaching a true fatigue failure of the panel or joint.

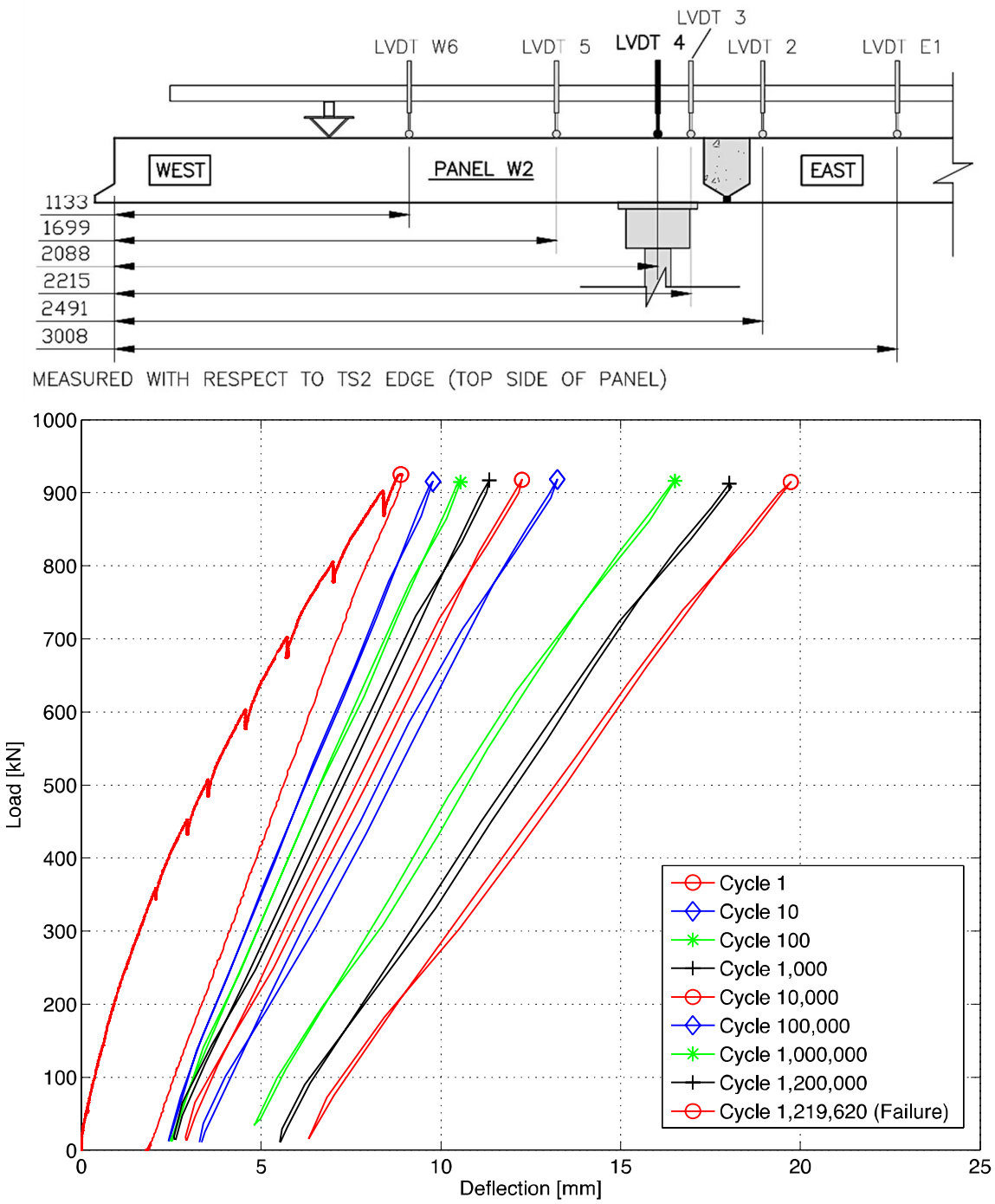

Figure 4-24 – Load-Deflection Curves at Log Number Cycles for LVDT 4 (Loading Point) [Test #3]

4.5.2 Crack Widths and Strains of Test Specimen #2 (Test #3)

4.5.2.1 Crack Widths

Two pi-gauges were used to monitor crack widths at locations of interest, namely across the PPCP/UHPC interface at the west and east sides of the west transverse joint. The maximum recorded crack widths plotted every ten thousand cycles is shown in Figure 4-25. It can be seen that the pi-gauge closer to the loading point (PI WJ-W) recorded a significantly higher crack width during the first cycle compared to PI WJ-E. Both gauges show that crack widths began increasing rapidly towards failure of the system as the studs fatigued and broke, eliminating structural fixity of the panel to the girders. Ultimate crack widths at failure were approximately 0.76 mm and 0.35 mm for the west and east interfaces of the west transverse joint respectably.

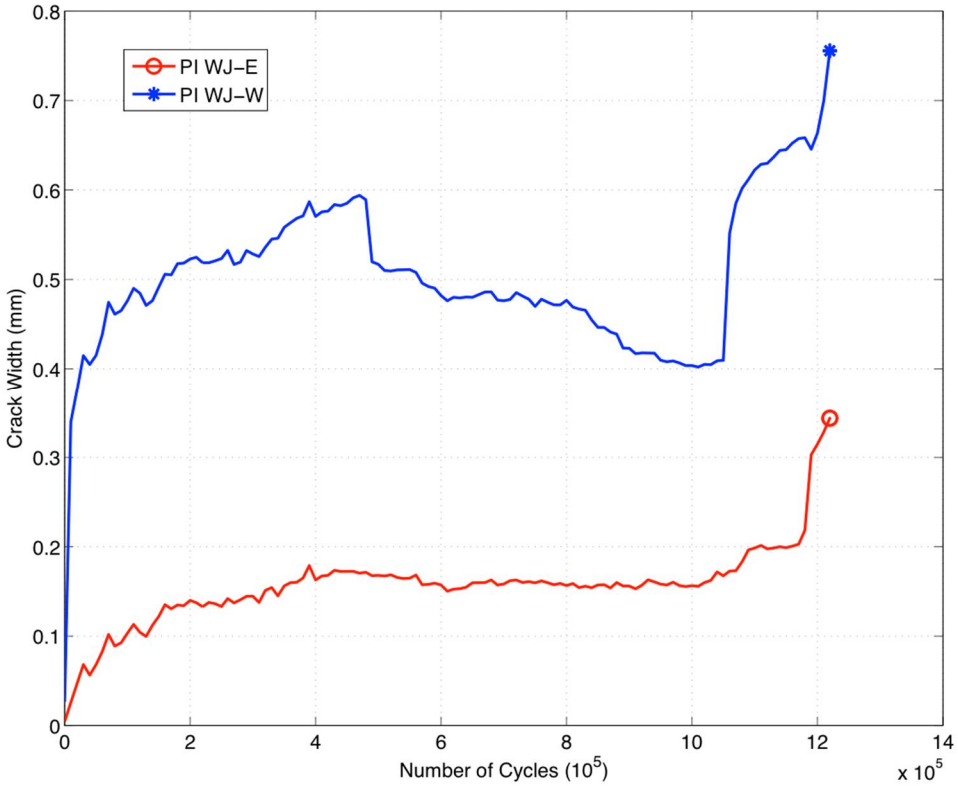

Figure 4-25 – Crack Widths Across the PPCP and UHPC Transverse Joint Interfaces in the West Joint (Test #3)

4.5.2.2 Transverse Joint Strains

Strains within the top mat of longitudinal reinforcement across the transverse joint were monitored to access the structural performance of the joint and its ability to transfer stresses from one PPCP to the next under fatigue loading. As previously discussed in Sub-section 3.4.3.3, three locations per transverse joint were instrumented: approximately 350mm in from the girder center line on either side, and at the midspan. Figures 4-26 through 4-28 depict the typical strains across the joint plotted at every ten thousand cycles at the locations depicted on the top right of each figure.

ESG W2-1 to C2-4 & ESG W2-3 to C2-6 (Strains 350mm in from Girder Center-Lines)

Unlike the strains captured during Test #1, there does not appear to be a trend in the strains shown in Figures 4-26 and 2-27. Overall, the strain levels are approximately one third at failure of those recorded during Test #1. This is likely due to the specimen geometry and the location of the loading point with respect to the monitored locations; due to the specimen geometry, it is not expected that significant longitudinal flexural strains would be occurring in the monitored locations.

Despite the lack of a clear trend, it appears as though the strains at the discrete points through the joint are very similar, indicating that there is an adequate level of continuity across the joint throughout the loading history. It should be noted that in Figure 4-27, ESG W2-3 was not recording for the first 580,000 cycles due to a technical error.

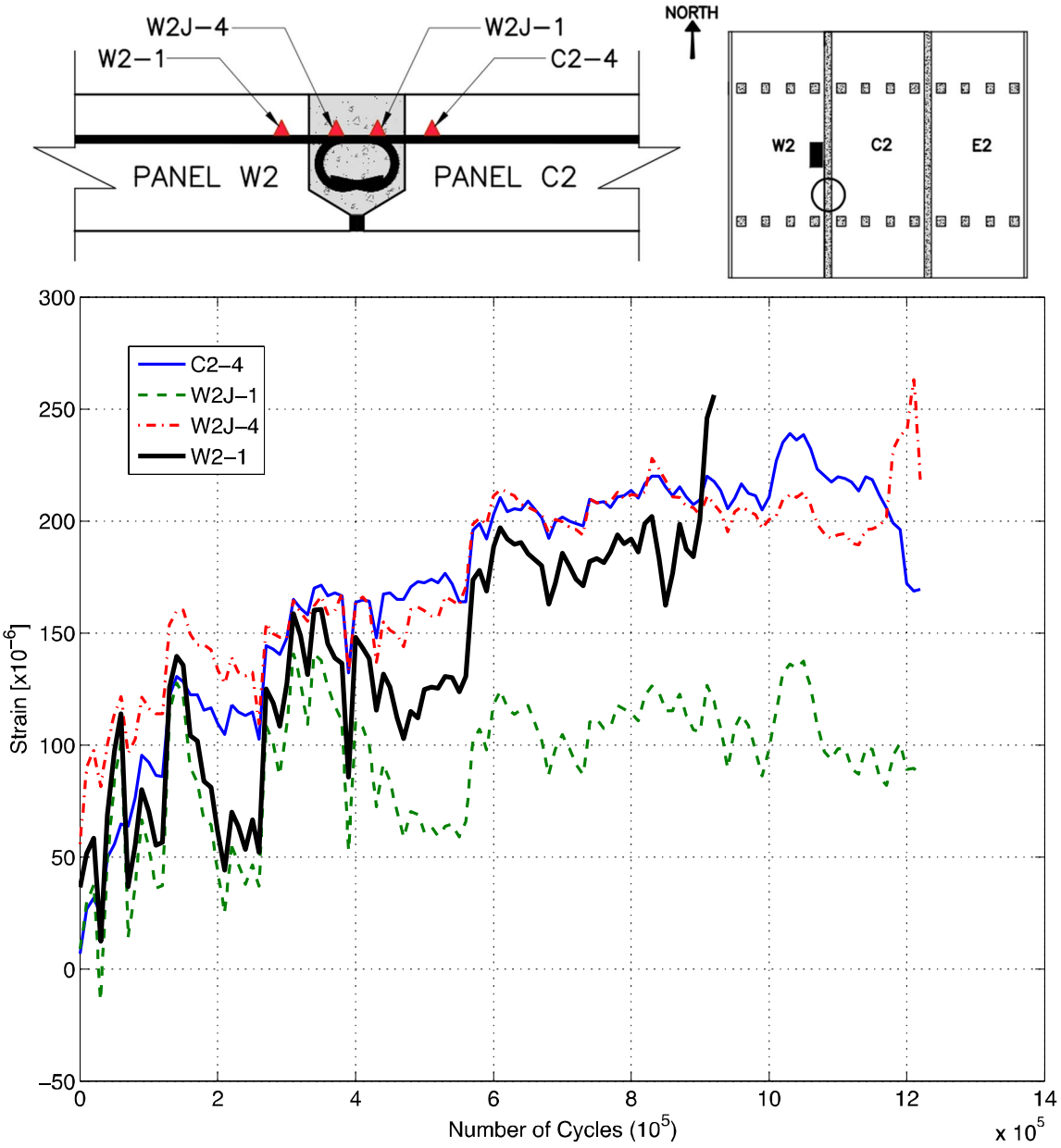

Figure 4-26 – Maximum Strains Every 10k Cycles Across West Joint from ESG W2-1 to C2-4 [Test #3]

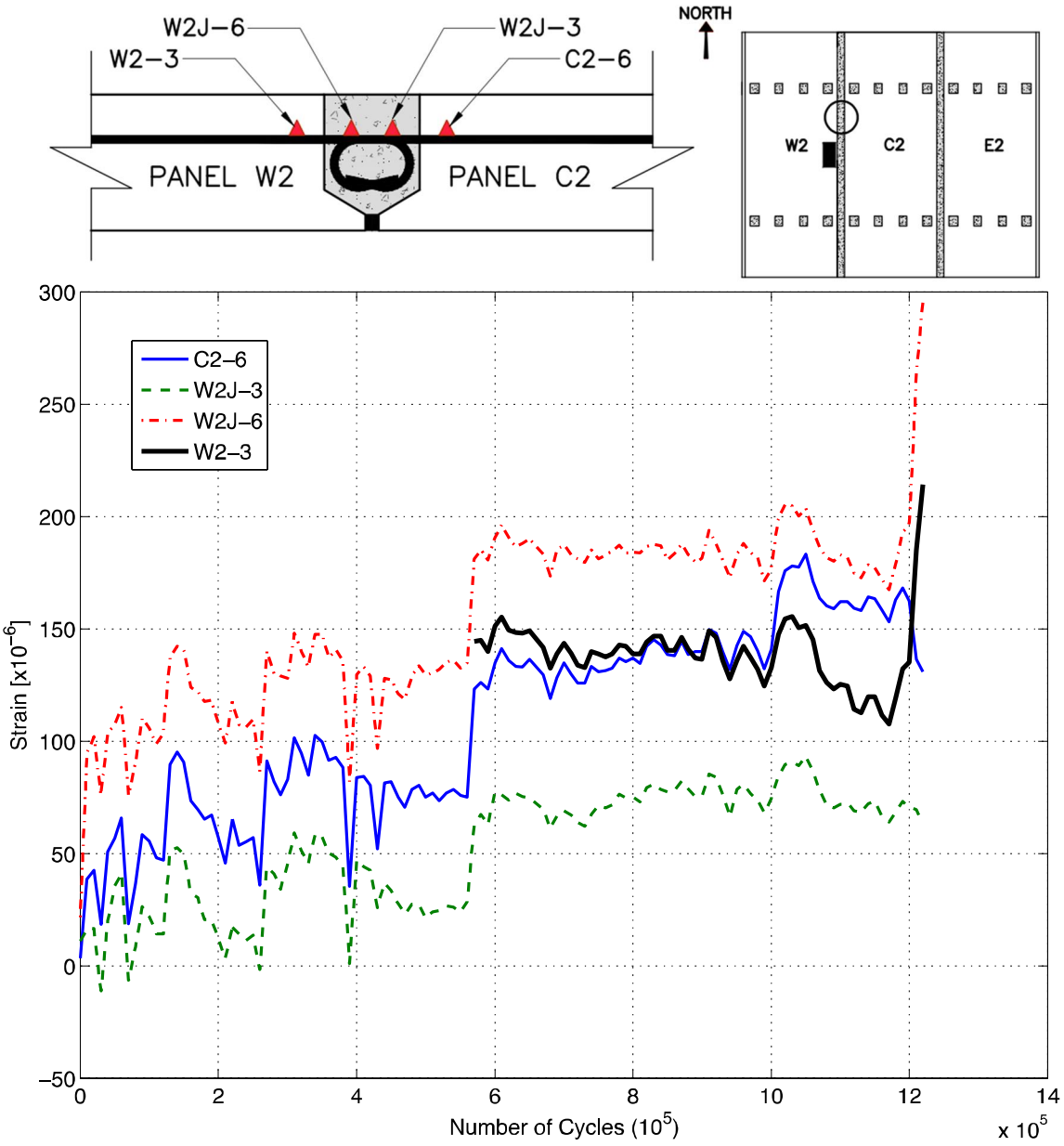

Figure 4-27 – Maximum Strains Every 10k Cycles Across West Joint from ESG W2-3 to C2-6 [Test #3]

ESG W2-2 to C2-5 (Strains at Midspan)

Similar to Test #1, the strains across the joint at the longitudinal centerline of the bridge were fundamentally different than the strains at the locations near the girders, as can be seen when comparing Figures 4-26 and 4-27 with Figure 4-28. From Figure 4-28, it is apparent that the west joint interface experienced significant tensile strains while the east joint interface experienced minimal strains. The strains decreased with distance from the loading point which was as expected. Overall, the trend in strains observed in Figure 4-28 agrees very strongly with that observed during both static Tests #1 and #4. The initial cycle caused significant strains in the ESGs closest to the loading point, and minimal tensile or compressive strains in the gauges furthest from the loading point which is similar to that shown in Figures 4-13 and 4-14 for Test #1 and Figure 4-43 for Test #4.

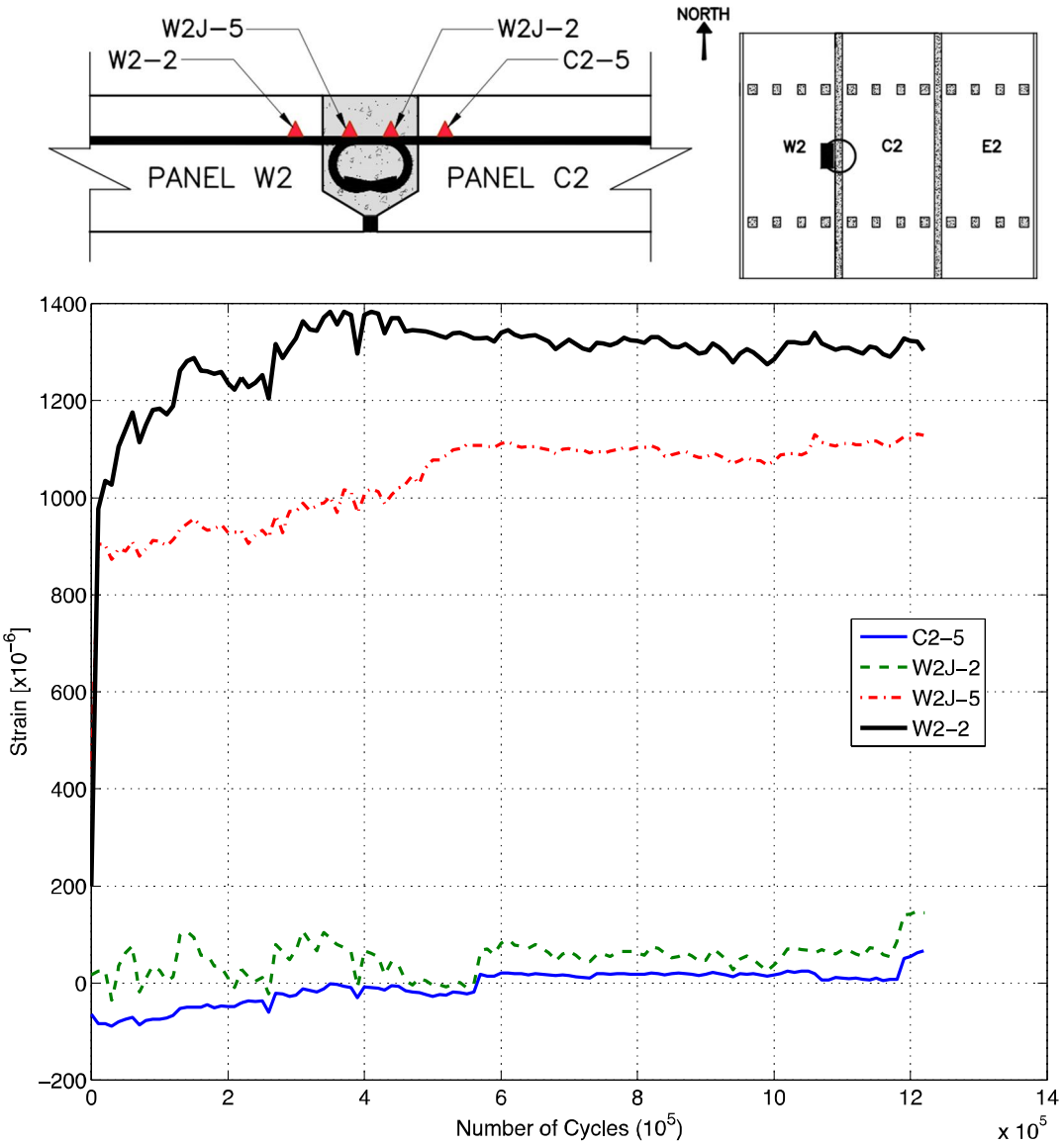

Figure 4-28– Maximum Strains Every 10k Cycles Across West Joint from ESG W2-2 to C2-5 [Test #3]

4.5.2.3 Crack Progression and Mapping

Cracks were mapped by the researchers at the onset of cracking (visually observed to occur at 450 kN), 500, 600, 700, 800, 900 kN during Cycle #1 and post failure. The visual crack mapping results are presented herein. Figures 4-29 and 4-30 depict the

progression of crack formation from 450 kN to 900 kN during Cycle #1. The post failure crack map is shown in Figure 4-31.

.

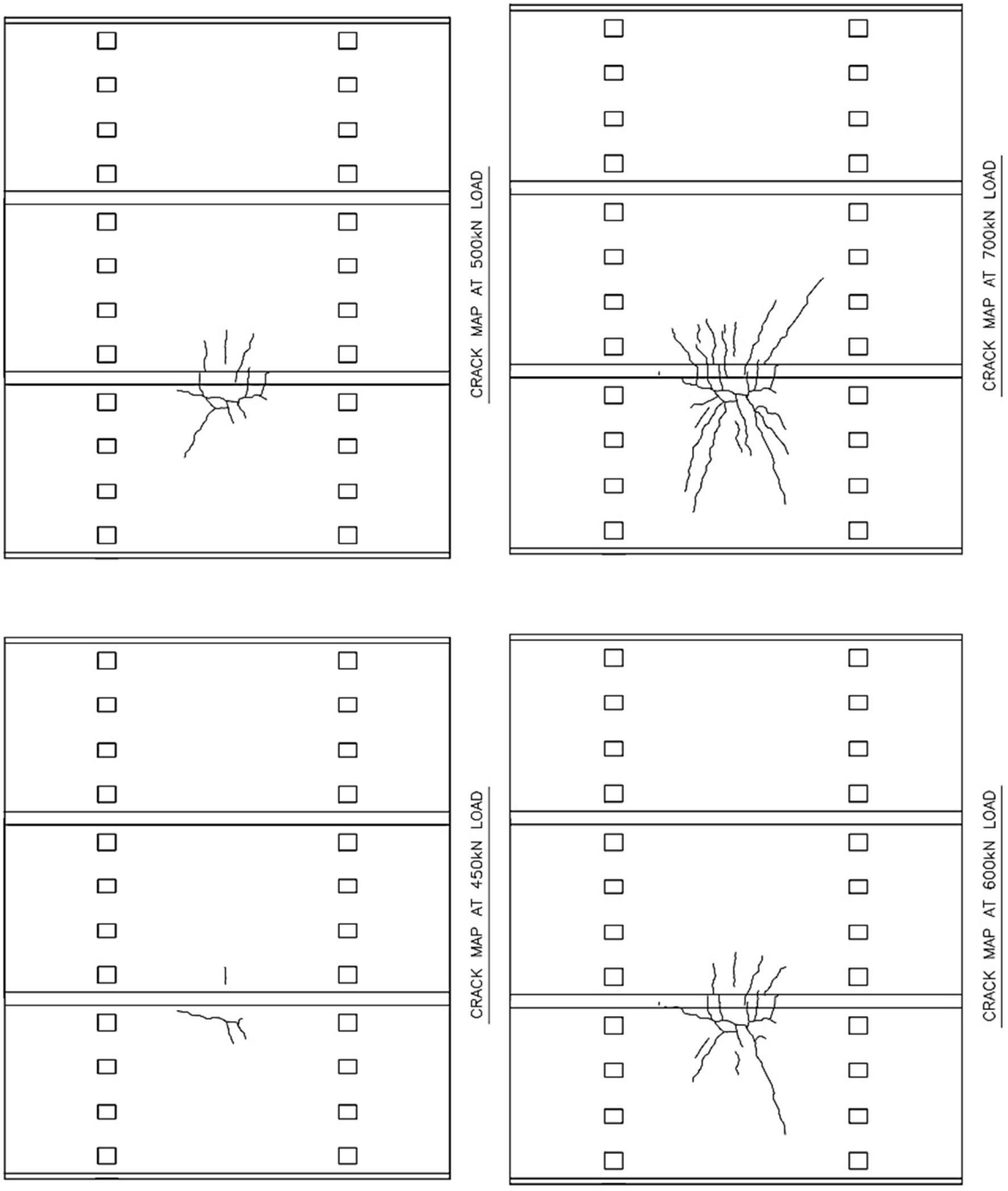

Figure 4-29 – Crack Progression from 450 kN to 700 kN (Test #3)

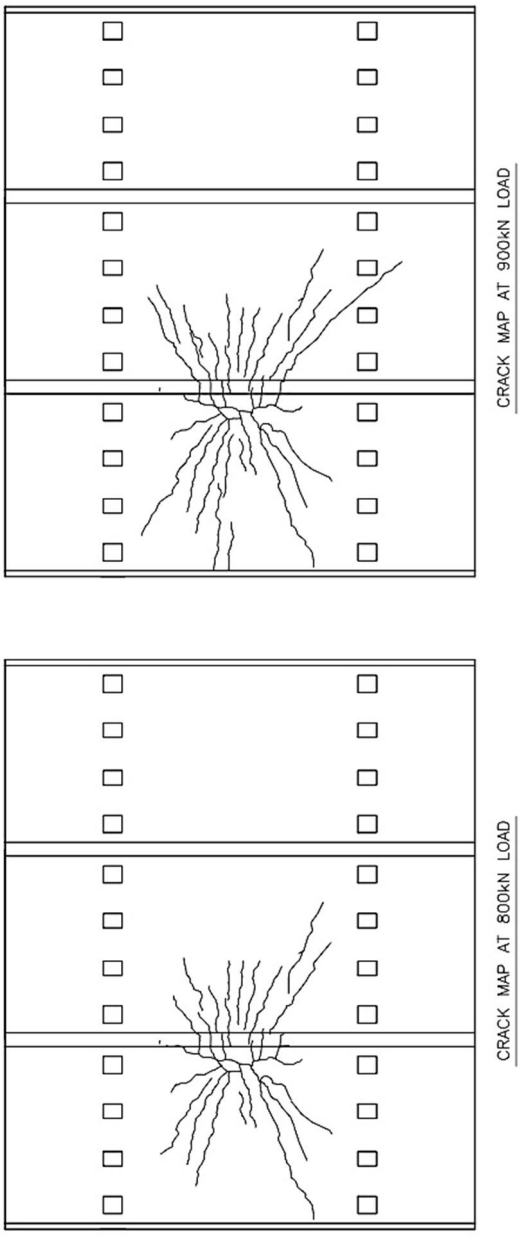

Figure 4-30 – Crack Progression from 800 kN to 900 kN (Test #3)

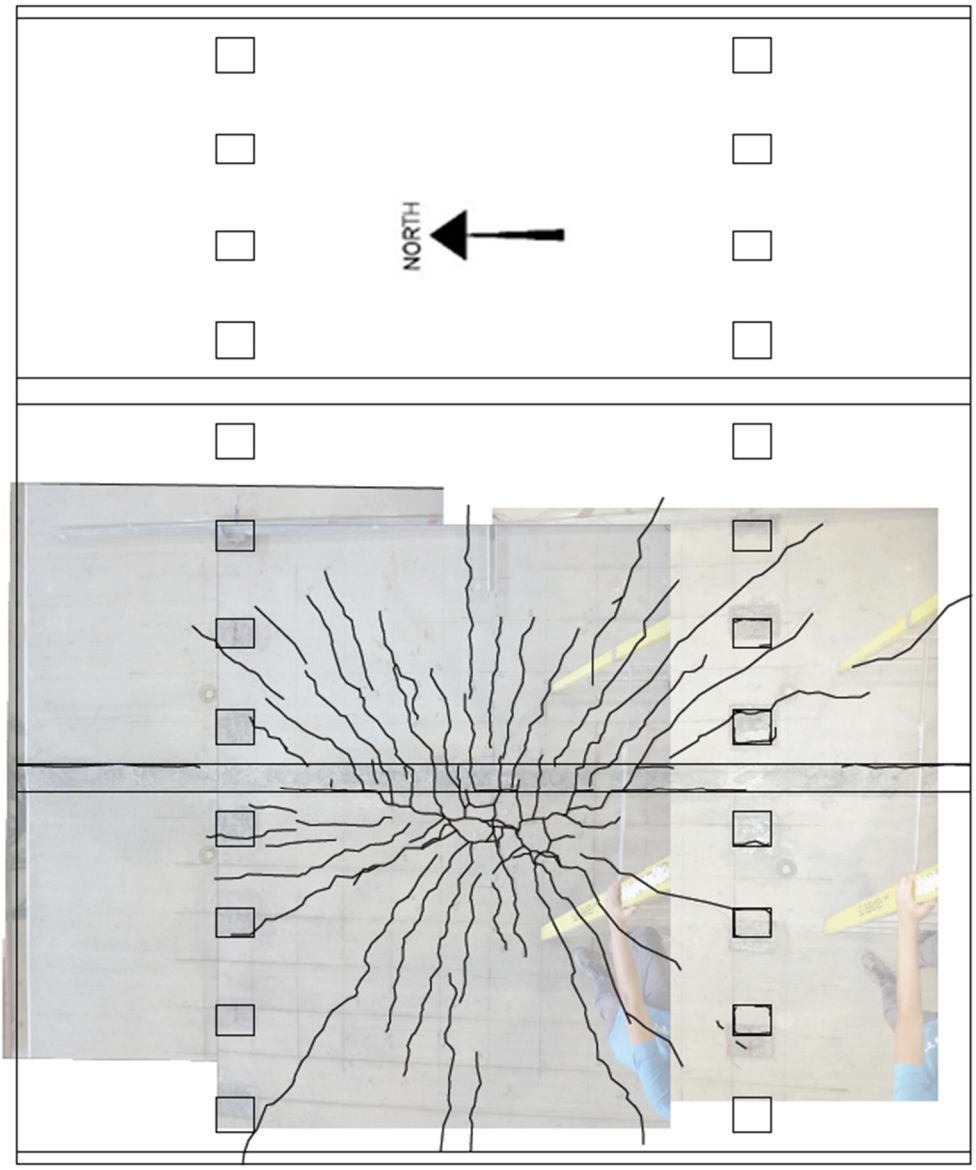

Figure 4-31 – Crack Mapping at Failure (Test #3)

Significant damage can be seen directly above the loading point with radial cracks extending outwards, characteristic of punching shear damage. A significant amount of transverse cracking along the joint was noted post failure however this cracking is attributed to the failure of the shear studs and subsequent lifting of the panels as

described in Sub-section 4.5.4; the extent of the observed lateral cracking would not be expected had the shear studs remained effective throughout the fatigue test.

4.5.3 Failure of Test Specimen #2 (Test #3)

Failure of the system was recorded at cycle 1,219,620 corresponding to the cycle in which Panel W2 began deflecting considerably due to total failure of the shear studs. As previously indicated, the true capacity of the precast system was not determined since a punching shear failure, as in the case of Test #1, did not occur. Therefore, it is unknown how many more cycles the system could have withstood prior to failing in punching shear. Sub-section 4.5.4 discusses the overall failure method and the resulting damage for Test #3.

4.5.4 TS2 Shear Stud Failure and Panel Damage (Test #3)

Due to the shear stud failures as a result of Test #2 encountered during the demolition (previously discussed in Sub-section 4.4.2), two full-depth shear pockets on Panel W2 were instrumented with ESGs as previously shown in Figures 3-43 and 3-44. The maximum strain in the studs recorded every 10,000 cycles is shown in Figures 4-32 and 4-33. Due to technical difficulties, the ESGs only began recording data at approximately cycle 560,000; therefore, it should be noted that the plotted strains provide an indication of the behaviour but do not represent the true strain as the effects of the first 560,000 cycles were not captured.

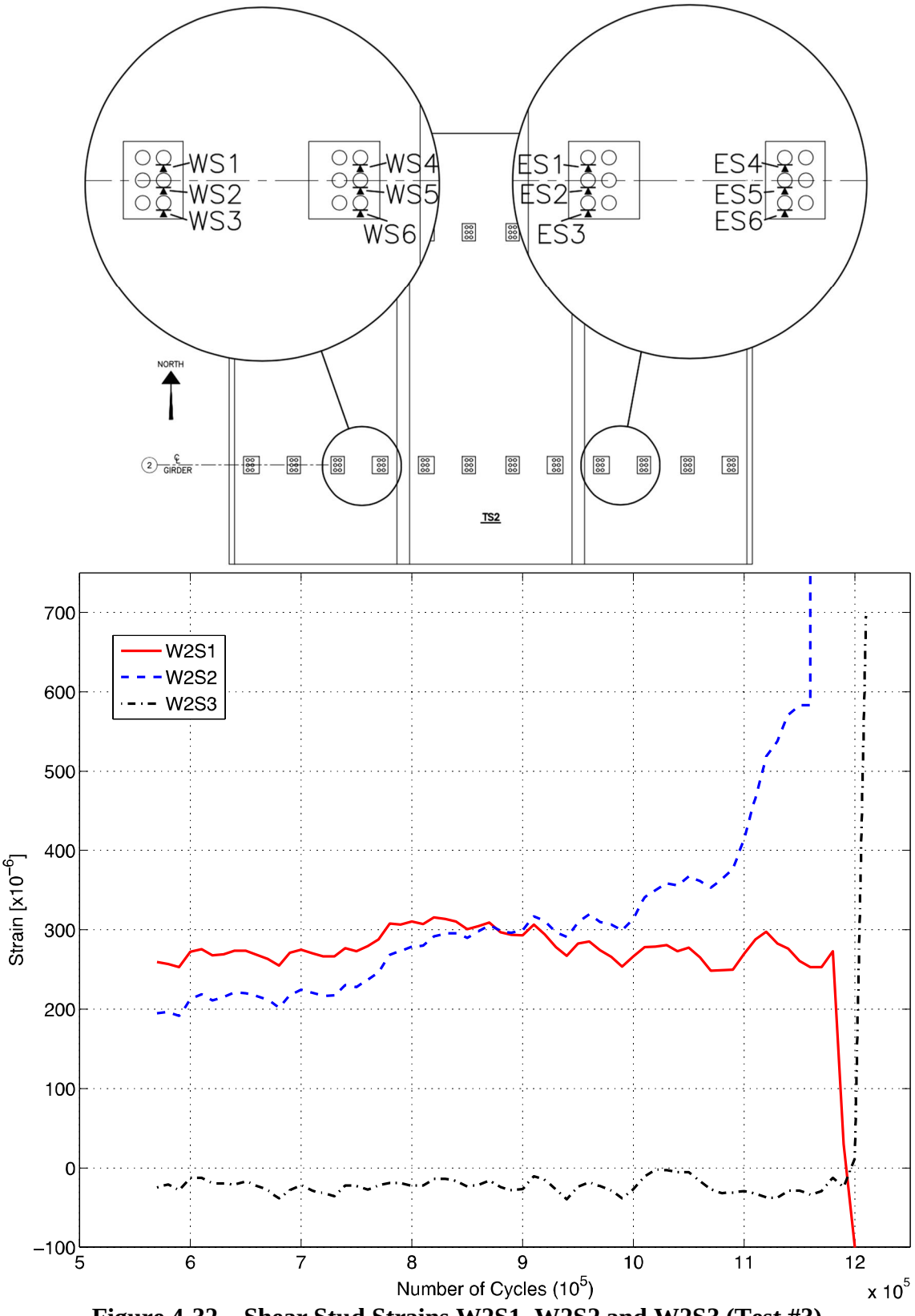

Figure 4-32 – Shear Stud Strains W2S1, W2S2 and W2S3 (Test #3)

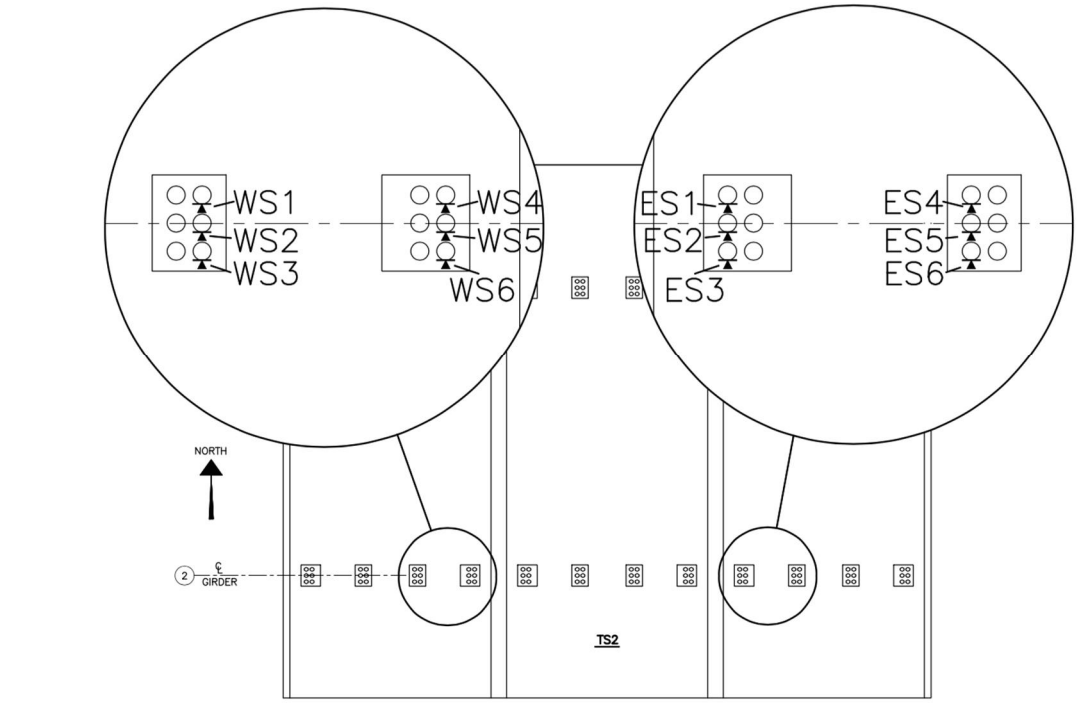

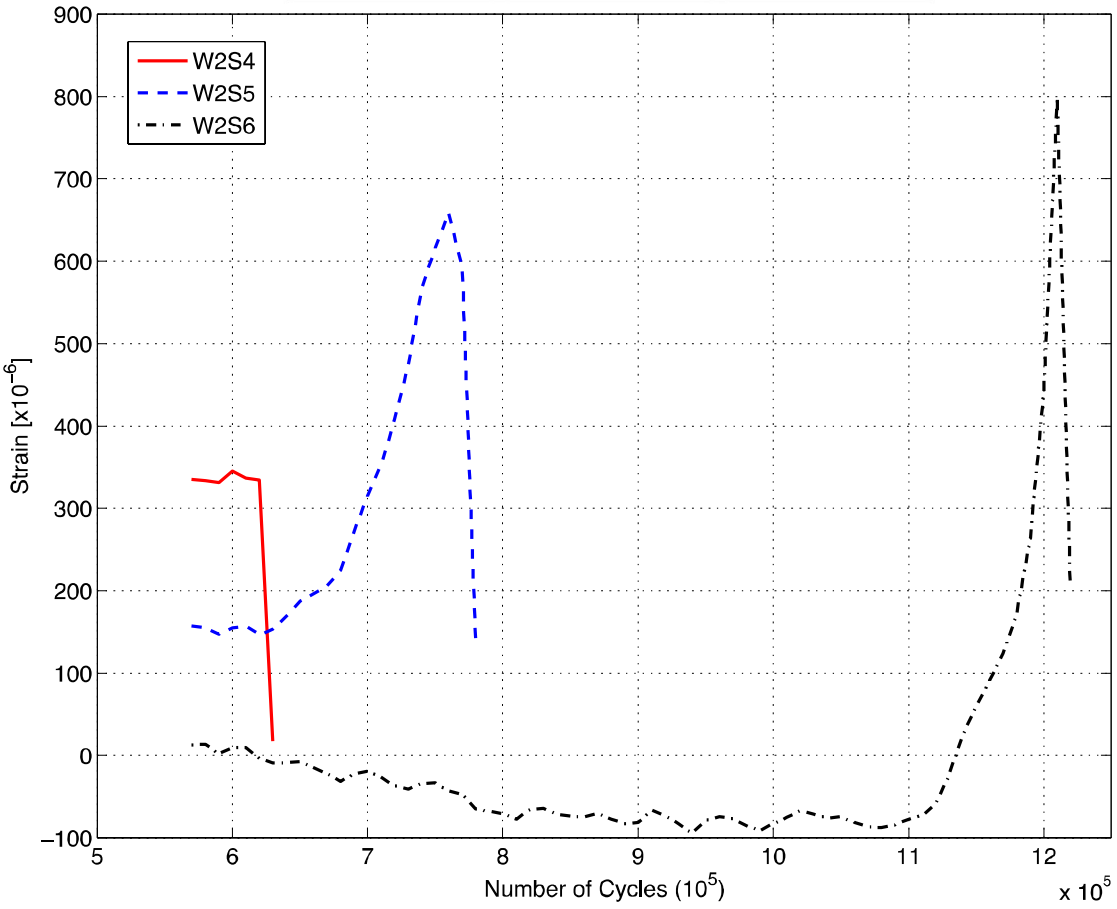

Figure 4-33 – Shear Stud Strains W2S4, W2S5 and W2S6 (Test #3)

From Figures 4-32 and 4-33, it can be seen that initially, the interior (W2S1 and W2S4) and center-line (W2S2 and W2S5) studs were subjected to tensile strains while the exterior (W2S3 and W2S6) studs were subjected to compressive strain; this observation is in agreement with the observed flexure of the overhangs at the peak of the fatigue cycle. As expected, the pocket closest to the loading point experienced the first stud failure. Stud W2S4 failed at approximately cycle 620,000, followed by stud W2S5 at approximately cycle 770,000. Once these two studs failed, the load was redistributed to the adjacent pockets.

Failure of studs W2S1 and W2S2 followed at approximately cycles 1,180,600 and 1,160,000 respectively. At this point, due to the failure of the interior and center-line studs, the exterior W2S3 and W2S6 studs would be subjected to large tensile forces and consequently failed shortly thereafter, both at approximately cycle and 1,190,000. It should be noted that although none of the other pockets in Panel W2 were instrumented, the panel was observed to lift off of the girder significantly during the last fatigue cycles indicating that the shear studs in the remaining pockets were likely failed as well.

Since Panel W2 was no longer attached to the girders by the studs, the loading caused the panel to begin rotating about the transverse joint; this induced significant flexural stresses causing cracking along the underside of Panel C2, as shown in Figures 4-34 and 4-35. In addition, full depth cracks through the panel in the vicinity of the joint as shown in Figure 4-36 were observed. These cracks appear to coincide with the joint interface and upon

demolition, it was determined that the significant loading likely caused cracking within the PPCP adjacent the joint interface.

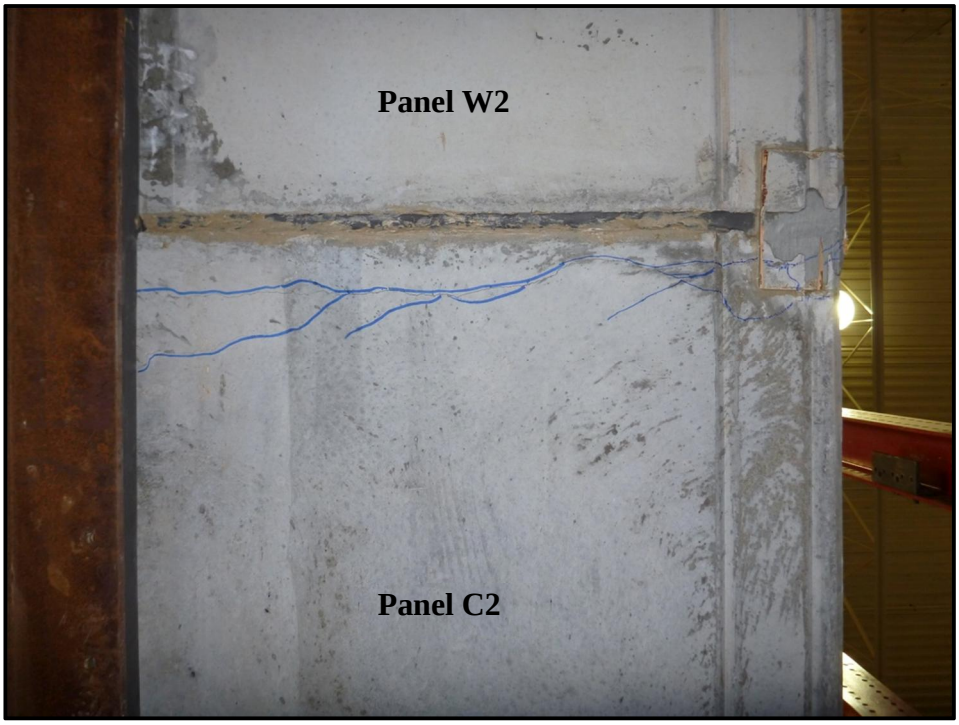

Figure 4-34 – Typical Cracks on Overhang Soffit (Test #3)

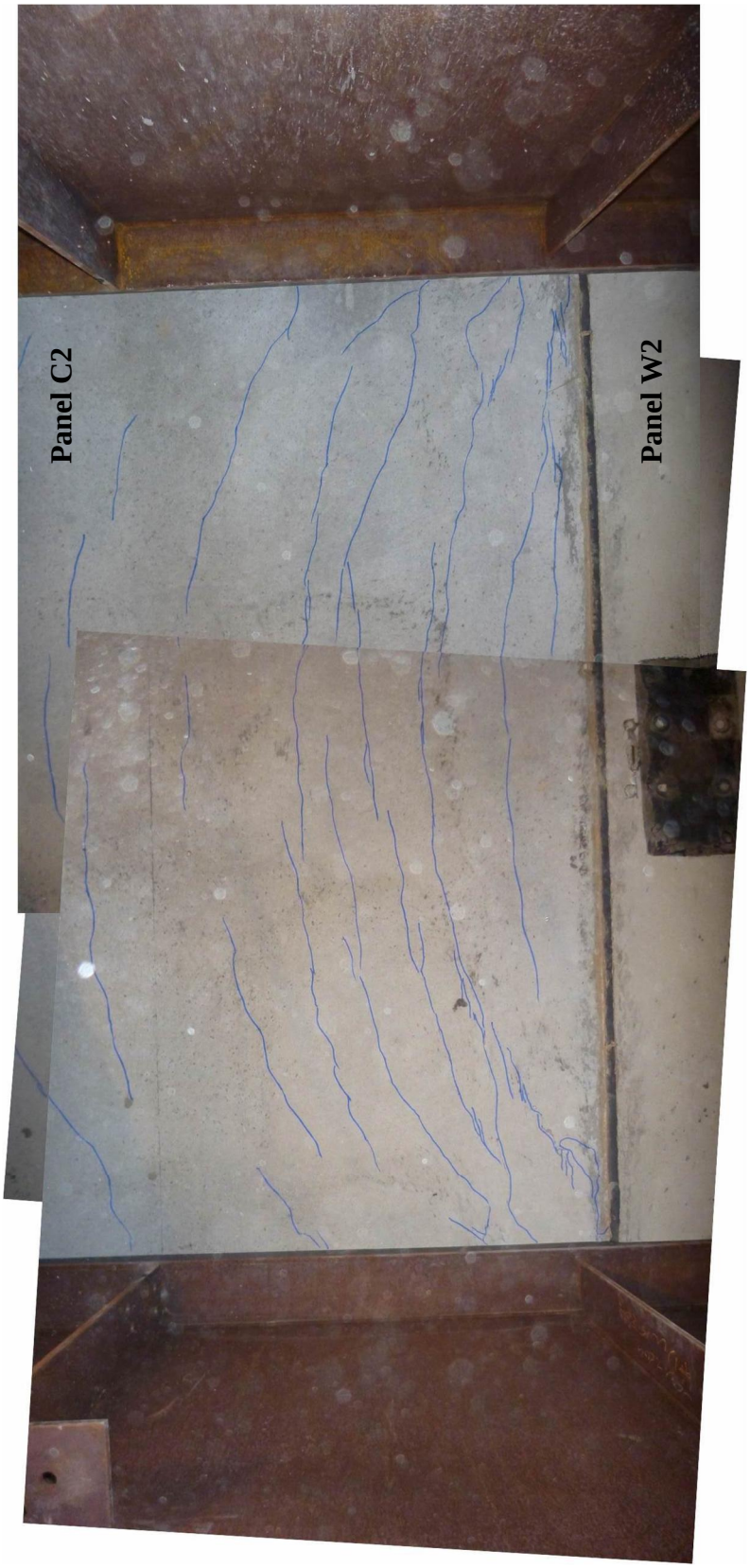

Figure 4-35 – Cracks on Deck Soffit Between Girders (Test #3)

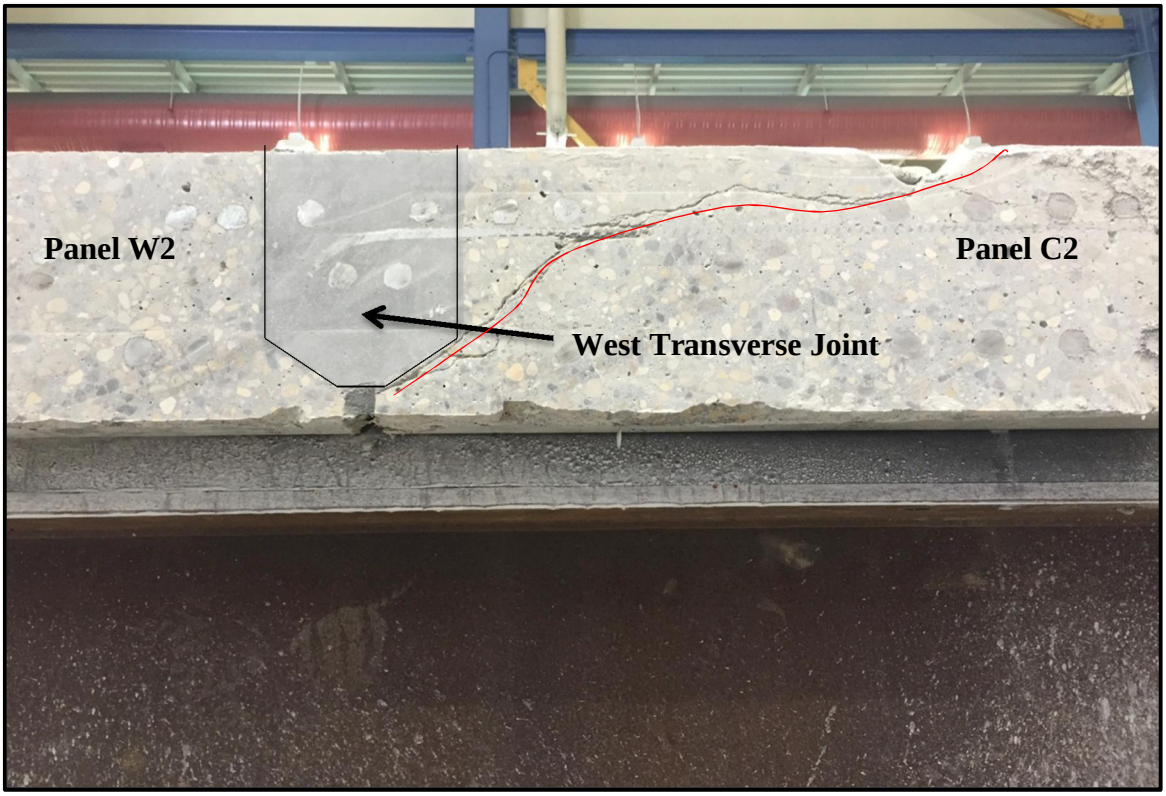

Figure 4-36 – Cracks in Panel C2 Due to Panel W2 Lifting During Failure (Test #3)

4.6 Static Test on TS2 – East Joint (Test #4)

The static test to failure of Panel E2 along the east transverse joint was the final test performed as part of this research program. Test #4 was performed on April 28, 2015. The experimental results and analysis of the data for this test is presented herein.

4.6.1 Deflection of Test Specimen #2 (Test #4)

A total of seven LVDTs were implemented above the bridge deck to monitor the deflection of the test specimen during Test #4 as shown in Figure 4-37 and schematically in Figure 4-38. The LVDTs were placed along the longitudinal centerline of TS2 at panel quarter points and within 50 mm of the UHPC joints on either side. The load-deflection curve for the LVDT placed directly above the loading location (LVDT 4) is shown in

Figure 4-38. It can be seen that the load vs. deflection curve is essentially linear until a load of approximately 325 kN is achieved at which point it is assumed that significant crack initiation occurred. For the purposes of comparison with other tests, the slope of the initial tangent has been found to be approximately 133 kN/mm.

To the naked eye, hairline cracks were observed on the deck at a load of 250 kN. However, as the initial tangent slope in Figure 4-38 suggests, the specimen behaved in a fairly linear matter until an approximate load of 400 kN; at this point, numerous cracks were visible and propagating rapidly. The irregularities in the curve between loads of 250 kN and 1000 kN are due to the pausing of the test to monitor crack growth. The loading was paused at 250, 300, 400, 500, 600, 700, 800, 900, and 1000 kN to allow the researchers an opportunity to mark cracks.

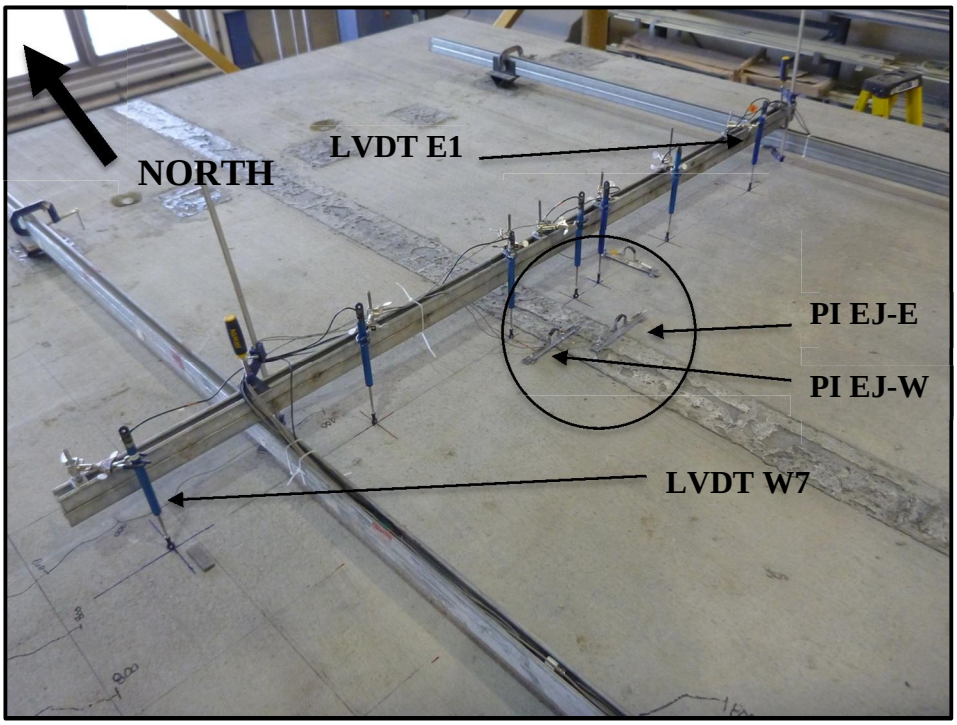

Figure 4-37 – LVDT and Pi-Gauge Set-up (Test #4)

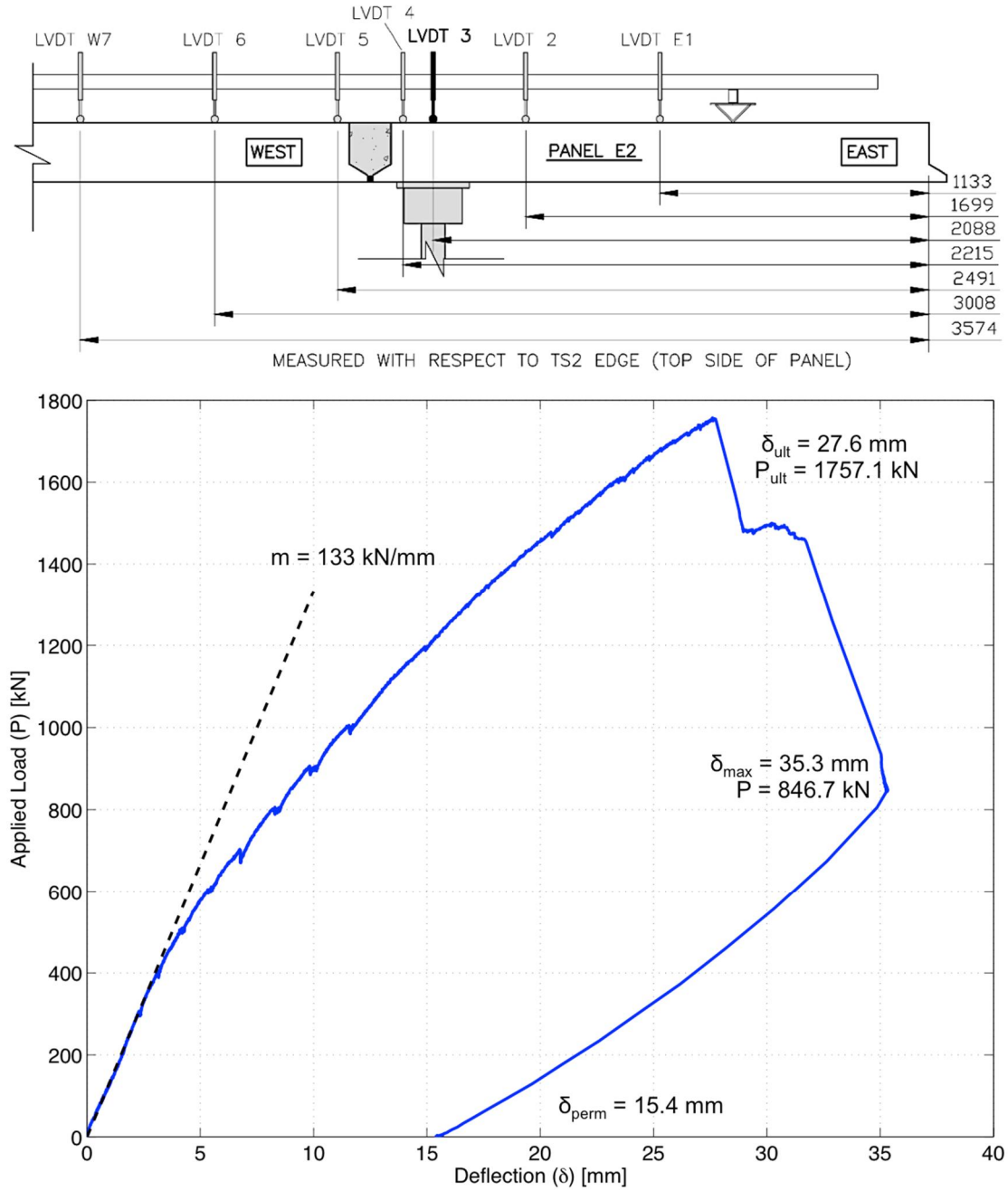

Figure 4-38 – Load-Deflection Curve for LVDT 3 (Loading Point) [Test #4]

From Figure 4-38, it can be seen that the specimen deflection begins to increase at a quicker rate nearing failure and reaches a value of 27.6 mm (δ_{ult}) at an ultimate load of 1757.1 kN (P_{ult}). Failure was marked by two sudden and significant drops in load to approximately 1500 kN and then 850 kN. The researchers continued to load the deck but

it was observed that the specimen continued deflecting (δ_{max} = 35.3 mm) without any recovery in load carrying capacity; thus the test was terminated and the specimen was unloaded. The specimen was observed to have a permanent deflection of 15.4 mm (δ_{perm}) at the loading location; this permanent deflection corresponds to approximately 56% of the ultimate deflection.

Longitudinal deflection profiles for TS2 are shown in Figure 4-39 at 25% of P_{ult}, 50% of P_{ult}, 75% of P_{ult}, 100% of P_{ult} and after unloading to capture the permanent deflection profile (corresponding to approximate loads of 440, 880, 1320, 1760 and 0 kN respectively). From this figure, it is evident that the deflections at up to and including the ultimate load were fairly symmetrical about the loading point and the slopes of the deflection profiles on either side of the joint are similar. Without studying the specimen crack widths and joint strains, there is no evidence in Figure 4-39 that the joint performed negatively; in fact, if the dashed lines indicating the boundaries of the east joint were not present in Figure 4-39, it would be difficult to differentiate this deflection profile from that of a monolithic CIP deck.

The permanent deflection profile in Figure 4-39 closely resembles the general deflection trend but has a maximum permanent deflection at the PPCP quarter point east of the east joint; this is due to the nature of the punching shear failure observed which is discussed in more detail Sub-section 4.6.3.

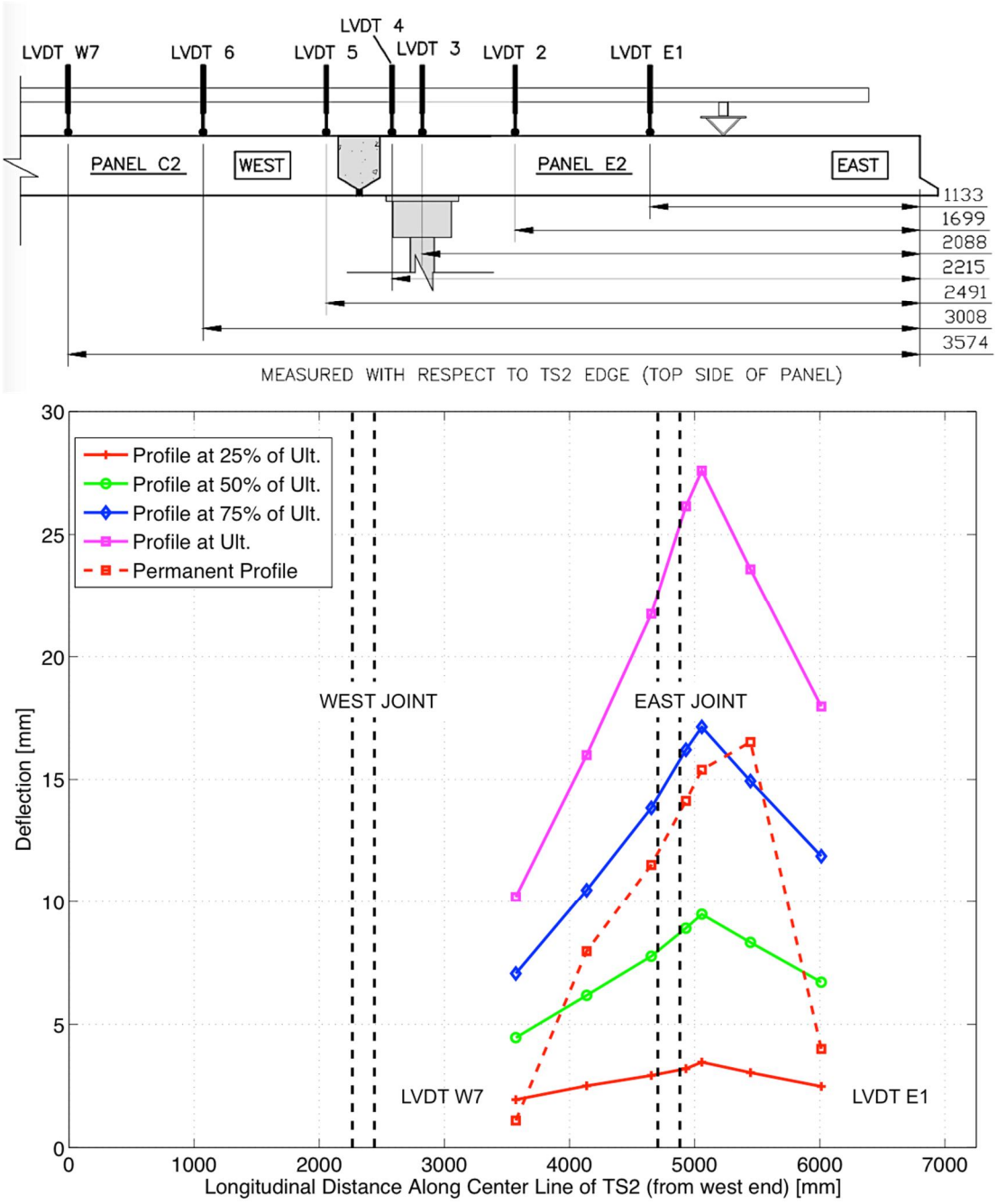

Figure 4-39 – Longitudinal Deflection Profiles (Test #4)

4.6.2 Crack Widths and Strains for Test Specimen #2 (Test #4)

4.6.2.1 Crack Widths

Due to the point of load application being immediately adjacent the east joint, it was expected that significant tensile stresses would be induced across the top of the UHPC joint. Therefore, two pi-gauges were placed across the PPCP and UHPC transverse joint interface, as shown in Figure 4-37, to determine if any cracks occurred during testing, possibly indicating the presence of debonding between the interfaces. Figure 4-40 provides the results of the pi-gauges placed across the east joints.

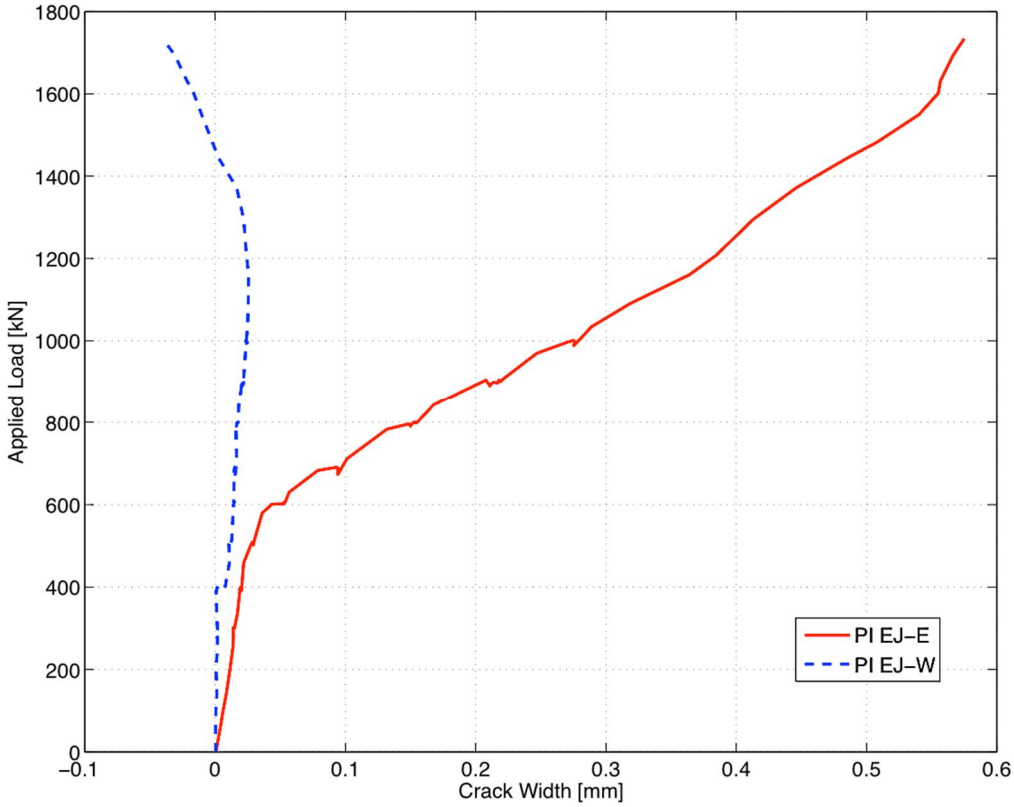

Figure 4-40 – Crack widths across the PPCP and UHPC transverse joint interfaces in the East Joint [Test #4]

A positive crack width suggests crack growth while a negative width suggests compression in the region of the pi-gauge indicating the presence of compressive forces across the top of the deck in this location. From Figure 4-40, it is evident that the pi-

gauge (PI EJ-E) across the Panel E2 – UHPC interface (east side of joint) began slowly reading positive crack growth before beginning to increase rapidly once approximately 600 kN of load was reached. An ultimate crack of approximately 0.58 mm was recorded at failure.

On the other hand, it is evident that the pi-gauge (PI EJ-W) across the Panel C2 – UHPC interface (west side of joint) began increasing minimally before going negative indicating very minor compressive stresses across this interface. This behaviour is consistent with that observed in Figure 4-5 during Test #1 in which one side of the joint experienced very minimal compressive strains while the other side of the joint experienced large tensile strains. In both the Test #1 and Test #4 cases, it is the pi-gauge on the side of the joint further from the loading point which appears to undergo compressive stresses.

4.6.2.2 Transverse Joint Strains

Strains within the top mat of longitudinal reinforcement across the transverse joints were monitored to access the structural performance of the joint and its ability to transfer stresses from one PPCP to the next. As previously discussed in Sub-section 3.4.3.3, three locations per transverse joint were instrumented: approximately 350mm in from the girder center line on either side, and at the midspan. Figures 4-41 through 4-43 depict the typical strains across the joint at the locations depicted on the top right of each figure.

ESG E2-1 to C2-1 & E2-3 to C2-3 (Strains 350mm in from Girder Center-Lines)

Overall, the strains across the joint at the locations near the girders were similar to those observed during Test #1 in the same locations. The strains shown in Figure 4-41 follow the expected behaviour of decreasing strain with increasing distance from the loading point throughout the majority of the test. The strains shown in Figure 4-42 varied slightly; the two sets of corresponding gauges on the same bar were very similar but there was a larger change in strain across the joint. This is likely due to cracking that may have intercepted the bar protruding into the joint from Panel E2 at around 700 kN of load.

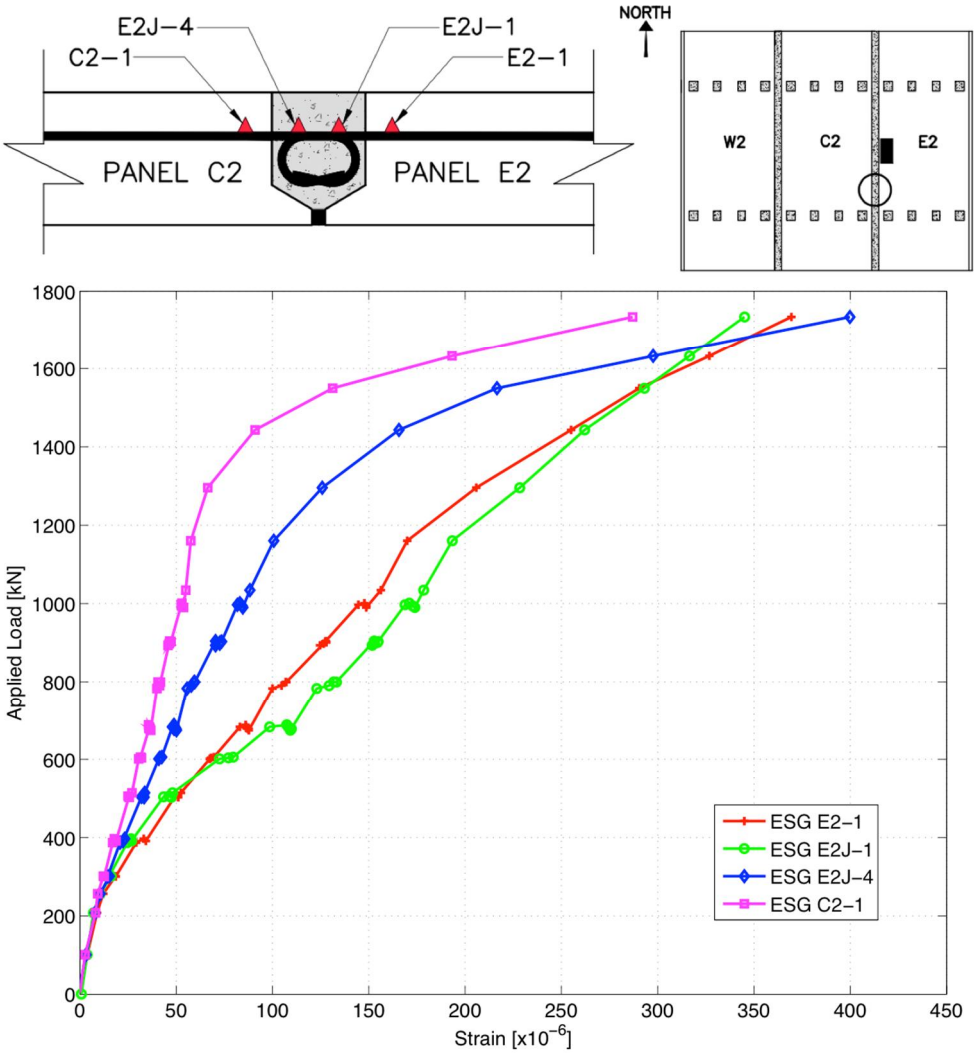

Figure 4-41 – Strains Across East Joint from ESG E2-1 to C2-1 [Test #4]

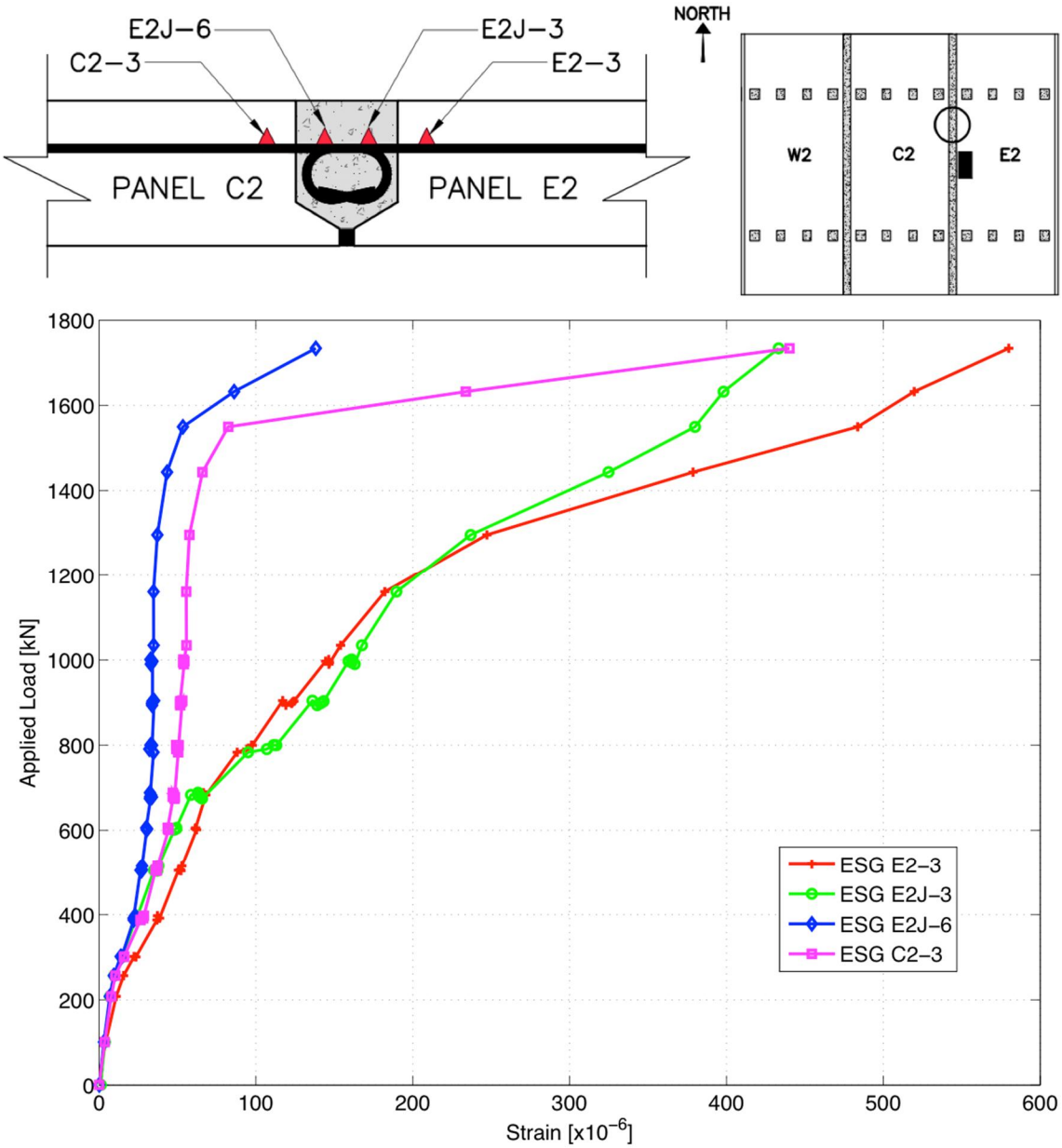

Figure 4-42 – Strains Across East Joint from ESG E2-3 to C2-3 [Test #4]

ESG E2-2 to C2-2 (Strains at Midspan)

The pi-gauges along the centerline of the specimen in line with the loading point displayed significantly different behaviour than those located near the girders. As shown in Figure 4-43, the strains in this location correspond clearly with the crack width data presented in Figure 4-40. It is shown that all gauges read minimal strains until

approximately 400 kN at which point the gauges further from the load (E2J-5 and C2-2) continued reading minimal compressive strains while the gauges closest to the point of load application (E2J-2 and E2-2) began reading increasing tensile strains. This trend is exactly as was observed with the crack widths which confirms that the east PPCP-UHPC interface developed tensile stresses while the west PPCP-UHPC interface developed compressive stresses.

Even though Test #4 had the point of load application much closer to a transverse joint than in Test #1, in which the point of load application was centered within Panel C1, the strain behaviour from the corresponding locations are quite similar. In Test #1, it was suspected that cracks developed near failure engaging the bar reading compressive strains, causing the bar to undergo a stress reversal and begin carrying tension. In Test #4, it is likely that cracks did not directly intercept the instrumented bar and thus no tensile strains in the bar was observed. In addition, the strains observed in Figure 4-43 correlate with the suspected inflection point observed in the deflection profiles shown in Figure 4-39.

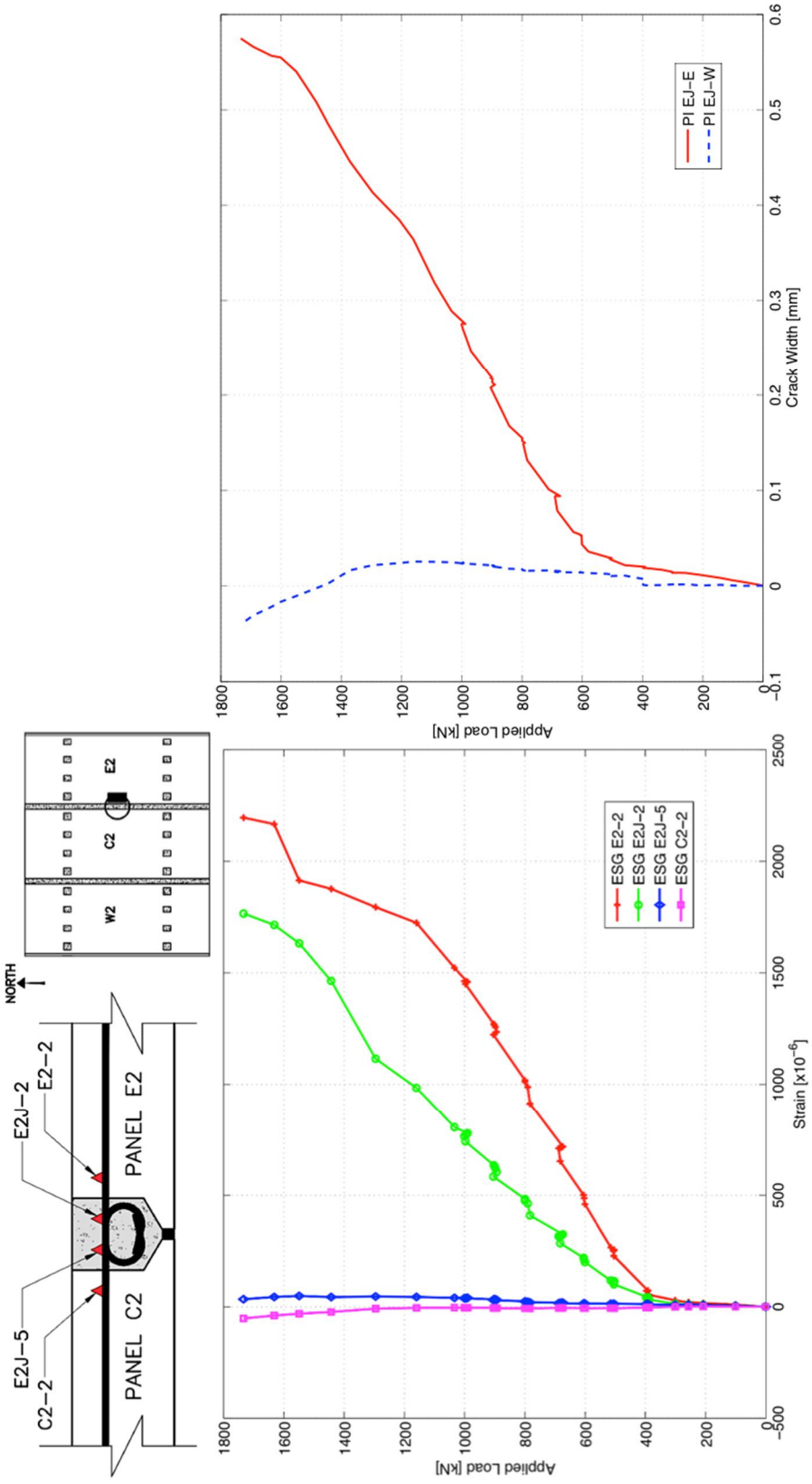

Figure 4-43 – Strains Across West Joint from ESG E2-2 to C2-2 [Test #4]

4.6.2.3 Crack Progression and Mapping

Cracks were mapped by the researchers at the onset of cracking (visually observed to occur at 250 kN), 300, 400, 500, 600, 700, 800, 900, 1000 kN and post failure. The visual crack mapping results are presented herein. Figures 4-44 and 4-46 depict the progression of crack formation from 250 kN to 1000 kN. It should be noted that only cracks formed during Test #4 are shown in these figures; cracks from Test #3 have not been shown. The post failure crack map is shown in Figure 4-48; cracks from Test #3 have been included in the post failure crack map for comparison.

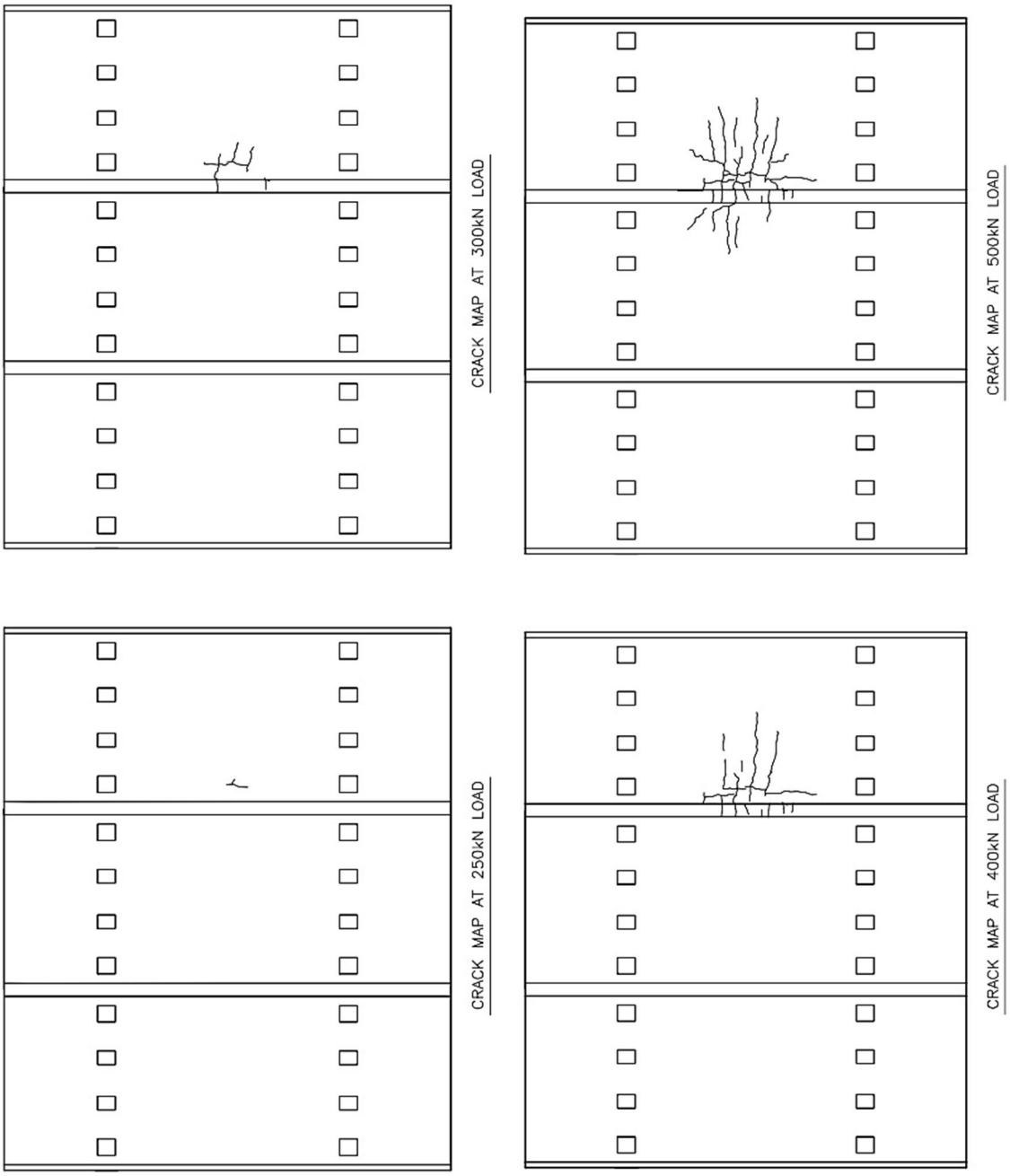

Figure 4-44 – Crack Progression from 250 kN to 500 kN (Test #4)

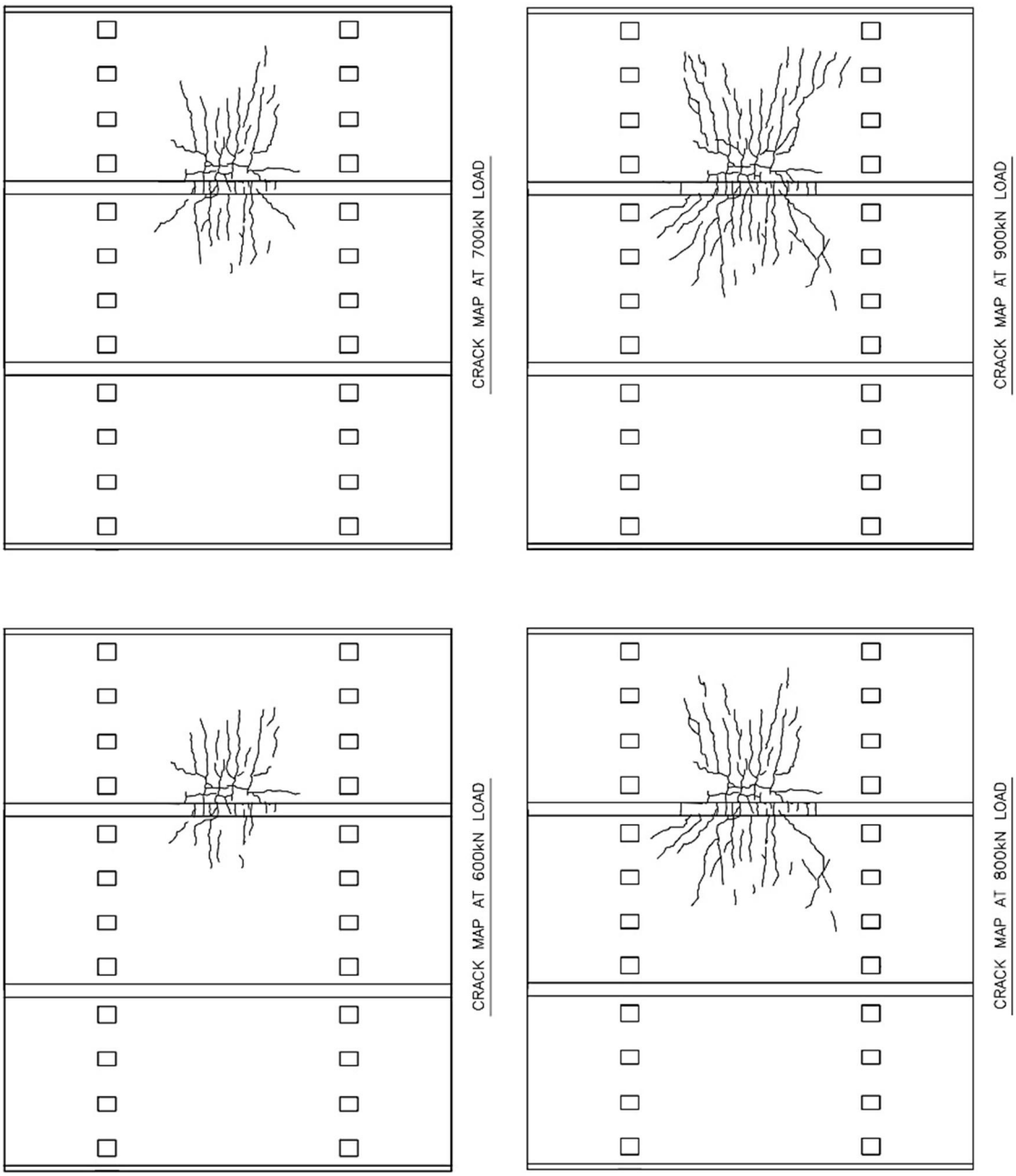

Figure 4-45 – Crack Progression from 600 kN to 900 kN (Test #4)

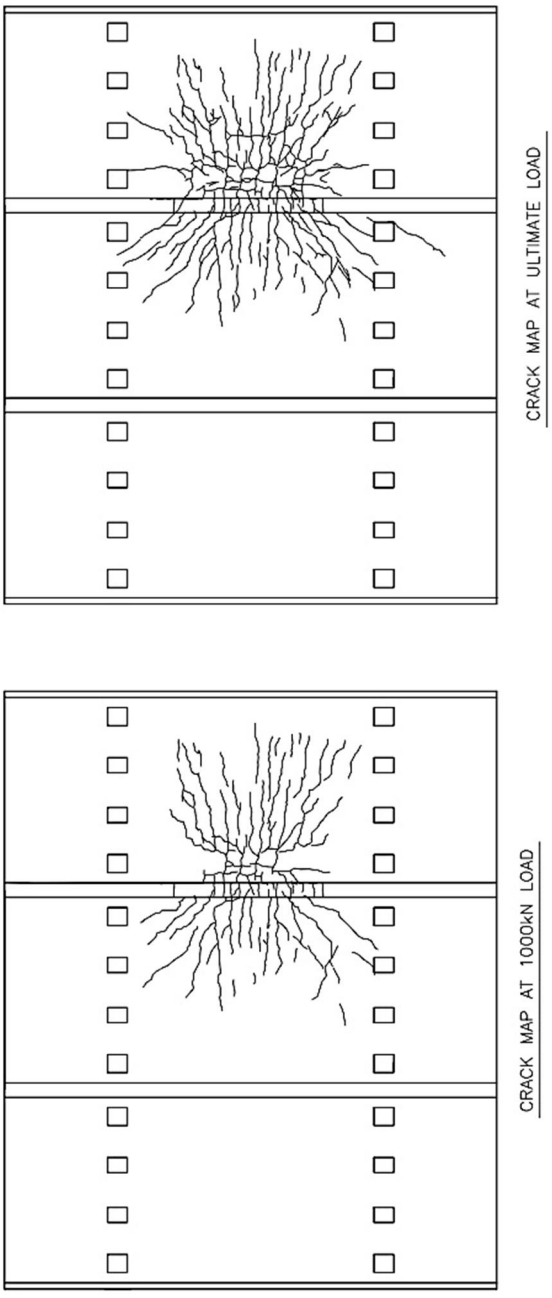

Figure 4-46 – Crack Progression from 900 kN to Failure (Test #4)

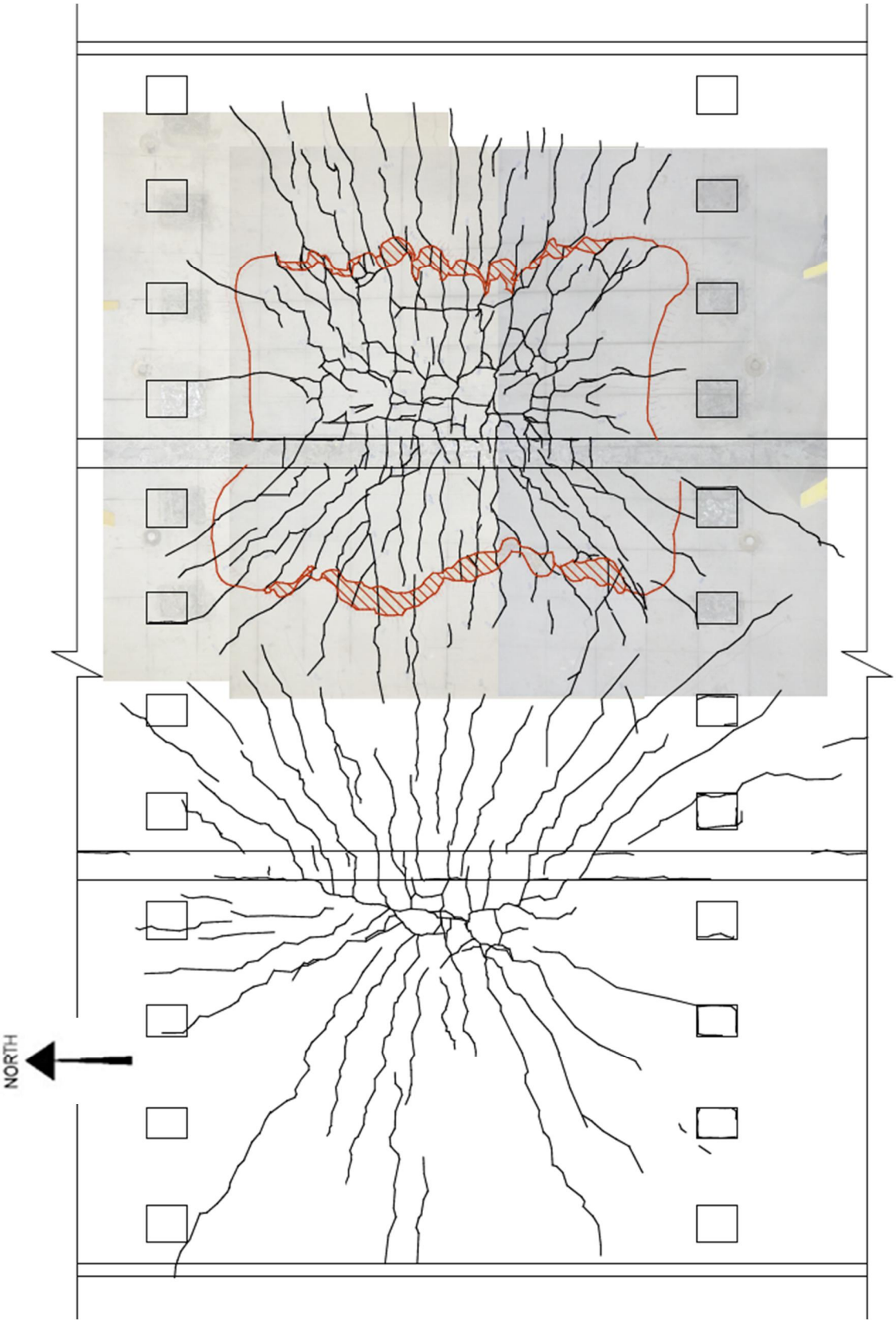

Figure 4-47 – Crack Map at Failure Showing Test #3 Cracks (Test #4)

It should be noted that the entire portion of the deck contained within the red boundary in Figure 4-47 is no longer intact due to delamination caused by punching shear. The hatched portion of the deck represents delaminated concrete that was easily removed by hand; the non-hatched portion of the deck is delaminated concrete held in place by the reinforcing steel (identified by finding the limits of the hollow sounding concrete when hit with a ballpeen hammer). Overall, this crack pattern is very typical of a punching shear failure for a traditional CIP deck.

4.6.3 Punching Shear Failure

Similarly to Test #1, TS2 failed in punching shear. The crack pattern and circumferential delamination typical of a punching shear failure is clearly visible in the post failure crack map in Figure 4-47. As can be seen in Figure 4-48, the damage on the soffit is contained primarily to the Panel E2 however the punching cone extended significantly into Panel C2 indicating that the joint transferred the loads from one panel to the next very well.

Figure 4-48 – Punching Shear Failure on Deck Soffit (Test #4)

4.7 Comparison of Test Results

Since Test #1 was performed centered on a panel, it can serve as a control test when comparing to Test #4 which was performed directly adjacent a transverse joint. By comparing these two tests, the performance of the joint relative to that of the panel can be studied. Many aspects of the two tests can be considered such as strains and crack widths however simply comparing the load-deflection curves of the two tests can provide an overall indication of the performance of the systems. A comparison of the load-deflection curves for Tests #1 and #4 is provided in Figure 4-49.

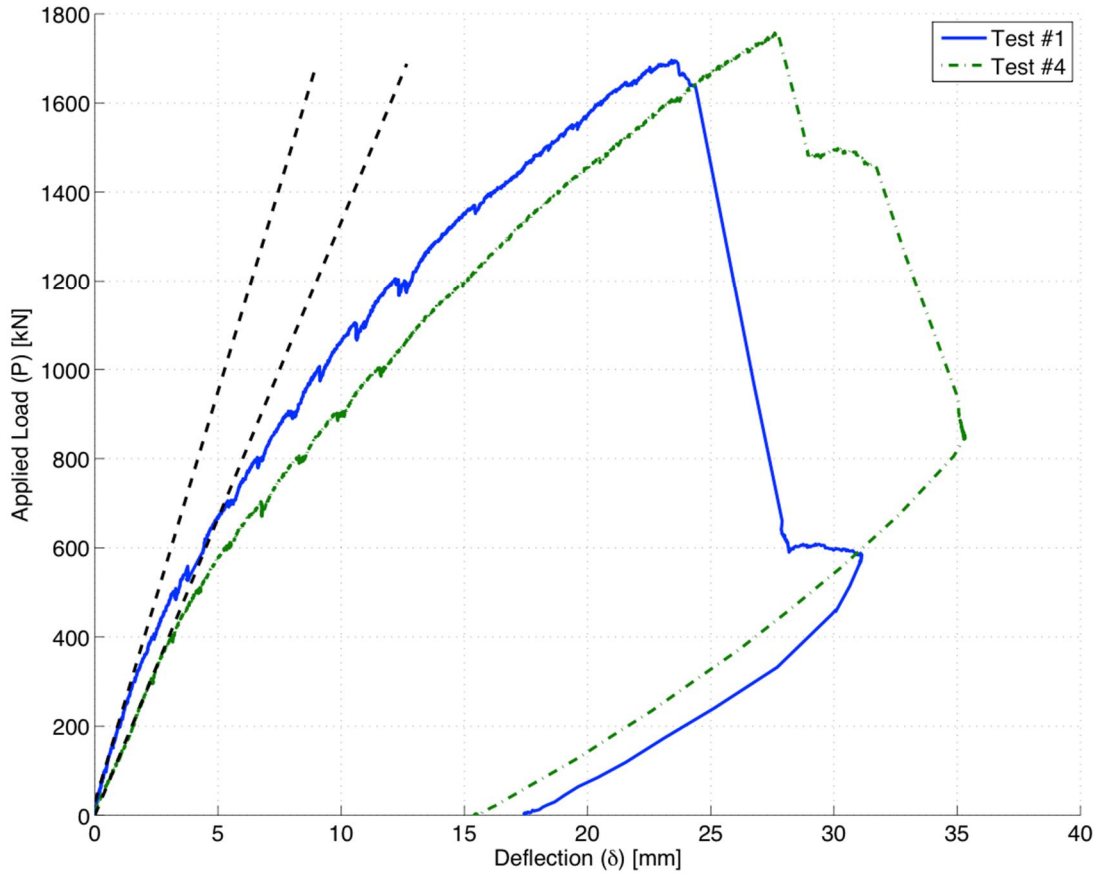

Figure 4-49 – Comparison of Static Tests – Load-Deflection Curves (Tests #1 & #4)

From Figure 4-49, it is evident that the load-deflection curve for Test #4 shows the system having a lower stiffness when loaded at the transverse joint. Due to the higher elastic modulus of UHPC compared to that of HPC, this is counter intuitive but can be likely explained by considering the material properties and loading conditions.

Although no significant joint interface cracking was observed during Test #4, the minimal distance from the point of high load application to the transverse joint likely caused extensive micro-cracking to occur within the joint. As these micro-cracks develop, the steel fibres within the UHPC matrix become engaged serving to provide a more ductile behaviour.

4.8 Yield Line and Punching Shear Analysis of Failure Loads

Three methods were used to predict the ultimate static failure load of the test specimens: yield line analysis, punching shear analysis utilizing AASHTO provisions, and punching shear analysis utilizing FEM PUNCH. A discussion of the analyses is presented herein.

4.8.1 Yield Line Analysis

The yield line analysis is an upper bound method that can be used to predict the ultimate failure load of a reinforced concrete slab. The ultimate load of a slab is estimated by postulating a collapse mechanism that is compatible with its support boundaries. The collapse mechanism is composed of plastic hinge lines, at which it is assumed that the reinforcement has yield. Using either the method of virtual work, or the method of equilibrium, the ultimate load can be predicted. Since the yield line method provides an

upper bound solution, it is necessary to postulate numerous possible collapse mechanisms, with the ultimate slab load being the minimum of that found for the various collapse mechanisms analyzed (Park and Gamble, 2000).

Often times, postulated collapse mechanisms can consist of yield lines inclined to the direction of the slab reinforcement. Johansen developed the Johansen yield line criterion in which the inclined yield line is considered as a series of infinitesimal steps in the x- and y-directions (Johansen, 1943). Assuming that the slab is isotropically reinforced, the ultimate bending capacity of the slab about the inclined yield line (m_{un}) has been generally accepted to be $m_{un} = m_{ux} = m_{uy}$ (Park and Gamble, 2000). Furthermore, in this case, the torsional moment of the slab about the yield line (m_{unt}) is zero. This greatly simplifies the yield line analysis as the principle bending moments (m_{ux} and m_{uy}) acting along the inclined yield line's projected x- and y- directions can be used to determine the ultimate load.

While it is advantageous to employ Johansen's yield line criterion in which $m_{un} = m_{ux} = m_{uy}$ and $m_{unt} = 0$, the derivation of these relationships applies only to isotropically reinforced concrete slabs. In reality, slabs are often orthotropically reinforced, thus modification to the slab is necessary to permit the use of Johansen's yield line criterion. The affinity theorem is frequently used when conducting a yield line analysis as it allows the orthotropic slab to be represented as an isotropic slab by modifying parameters of the orthotropic slab by the coefficient of orthotropy (μ) (Park and Gamble, 2000). The coefficient of orthotropy is commonly taken as the ratio between the ultimate bending

moment resistances in the x- and y-direction, and it is typically < 1. The orthotropic and equivalent isotropic representation of the test specimens is shown in Figure 4-50.

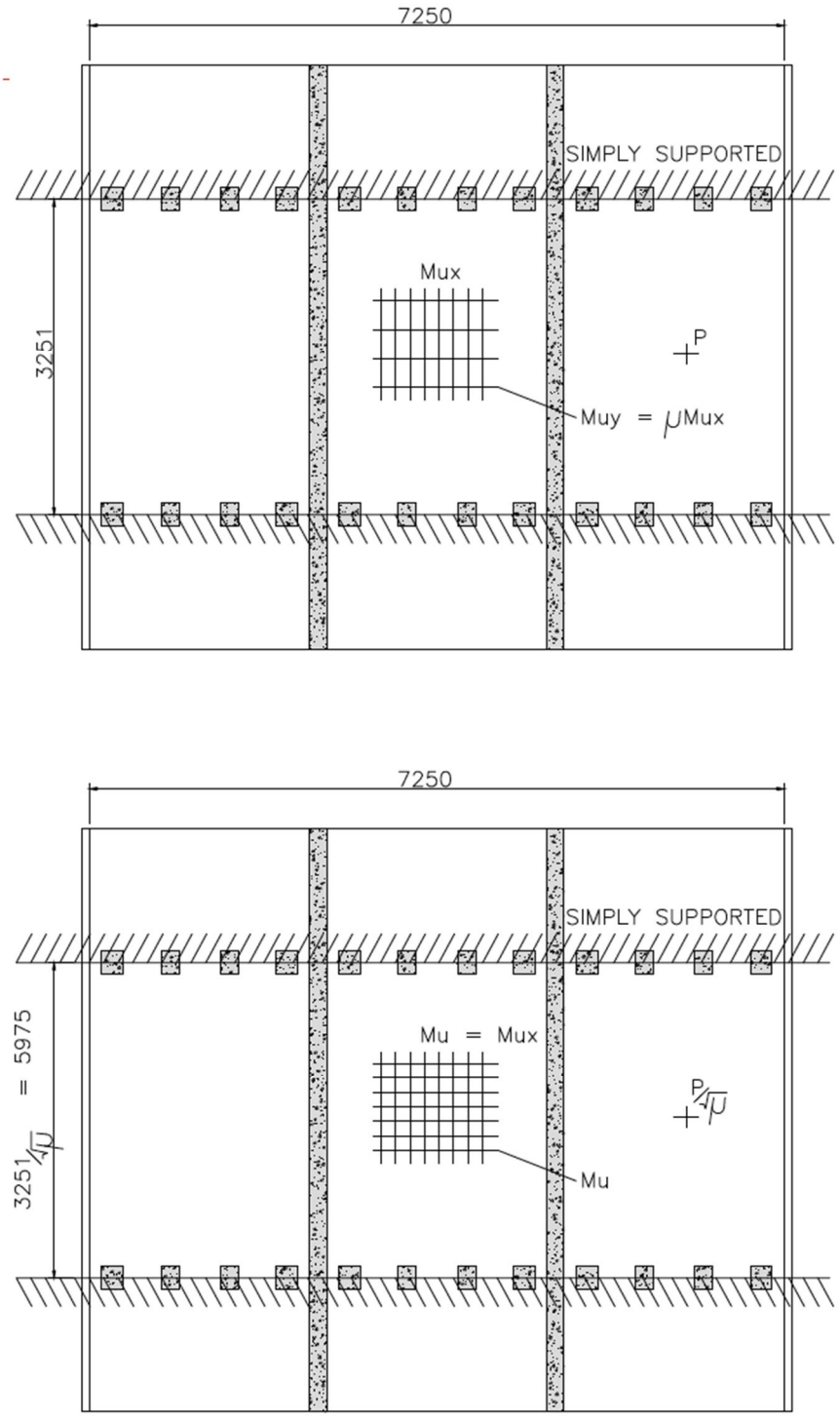

Figure 4-50 – Affine Transformation for Yield Line Analysis

Six different collapse mechanisms were postulated and analyzed assuming that the deck is simply supported along the girder lines and free at the transverse ends. The six modes along with their corresponding ultimate loads are shown in Figures 4-51 and 4-52. Detailed calculations are presented in Appendix C. Modes (a) through (d) represented Test #1 and Modes (e) and (f) represented Test #4. Modes (a) and (e) were the governing failure modes corresponding to Test #1 and Test #4 respectively. The analysis predicted an ultimate load of 945 kN for the load centered within the panel, and 2198 kN for the load adjacent the transverse UHPC joint.

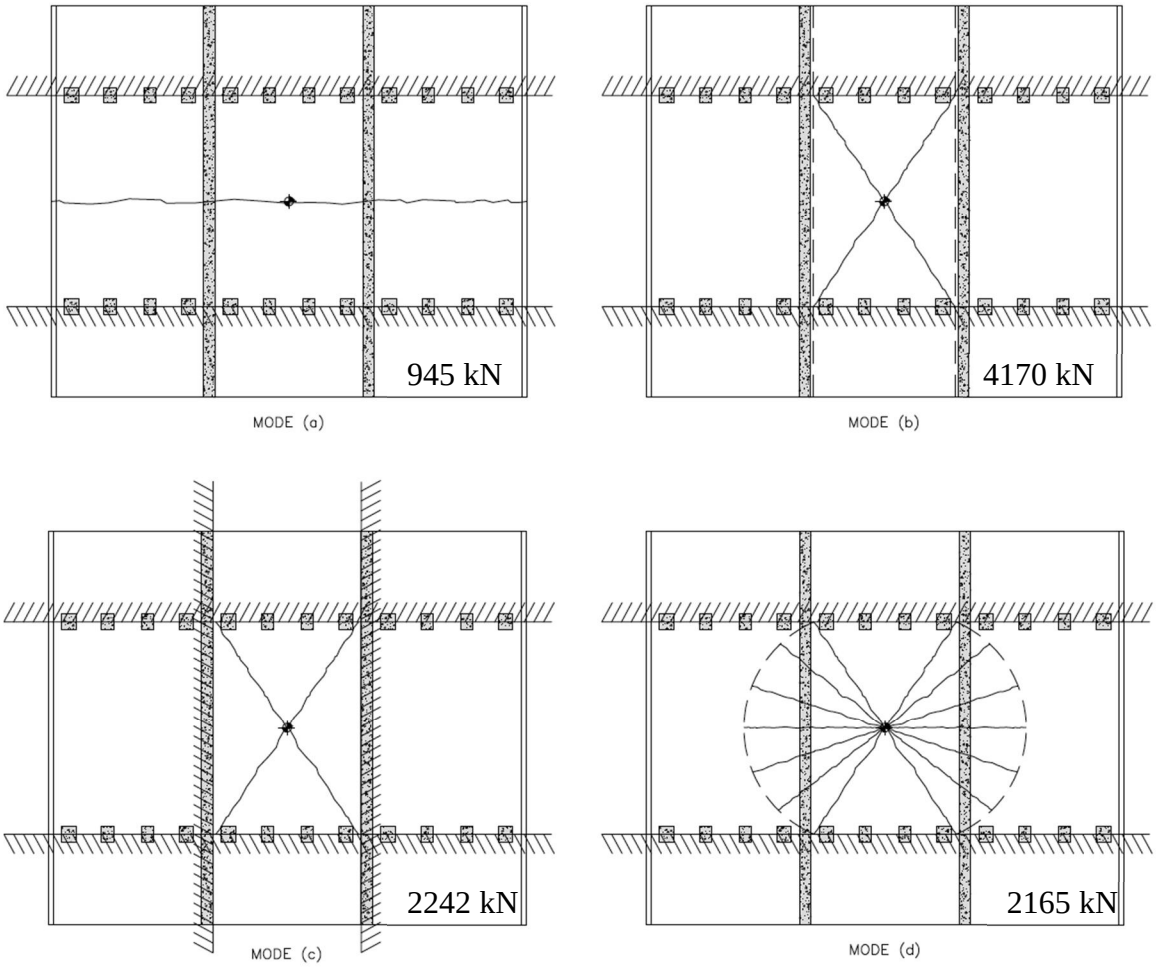

Figure 4-51 – Yield Line Analysis Failure Modes (a) to (d)

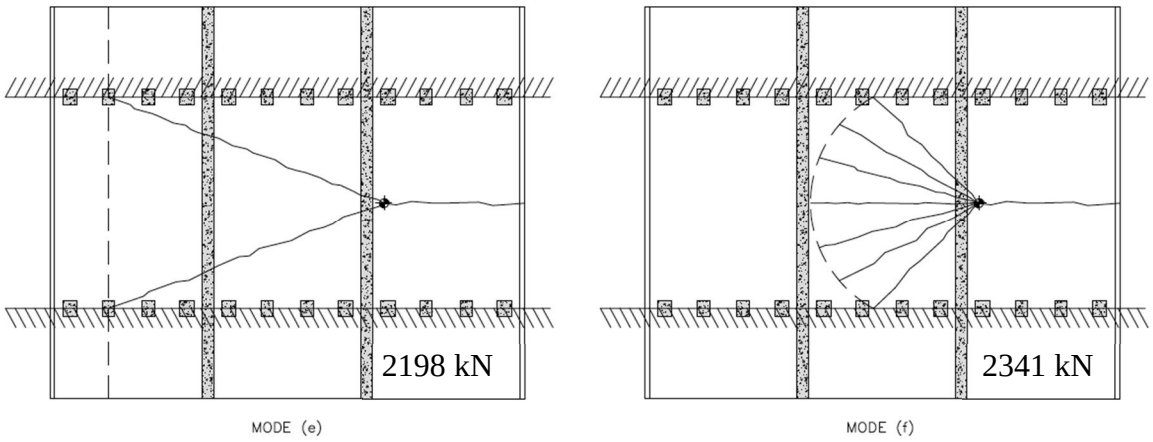

Figure 4-52 – Yield Line Analysis Failure Modes (e) & (f)

As expected, for the case of the load centered on the panel (Test #1), the yield line analysis (Mode (a)) predicted an ultimate load of 945 kN which is less than that observed during testing. It should be noted that the yield line theory provides a good indication of ultimate capacities only when the postulated collapse mechanism forms *without* the development of internal membrane forces. Due to the boundary conditions imposed by the girders, it would be expected that membrane action would develop in a deck of this nature. As discussed in Subsection 4.8.2, the significant observed failure loads resulting in punching shear failures are likely the result of internal arching action, thus explaining why the observed failure loads were higher than the upper bounds suggested by the yield line theory.

On the other hand, for the case of the load adjacent the transverse joint (Test #4), the yield line analysis (Mode (e)) predicted an ultimate load of 2198 kN which is greater than that observed during testing. It should be noted that the yield lines shown in Mode (e) and (f) are the optimized to provide a minimum load and are not similar in nature to the failure mechanism observed during testing.

4.8.2 Punching Shear using PUNCH

It has been well documented that concrete slab-on-girder bridge decks develop an internal arching action that leads to a punching shear failure mode under wheel loads significantly higher than the theoretical flexural failure load of the bridge deck (J. Newhook, A. Mufti, 2003). This theory held true for the PPCPs jointed with UHPC as the test specimen ultimately failed in punching shear as expected. The punching shear failure is shown in Figure 4-53, obtained during the demolition of the test specimen.

Figure 4-53 – Punching Shear Failure of Test Specimen #1 (Cut at Centerline of Panel/Loading Point)

PUNCH is a program developed to predict the behaviour of laterally restrained concrete slab-on-girder bridge decks under wheel loading. While PUNCH was developed specifically for use with the steel-free concrete bridge deck system, it can also be used to model isotropically reinforced concrete deck slabs (J. Newhook, A. Mufti, 2003). Even though the PPCPs used in this research program are neither part of a steel-free deck slab system nor isotropically reinforced, PUNCH has been used to compare the actual performance of the PPCPs with the expected results for a conventional isotropically reinforced concrete deck slab.

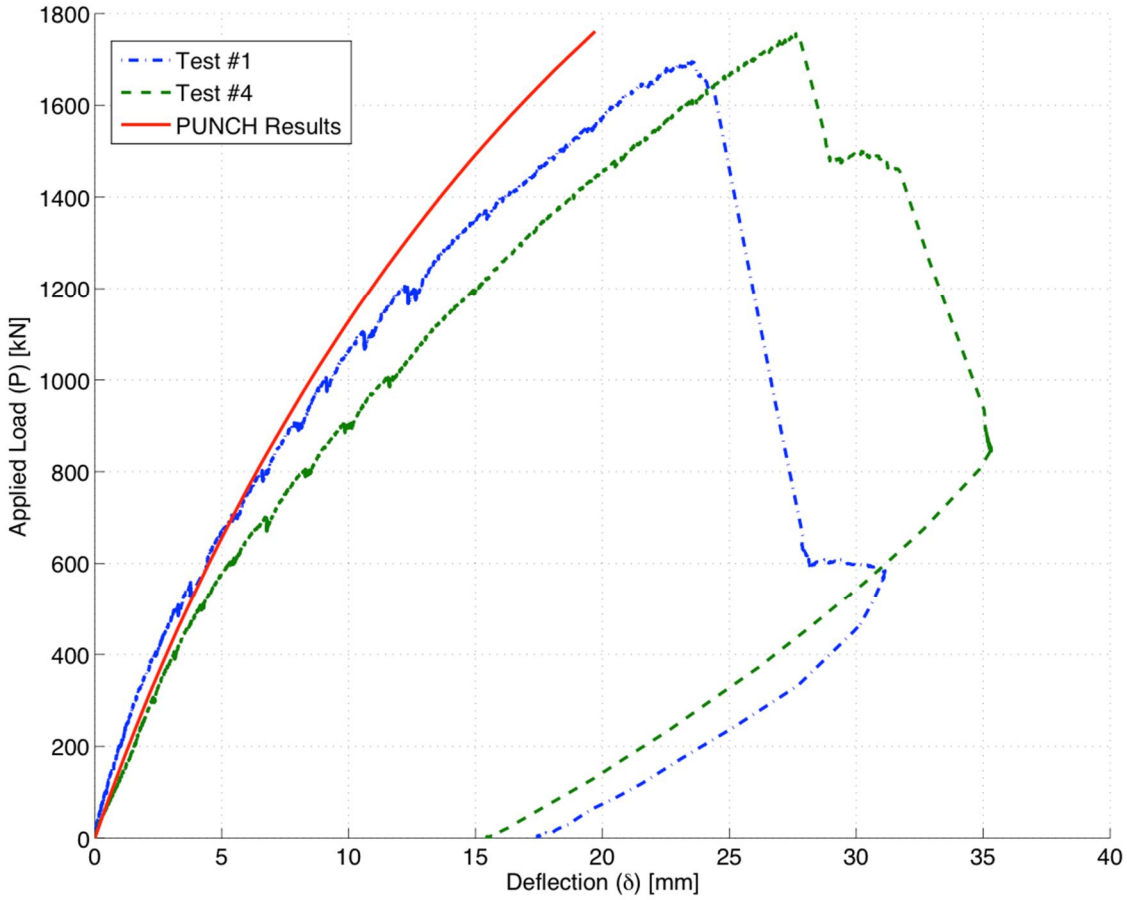

Figure 4-54 – Comparison Between Experimental and Theoretical PUNCH Test Results (Test #1)

As can be seen in Figure 4-54, PUNCH predicted the initial portion of the load deflection curve until approximately 1000 kN well. While the curve from 1000 kN to failure varies slightly, it should be noted that the magnitude of the predicted failure load is very similar and the predicted deflection at failure only varies by approximately 4 mm. The higher stiffness observed in the test specimen at low load levels is likely due to the fact that PUNCH does not take prestressing into account; the PPCPs were each prestressed with six low-relaxation strands. Overall, PUNCH appears to provide a fair indication of the expected performance of PPCP and UHPC systems.

Chapter 5

Conclusions

5.1 Introduction

This research program was undertaken to investigate the static and fatigue performance of full-depth precast bridge deck systems utilizing UHPC as a joint-fill material subjected to negative bending. The following Chapter presents the conclusions of this research.

5.2 Conclusions

The following Sub-sections provide the research program conclusions related to constructability, static performance, and fatigue performance.

5.2.1 Literature Review

1. The use of UHPC as a joint fill material was well documented, especially in Ontario, Canada by the Ministry of Transportation of Ontario (MTO). Although it has been widely used on simply supported structures, only one truly continuous bridge structure – the Keg Creek demonstration bridge – with UHPC joints was noted at this time. The Keg Creek Bridge ultimately required a post-tensioning retrofit across the transverse UHPC joint when laboratory testing showed unsatisfactory performance of joint when subjective to negative moment.
2. Current bridge code provisions for UHPC in the AASHTO LRFD specifications and in CAN/CSA S6-06 were studied. Although the use of precast bridge deck panels are mentioned, no significant design provisions exist for such systems. In addition, the code is silent on the use of UHPC as a joint fill material.

5.2.2 Constructability

1. The installation of the shear studs prior to the placement of the panels is not recommended, as it was not possible to install the panels without damage due to the geometric conflicts presented in Sub-section 3.2.5.
2. Mixing of the UHPC material required the use of specialized concrete mixers to properly mix the UHPC material. The logistics and procurement process for the specialized mixers must be considered in advance for any future project.
3. The UHPC surface finish obtained on the test specimens constructed as part of this research program was not desirable. A thin crust overtop an air layer developed in the UHPC during curing. Removal of the thin UHPC crust revealed apparently sound UHPC, however no testing was performed on the in-situ material to verify its durability. This crust should not be an issue if the structure is to receive an asphaltic riding surface.

5.2.2 Static Performance

1. The response of the system during Test #1 (load centered on panel) was very similar to that of Test #4 (load adjacent transverse joint). In both cases, the joints transferred stresses from one panel to the next in a satisfactory manner.
2. Both Tests #1 and #4 failed in a punching shear failure. This is the same failure mode that would be expected for a conventional monolithic cast-in-place deck. The fact that Test #4 (load adjacent transverse joint) failed in punching shear is very favorable as the punch cone extended well into the adjacent panel. Rather

than simply shearing at the UHPC-PPCP interface, the transverse joint successfully transferred the significant shear stresses.

3. Overall, both test specimens displayed the structural performance required by current bridge codes with respect to load carrying capacity. The system sustained a failure load of approximately 16 times the design wheel load of 108 kN for the HSS30 design vehicle often used in Manitoba (modified AASHTO MSS 27); or approximately 23 times the design wheel load of 72.5 kN for the HL-93 design vehicle specified by AASHTO.

5.2.3 Fatigue Performance

1. Test #2 (load adjacent transverse joint) was simply a trial test and the specimen was only subjected to approximately 575,000 cycles. Throughout testing, minimal stiffness degradation and energy dissipation were observed indicating that the specimen was far from failure when the test was terminated.
2. Test #3 (load adjacent transverse joint) failed at approximately 1,220,000 cycles due to fatigue of the shear studs. Throughout testing, minimal stiffness degradation and energy dissipation were observed indicating that the specimen was far from failure. Due to the testing method, the shear studs prematurely failed in fatigue and the test was terminated. Had the shear studs not failed, it is expected that the PPCP and UHPC system would have reached 2,000,000 fatigue cycles without failing. In order to improve the overall fatigue performance of the system, the diameter and/or number of shear studs per shear pocket would have to be increased.

5.2.4 Analysis

1. The ultimate capacities of the test specimens were compared to those calculated using the yield line analysis. The yield line analysis is allowed by the bridge codes as a method of verifying adequate structural capacity. It was determined that the governing yield line failure mode predicted a capacity much lower than that observed in testing. The corresponding yield line failure mode was also fundamentally different from the punching shear failure mode observed in testing.
2. The bridge sustained a failure load higher than its theoretical bending capacity due to the presence of internal arching action. Although the span between girders was quite large, significant arching was still developed.
3. PUNCH was utilized to predict the load-deflection curve and ultimate failure load of the test specimens. PUNCH's predictions were very similar to the performance observed in testing with a predicted failure load within 5% of that observed. Overall, PUNCH provides a very good prediction of the systems performance.

References

AASHTO. (2007). *LRFD Bridge Design Specifications.* American Association of State Highway and Transportation Officials.

AFGC. (2012). *Ultra High Performance Fibre-Reinforced Concretes - Interim Recommendations.* Association Francaise de Genie Civil. AFGC.

Ahlborn, T. M.; Peuse, E. J.; Misson, D. I. (2008). *Research Report RC-1525 Ultra-High Performance Concrete for Michigan Bridges Material Performance - Phase 1.* Michigan Department of Transportation, Construction and Technology Division. Houghton: MDOT.

ASCE. (2013). *2013 Report Card for America's Infrastructure.* American Society of Civil Engineers

Badie, S. S.; Tadros, M. K. (2008). *NCHRP Report 584 Full-Depth Precast Concrete Bridge Panel Systems.* Final , NCHRP, Washington D.C.

Badie, S. S.; Tadros, M. K.; Usdan, R .M M. (2009, April). Full-Depth, Precast Concrete Bridge Deck Panel Systems. *Concrete International* , 53-58.

Blais, Y. P.; Couture, M. (1999, Sept-Oct). Precast, Prestressed Pedestrian Bridge - World's First Reactive Powder Concrete Structure. *PCI Journal* , 60-71.

CAN/CSA. (2006). *CAN/CSA S6-06 Canadian Highway Bridge Design Code.* Canadian Standards Association.

Chavel, B. (2012). *FHWA-IF-12-052 Steel Bridge Design Handbook: Bridge Deck Design.* Technical Report, Federal Highway Administration, Washington D.C.

Federation of Canadian Municipalities. (2012). *Canadian Infrastructure Report Card - Volume 1: 2012 Municipal Roads and Water Systems.* Project Steering Committee.

Fowler, J. (2008). Full-Depth Precast Concrete Bridge Deck Construction. *Bridges - Links to a Sustainanle Future - 2008 Annual Conference of the Transportation Association of Canada.* Toronto, ON: Transportation Association of Canada.

Graybeal, B. (2006). *FHWA-HRT-06-103 Material Property Characterization of Ultra-High Performance Concrete.* Federal Highway Administration . McLean: FHWA.

Graybeal, B. (2010). *FHWA-HRT-11-023 Behaviour of Field-Cast Ultra-High Performance Concrete Bridge Deck Connections Under Cyclic and Static Loading.* Federal Highway Administration. McLean: FHWA.

Hansen, L.; Jensen, B. (1999). A New Building System Using Joints of Ultra-High Strength Fiber Reinforced Concrete. *International Conference on Innovation in Concrete Structures: Design and Construction* (pp. 544-552). Dundee: Thomas Telford Ltd.

Hartwell, D. (2011). *Laboratory Testing of Ultra High Performance Concrete Deck Joints for use in Accelerated Bridge Construction.* M.Sc. Thesis, Iowa State University, Civil and Environmental Engineering.

Issa, M. A.; Yousif, A. A.; Issa, M. A. (2000, May-June). Experimental Behaviour of Full-Depth Precast Concrete Panels for Bridge Rehabilitation. *ACI Structural Journal* , 397-407.

Issa, M. A.; Yousif, A. A.; Issa, M. A.; Kaspar, I. I.; Khayyat, S. Y. (1995, May-June). Field Performance of Full Depth Precast Concrete Panels in Bridge Deck Reconstruction. *PCI Journal* , 82-94.

Johansen K. W. (1943) Brudlinieteorier, Copenhagen: Gjellerup Forlag. (English translation: Yield-Line Theory, London: Cement and Concrete Association, 1962).

Kenedi, W. (n.d.). Prefabricated Bridge Replacements. Ontario, Canada: Ministry of Transportation .

Kosmatka, S. H.; Kerkhoff, B.; Panarese, W. C. (2011). *Design and Control of Concrete Mixtures - The Guide to Application, Methods, and Materials* (Eighth Canadian Edition ed.). Ottawa, ON, Canada: Cement Association of Canada.

Lafarge Ductal. (2015). *Ductal Operating Procedure 5.4 - Cylinder End Grinding.* Version 2.

Markowski, S. M. (2005). *Experimental and Analytical Study of Full-Depth Precast/Prestressed Concrete Deck Panels for Highway Bridges.* University of Wisconsin-Madison, Civil and Environmental Engineering. University of Wisconsin-Madison.

MMM Group Limited. (2012). *Engineering Services for Preliminary Design of MAJOR REHABILITATION WORKS for the Bridge Structure on PTH 23 over Red River (Bridge Site No.: 271-00).* Preliminary Design Report, Winnipeg, MB.

Newhook, J.; Mufti, A. (2003). *PUNCH - User and Theoretical Manual.* ISIS Canada Research Network. Winnipeg: ISIS Canada Research Network.

Park, R.; Gamble, W. L. (2000). *Reinforced Concrete Slabs - Second Edition.* John Wiley & Sons, Inc.

Perry, V. H.; Royce., M. (2010). Innovative Field-Cast UHPC Joints for Bridge Decks (Side-by-Side Deck Bulb Tees), Village of Lyons, New York: Design, Prototyping, Testing and Construction. *3rd fib International Conference 2010.* Perry and Royce.

Perry, V. H.; Scalzo, P.; Weiss, G. (2007). Innovative Field Cast UHPC Joints for Precast Deck Panel Bridge Superstructures - CN Overhead Bridge at Rainy Lake, Ontario. *2007 Concrete Bridge Conference*.

PCI. (2011). *State-of-the-Art Report on Full-Depth Precast Concrete Bridge Deck Panels.* Chicago, IL: Precast Prestressed Concrete Institute.

Russell, H.; Graybeal, B. (2013). *FHWA-HRT-13-060 - Ultra-High Performance Concrete: A State-of-the-art Report for the Bridge Community.* Federal Highway Administration. McLean: FHWA.

Sullivan, S. (2007). *Construction and Behaviour of Precast Bridge Deck Panel Systems.* Virginia Polytechnic Institute and State University, Civil and Environmental Engineering. Virginia Polytechnic Institute and State University.

TRB. (2013). *A Toolkit for Accelerated Bridge Construction* . SCHRP 2. Washinton D.C.: Transportation Research Board.

Appendix A

UHPC Product Data Sheet

PRODUCT DATA SHEET

JS1000

Ductal®

LAFARGE

bringing materials to life™

JS1000

field-cast joint fill solutions for precast deck panel bridges

Ductal® JS1000 offers a combination of superior properties including strength, durability, fluidity and increased bond capacity. By utilizing these superior properties in conjunction with precast deck panels, engineers can create optimized solutions for advanced precast bridge deck systems – with simplified fabrication and installation processes.

Reinforced with steel fibers, Ductal® JS1000 is significantly stronger than conventional concrete and performs better in terms of abrasion and chemical resistance, freeze-thaw, carbonation and chloride ion penetration.

Because of its optimized gradation of the raw material components, Ductal® is also denser than conventional concrete. This "denseness", along with nanometer sized non-connected pores throughout its cementitious matrix, attributes to its remarkable imperviousness and durability against adverse conditions or aggressive agents.

PHYSICAL PROPERTIES

Characteristic Values for Design						
	Test Data					
	Mean		Standard Deviation		Design Values	
	MPa	psi	MPa	psi	MPa	psi
Compression	140	20,000	10	1,400	100	14,500
Flexural	30	4,300	5	700	-	-
Direct Tension f_{tj}	8	1,160	1	145	5	725
	GPa	ksi	GPa	ksi	GPa	ksi
Youngs Modulus	50	7,200	2	300	45	6,500

JS1000

DURABILITY

• Carbonation penetration depth	<0.5 mm
• Freeze/thaw (after 300 cycles)	100%
• Salt-scaling	<0.10 g/m^2

OTHER PROPERTIES

• Density	2.4 – 2.6 S.G.
• Capillary porosity (>10mm)	<1%
• Total porosity	2 – 6%
• Creep coefficient	0.2-0.5

COMPONENTS

A) Premix - silica fume, ground quartz, sand, cement
B) High tensile steel fibers - 0.2 mm (0.008 in) diameter x 14 mm (0.5 in) long (>2000 MPa/ 290 psi)
C) Admixture - high range water reducer/ 3rd generation
+ Water and/or ice

BATCHING

High shear mixers and an ambient temperature above 16ºC (60ºF) are recommended to successfully produce Ductal® JS1000. Onsite technical assistance by a Lafarge representative is recommended.

PLACING

Ductal® JS1000 can be placed by pouring with the use of a bucket, wheelbarrow or buggy. Any exposed Ductal® surfaces should be covered with poly or vapor barriers to prevent surface dehydration.

JOINT REINFORCING

To minimize any corrosion potential of the reinforcing between the precast panel and joints, non-corrosive rebar (such as GFRP or stainless steel) may be used. Black rebar reinforcement may also be utilized for bottom mat connection.

DESIGN

The high strength of Ductal® JS1000 allows for reduced joint widths. When designing a joint using Ductal® JS1000, the characteristic design values can be reached within 96 hours of casting -- as long as ambient temperatures above 16ºC (60ºF) are ensured. Please contact a Lafarge representative when designing joints with Ductal® JS1000.

Add value with Ductal® JS1000

- improved durability
- increased usage life
- superior freeze/thaw resistance
- impact & abrasion resistance
- reduced joint width and complexity
- dimensional stability
- flexural strength
- lower permeability
- superior toughness
- low chloride ion diffusion
- ductility
- faster construction
- improved resistance to continuous flexing across the joints (from truck loads)
- reduced maintenance
- extremely low porosity
- reduced traffic disruption & risk
- cost effective

Lafarge Canada Inc.
1200, 10655 Southport Road S.W.
Calgary, Alberta, Canada T2W 4Y1
Email: ductal@lafarge-na.com • Tel: 403-271-9110
Toll free: 1-866-238-2825 • www.imagineductal.com

25% Post Consumer

LAFARGE

This page intentionally left blank

Appendix B

Materials Testing Results

Table B.1 – UHPC Compression Test Results for TS1

Cylinder Age at Test (Days)	Cylinder ID Number	Levelness (mm)[1]	Height (mm)	Failure Load (lbf)	Compressive Strength (MPa)	Average Compressive Strength (MPa)	SD	CV
7	4	-[2]	-[2]	131090	128	145	3.90	2.7
	8	0.32/0.37	149	151620	148			
	15	0.06/0.26	148	144100	141			
	19	0.45/0.36	148	150200	147			
14	1	0.20	146	159250	155	166	7.54	4.5
	5	0.64/0.52	145	172050	168			
	6	0.36/0.33	148	175760	171			
	20	0.54/0.78	147	175270	171			
28	3[3]	0.35/0.32	148	193850	189	181	14.23	7.9
	10[3]	0.22/0.28	150	201580	197			
	14[3]	0.42/0.38	148	178520	174			
	18[3]	0.14/0.17	146	169310	165			
72	7[4]	0.21/0.10	150	189450	185	188	6.20	3.3
	9[4]	0.09/0.11	148	187760	183			
	11	0.12/0.06	148	201930	197			
	17	0.52/0.49	147	191600	187			
268	2	0.33/0.37	145	220230	215	218	4.50	2.1
	12	0.47/0.40	149	226390	221			
	13	0.38/0.37	147	218430	213			
	16	0.58/0.48	147	227910	222			

Notes:

[1]The measured levelness is expressed as the difference in cylinder height between the center of the cylinder end face and a random point on the end face found to provide the largest difference. A measurement for each cylinder end is provided. The max allowable between the end face center and edge is 0.33 mm corresponding to 0.5°.

[2]Cylinder was badly damaged during grinding. It was still tested in compression but the result was not taken into account in calculations.

[3]Tested by a different machine operator unfamiliar with testing of UHPC. Conformance with the testing specifications cannot be guaranteed.

[4]Cylinder had chipped edges from grinding process. Result still considered in calculations.

Table B.2 – UHPC Compression Test Results for TS2

Cylinder Age at Test (Days)	Cylinder ID Number	Levelness (mm)[1]	Height (mm)	Failure Load (lbf)	Compressive Strength (MPa)	Average Compressive Strength (MPa)	SD	CV
36	16	0.12/0.16	141	192470	188	172	17.05	9.9
	10	0.26/0.26	142	174730	170			
	3	0.11/0.11	132	188290	184			
	15	0.03/0.11	136	151050	147			
	13	0.11/0.14	137	140820	137			
	5	0.22/0.26	143	185760	181			
	14	0.07/0.13	142	181160	177			
	4	0.09/0.12	142	179970	176			
	9	0.37/0.38	144	193960	189			
	18	0.09/0.10	141	179530	175			
97	1	0.21/0.25	139	200570	196	188	12.44	6.6
	2	0.31/22	139	202550	198			
	6	0.28/0.15	139	170270	166			
	7	0.31/0.31	142	195570	191			
	8	0.07/0.10	142	176660	172			
	11	0.06/0.12	144	188530	184			
	12	0.11/0.14	142	189690	185			
	17	0.09/0.16	143	208370	203			
	19	0.16/0.17	141	202790	198			

Notes:

[1]The measured levelness is expressed as the difference in cylinder height between the center of the cylinder end face and a random point on the end face. A measurement for each cylinder end is provided. The max allowable between the end face center and edge is 0.33 mm corresponding to 0.5°.

Table B.3 – UHPC QC Test Results for TS1[1]

Batch #	Batch Time		Temperature (°C)		Flow (mm)		Comments
	Start	Finish	Ambient	Ductal	Static	Dynamic	
1	10:28 AM	10:54 AM	17	27	235	245	NA
2	11:42 AM	12:20 PM	18	27	240	250	Cast cylinders, fiber dose may have been 4 kg short
3	1:27 PM	2:04 PM	18	28	235	245	Half batch

Notes:
[1]Tests conducted by qualified UHPC material supplier and report submitted to researchers.

Table B.4 – UHPC QC Test Results for TS2[1]

Batch #	Batch Time		Temperature (°C)		Flow (mm)		Comments
	Start	Finish	Ambient	Ductal	Static	Dynamic	
1	9:14 AM	9:40 AM	19	27	240	250	NA
2	10:28 AM	10:50 AM	20	25	240	250	Cast cylinders

Notes:
[1]Tests conducted by qualified UHPC material supplier and report submitted to researchers.

Table B.5 – PPCP Compression Test Results for Panels W1 and W2

Cylinder Age at Test (Days)	Cylinder ID Number	Failure Load (lbf)	Compressive Strength (MPa)	Average Compressive Strength (MPa)	SD	CV
</= 1[1]	W1-1c	-	33.8	N/A	N/A	N/A
	W1-2c	-	34.3			
	W1-3c	-	37.5			
	W1-4c	-	38.5			
	W1-5c	-	37.7			
	W2-1c	-	32.4	N/A	N/A	N/A
	W2-2c	-	34.8			
	W2-3c	-	36.8			
	W2-4c	-	37.1			
	W2-5c	-	38.3			
7[2]	W1-6c	-	80.1	N/A	N/A	N/A
	W2-6c	-	72.9	N/A	N/A	N/A
28	W1-7c	155360	85.4	71.7	18.56	5.35
	W1-8c	92050	50.6			
	W1-9c	144040	79.2			
	W2-7c	150240	82.6	82.3	0.43	25.87
	W2-8c	148740	81.8			
	W2-9c	149820	82.4			
482	W1-10c	177970	97.9	101.2	3.65	3.61
	W1-11c	191160	105.1			
	W1-12c	183210	100.7			
	W2-10c	161850	89.0	83.5	15.2	18.20
	W2-11c	120630	66.3			
	W2-12c	173170	95.2			

Notes:
[1]Tests conducted by PPCP manufacturer at various times throughout the day to verify release strength; no statistical data is provided for these tests as the concrete specimens were not all the same age.
[2]Tests by PPCP manufacturer.

Table B.6 – PPCP Compression Test Results for Panels E1 and E2

Cylinder Age at Test (Days)	Cylinder ID Number	Failure Load (lbf)	Compressive Strength (MPa)	Average Compressive Strength (MPa)	SD	CV
</= 1[1]	E1-1c	-	31.3	N/A	N/A	N/A
	E1-2c	-	36.5			
	E1-3c	-	35.9			
	E1-4c	-	36.1			
	E2-1c	-	28.9	N/A	N/A	N/A
	E2-2c	-	33.8			
	E2-3c	-	35.4			
	E2-4c	-	35.0			
	E2-5c	-	35.7			
7[2]	E1-6c	-	63.3	N/A	N/A	N/A
	E2-6c	-	68.8	N/A	N/A	N/A
28	E1-7c	148250	81.5	81.3	2.52	3.10
	E1-8c	152240	83.7			
	E1-9c	143110	78.7			
	E2-7c	134050	73.7	75.1	1.70	2.27
	E2-8c	135870	74.7			
	E2-9c	140090	77.0			
419	E1-10c	169280	93.1	92.8	3.37	3.64
	E1-11c	174600	96.0			
	E1-12c	162360	89.3			
480	W2-10c	150100	82.5	77.0	7.85	10.19
	W2-11c	129920	71.4			

Notes:
[1]Tests conducted by PPCP manufacturer at various times throughout the day to verify release strength; no statistical data is provided for these tests as the concrete specimens were not all the same age.
[2]Tests performed by PPCP manufacturer.

Table B.7 – PPCP Compression Test Results for Panels C1 and C2

Cylinder Age at Test (Days)	Cylinder ID Number	Failure Load (lbf)	Compressive Strength (MPa)	Average Compressive Strength (MPa)	SD	CV
</= 1[1]	C1-1c	-	35.0	N/A	N/A	N/A
	C1-2c	-	36.9			
	C1-3c	-	37.8			
	C2-1c	-	38.1	N/A	N/A	N/A
	C2-2c	-	39.4			
	C2-3c	-	38.4			
7[2]	C1-4c	-	77.7	N/A	N/A	N/A
	C2-4c	-	76.1	N/A	N/A	N/A
28	C1-5c	142670	78.4	75.2	5.56	7.38
	C1-6c	125180	68.8			
	C1-7c	142690	78.5			
	C2-5c	137210	75.4	74.0	4.62	6.24
	C2-6c	141510	77.8			
	C2-7c	125280	68.9			
476[3]	C2-8c	161110	88.6	89.6	3.57	3.98
	C2-9c	157620	86.7			
	C2-10c	170200	93.6			

Notes:

[1]Tests conducted by PPCP manufacturer at various times throughout the day to verify release strength; no statistical data is provided for these tests as the concrete specimens were not all the same age.

[2]Tests performed by PPCP manufacturer.

[3]C1 concrete cylinders misplaced therefore no long-term compressive strength results provided.

Table B.8 – PPCP Splitting Tension Test Results for Panels W1 and W2

Cylinder Age at Test (Days)	Cylinder ID Number	Failure Load (lbf)	Splitting Tensile Strength (MPa)	Average Splitting Tensile Strength (MPa)	SD	CV
14	W1-1t	36370	5.0	5.3	0.49	9.21
	W1-2t	42470	5.8			
	W1-3t	36320	5.0			
	W2-1t	32110	4.4	4.7	0.45	9.54
	W2-2t	32990	4.5			
	W2-3t	38190	5.2			
28	W1-4t	40920	5.6	5.7	0.18	3.09
	W1-5t	43130	5.9			
	W1-6t	40880	5.6			
	W2-4t	45010	6.2	6.1	0.54	8.95
	W2-5t	47670	6.6			
	W2-6t	39890	5.5			
482	W1-7t	37590	5.2	5.5	0.35	6.39
	W1-8t	40300	5.5			
	W1-9t	42730	5.9			
	W2-7t	35610	4.9	4.9	0.15	2.95
	W2-8t	35060	4.8			
	W2-9t	37110	5.1			

Table B.9 – PPCP Splitting Tension Test Results for Panels E1 and E2

Cylinder Age at Test (Days)	Cylinder ID Number	Failure Load (lbf)	Splitting Tensile Strength (MPa)	Average Splitting Tensile Strength (MPa)	SD	CV
14	E1-1t	39740	5.5	5.7	0.49	8.55
	E1-2t	45710	6.3			
	E1-3t	39370	5.4			
	E2-1t	34480	4.7	5.1	0.34	6.72
	E2-2t	39300	5.4			
	E2-3t	38070	5.2			
28	E1-4t	39150	5.4	5.8	0.52	9.05
	E1-5t	40910	5.6			
	E1-6t	46460	6.4			
	E2-4t	34320	4.7	4.9	0.38	7.62
	E2-5t	34200	4.7			
	E2-6t	38990	5.4			
480	E1-7t	41000	5.6	5.4	0.21	3.86
	E1-8t	38320	5.3			
	E1-9t	38550	5.3			
	E2-7t	32320	4.4	4.8	0.38	7.79
	E2-8t	35750	4.9			
	E2-9t	37750	5.2			

Table B.10 – PPCP Splitting Tension Test Results for Panels C1 and C2

Cylinder Age at Test (Days)	Cylinder ID Number	Failure Load (lbf)	Splitting Tensile Strength (MPa)	Average Splitting Tensile Strength (MPa)	SD	CV
14	C1-1t	38940	5.4	5.4	0.05	0.90
	C1-2t	39630	5.4			
	C1-3t	39420	5.4			
	C2-1t	33050	4.5	4.6	0.26	5.66
	C2-2t	35890	4.9			
	C2-3t	32260	4.4			
28	C1-4t	40450	5.6	5.3	0.36	6.90
	C1-5t	38960	5.4			
	C1-6t	35320	4.9			
	C2-4t	31500	4.3	4.6	0.45	9.82
	C2-5t	31110	4.3			
	C2-6t	36940	5.1			
476[1]	C2-7t	38910	5.3	5.0	0.98	19.69
	C2-8t	41440	5.7			
	C2-9t	28050	3.9			

Notes:
[1]C1 concrete cylinders misplaced therefore no long-term splitting tensile strength results provided.

Appendix C

Yield Line Theory Analysis

MODE (a)

Diagram:

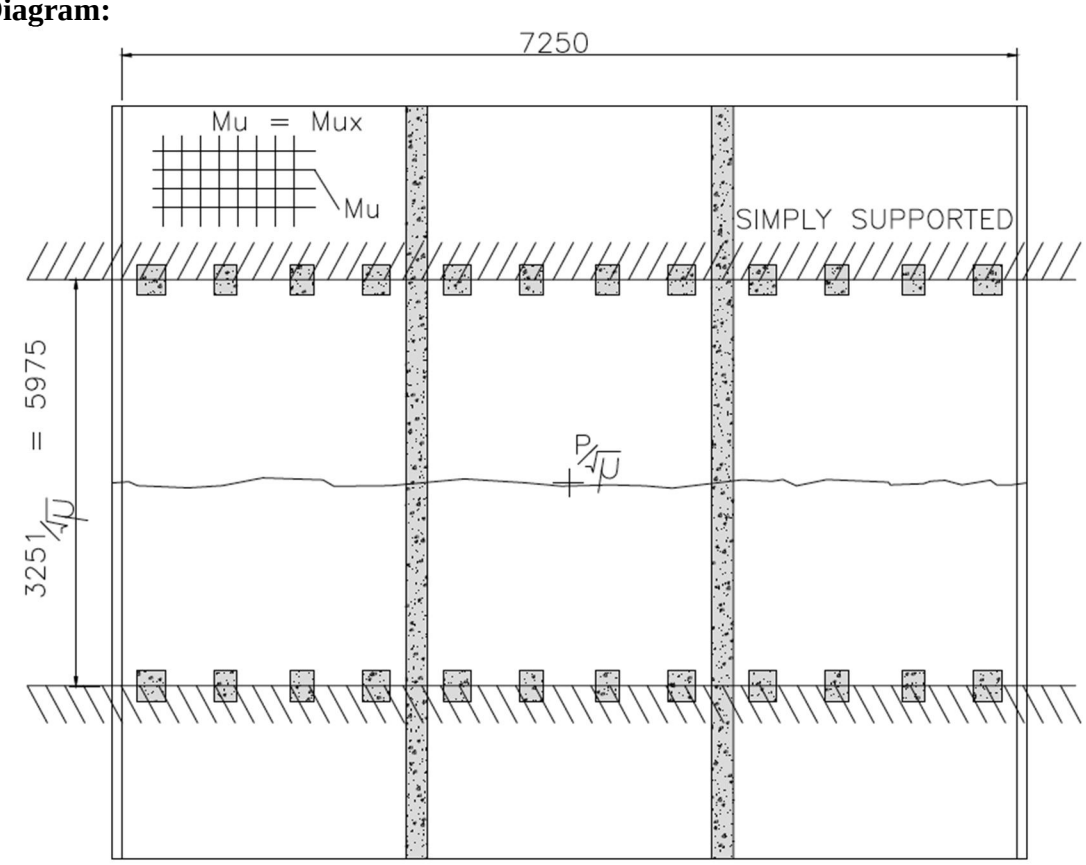

Internal Work:

$$\boldsymbol{Internal\ work = 2 * M_u * L_y * \frac{\delta}{0.5 * L_x}}$$

External Work:

$$\boldsymbol{External\ work = \frac{P}{\sqrt{\mu}} * \delta}$$

Where:

$$\boldsymbol{M_{ux} = 358\ kNm/m}$$
$$\boldsymbol{M_{uy} = 106\ kN\ m/m}$$

$$\boldsymbol{\mu = \frac{M_{uy}}{M_{ux}} = 0.296}$$

$$\boldsymbol{M_u = M_{ux}}$$

$$L_x = 5.975\ m$$
$$L_y = 7.250\ m$$

Equate *Internal* and *External Work* → solve for P:

$$2 * M_u * L_y * \frac{\delta}{0.5 * L_x} = \frac{P}{\sqrt{\mu}} * \delta$$

Therefore:

$$P = 945\ kN$$

MODE (b)

Diagram:

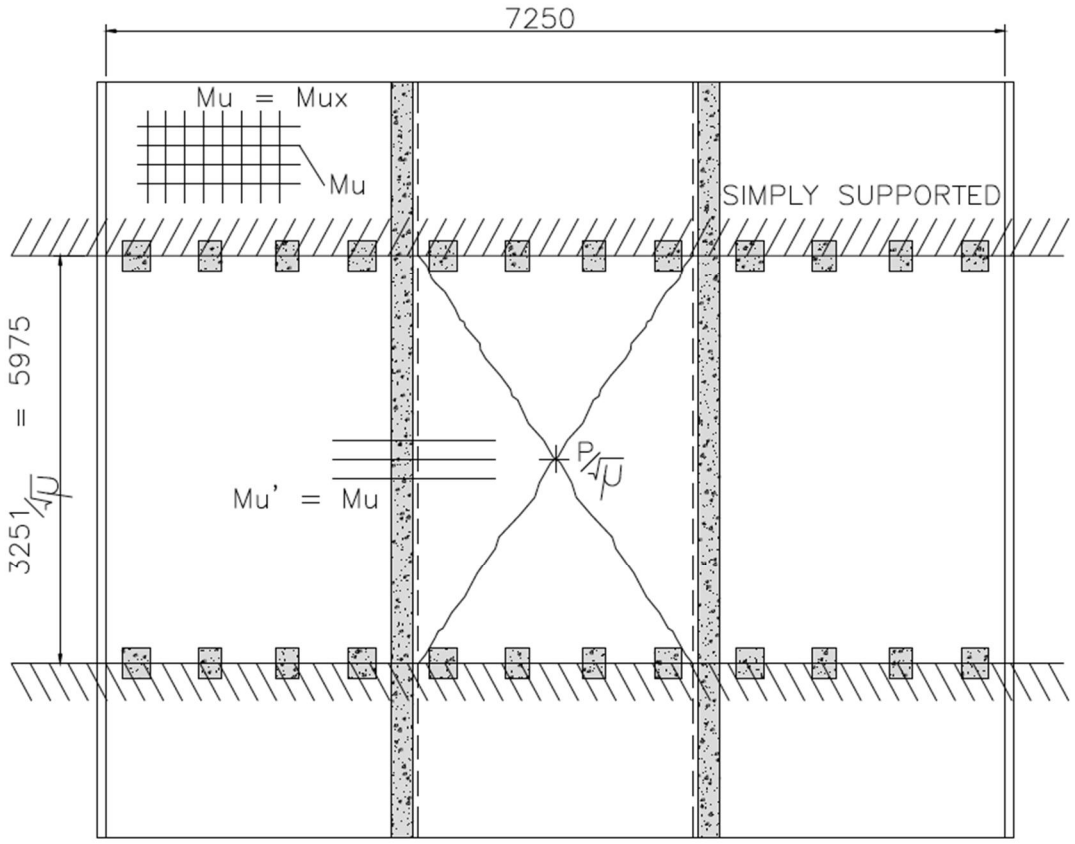

Internal Work:

$$\boldsymbol{Internal\ work = 2 * M_u * L_y * \frac{\delta}{0.5 * L_x} + 2 * (M_{u'} + M_u) * L_x * \frac{\delta}{0.5 * L_y}}$$

External Work:

$$\boldsymbol{External\ work = \frac{P}{\sqrt{\mu}} * \delta}$$

Where:

$$\boldsymbol{M_{ux} = 358\ kNm/m}$$
$$\boldsymbol{M_{uy} = 106\ kN\ m/m}$$

$$\boldsymbol{\mu = \frac{M_{uy}}{M_{ux}} = 0.296}$$

$$\boldsymbol{M_u = M_{u'} = M_{ux}}$$

$$L_x = 5.975\ m$$
$$L_y = 2.415\ m$$

Equate *Internal* and *External Work* → solve for P:

$$2 * M_u * L_y * \frac{\delta}{0.5 * L_x} + 2 * (M_{u'} + M_u) * L_x * \frac{\delta}{0.5 * L_y} = \frac{P}{\sqrt{\mu}} * \delta$$

Therefore:

$$P = 4170\ kN$$

MODE (c)

Diagram:

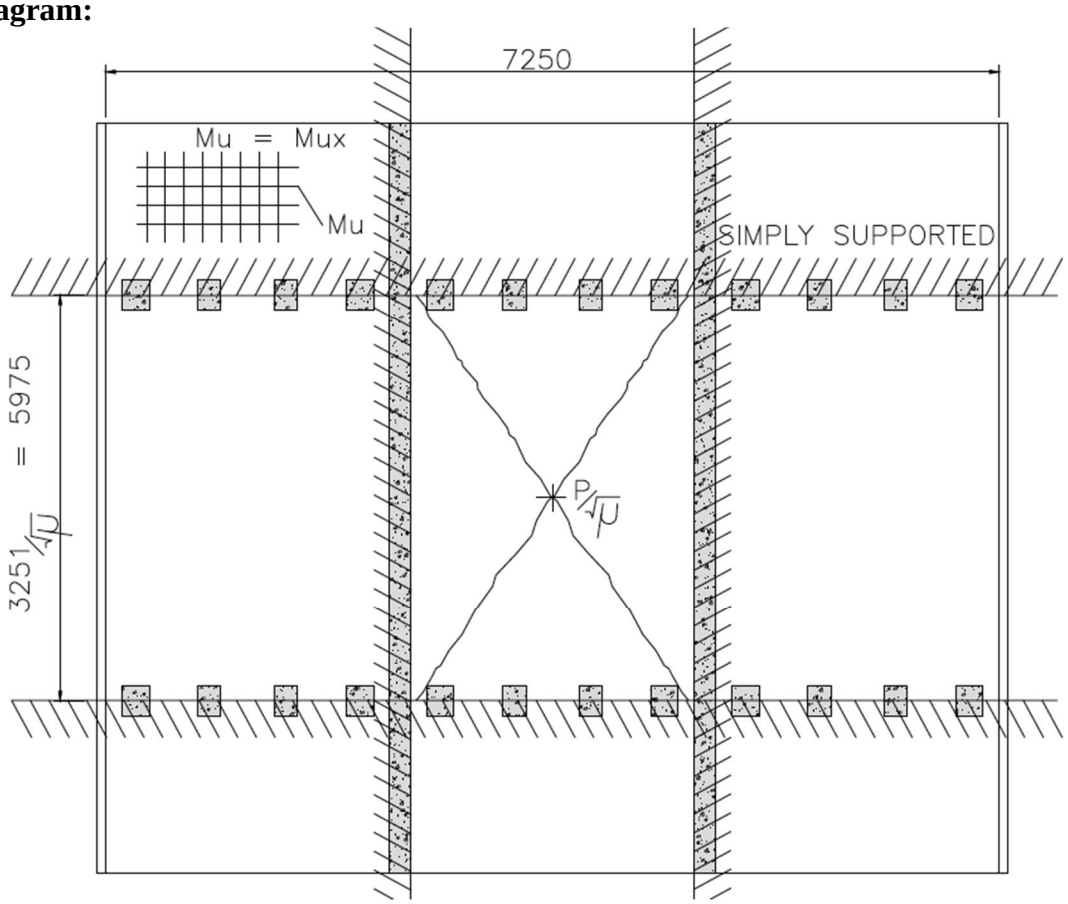

Internal Work:

$$\boldsymbol{Internal\ work = 2 * M_u * L_y * \frac{\delta}{0.5 * L_x} + 2 * M_u * L_x * \frac{\delta}{0.5 * L_y}}$$

External Work:

$$\boldsymbol{External\ work = \frac{P}{\sqrt{\mu}} * \delta}$$

Where:

$$\boldsymbol{M_{ux} = 358\ kNm/m}$$
$$\boldsymbol{M_{uy} = 106\ kN\ m/m}$$

$$\boldsymbol{\mu = \frac{M_{uy}}{M_{ux}} = 0.296}$$

$$\boldsymbol{M_u = M_{u'} = M_{ux}}$$

$$L_x = 5.975\ m$$
$$L_y = 2.415\ m$$

Equate *Internal* and *External Work* → solve for P:

$$2 * M_u * L_y * \frac{\delta}{0.5 * L_x} + 2 * M_u * L_x * \frac{\delta}{0.5 * L_y} = \frac{P}{\sqrt{\mu}} * \delta$$

Therefore:

$$P = 2242\ kN$$

MODE (d)

Diagram:

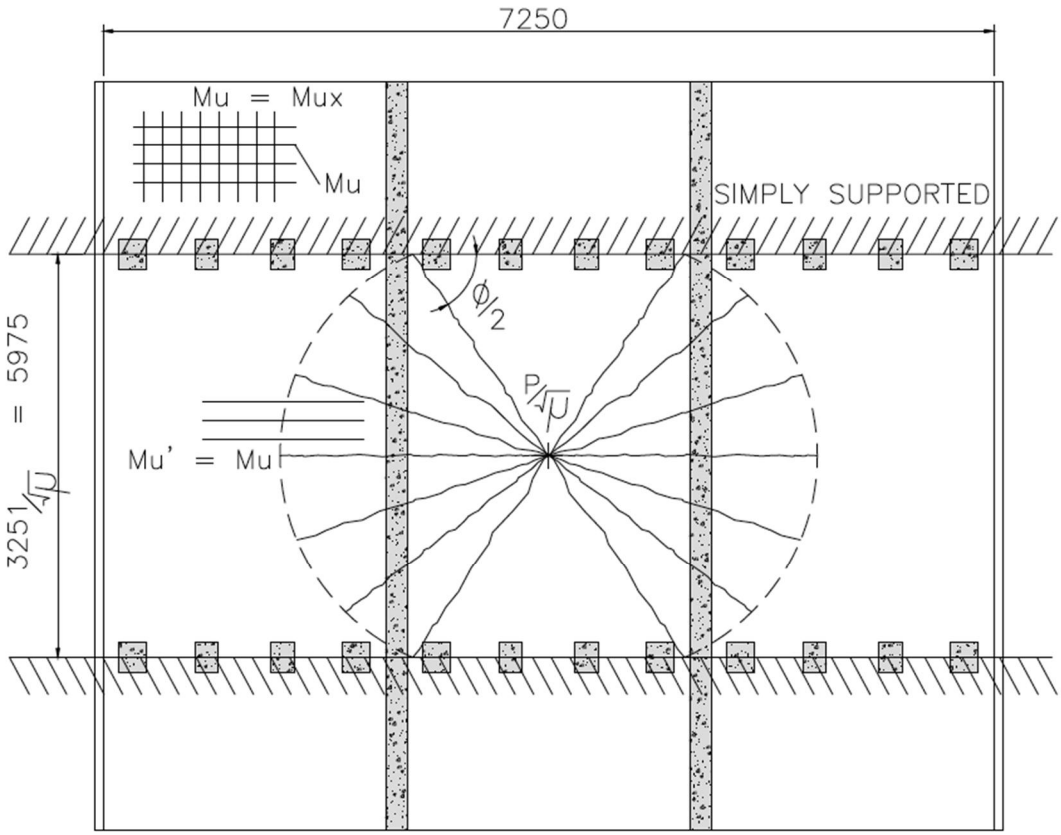

Internal Work:

$$\boldsymbol{Internal\ work = 2 * M_u * L_y * \frac{\delta}{0.5 * L_x} + 2 * (M_u + M_{u'}) * \Phi * \delta}$$

External Work:

$$\boldsymbol{External\ work = \frac{P}{\sqrt{\mu}} * \delta}$$

Where:

$$\boldsymbol{M_{ux} = 358\ kNm/m}$$
$$\boldsymbol{M_{uy} = 106\ kN\ m/m}$$

$$\boldsymbol{\mu = \frac{M_{uy}}{M_{ux}} = 0.296}$$

$$\boldsymbol{M_u = M_{u'} = M_{ux}}$$

$$L_x = 5.975\ m$$
$$L_y = 2.415\ m$$

$$\phi/_2 = tan^{-1}\left(\frac{0.5 * L_x}{0.5 * L_y}\right) = 68^\circ\ therefore, \phi = 136^\circ\ or\ 0.756\pi\ radians$$

Equate *Internal* and *External Work* → solve for P:

$$2 * M_u * L_y * \frac{\delta}{0.5 * L_x} + 2 * (M_u + M_{u'}) * \Phi * \delta = \frac{P}{\sqrt{\mu}} * \delta$$

Therefore:

$$P = 2165\ kN$$

MODE (e)

Diagram:

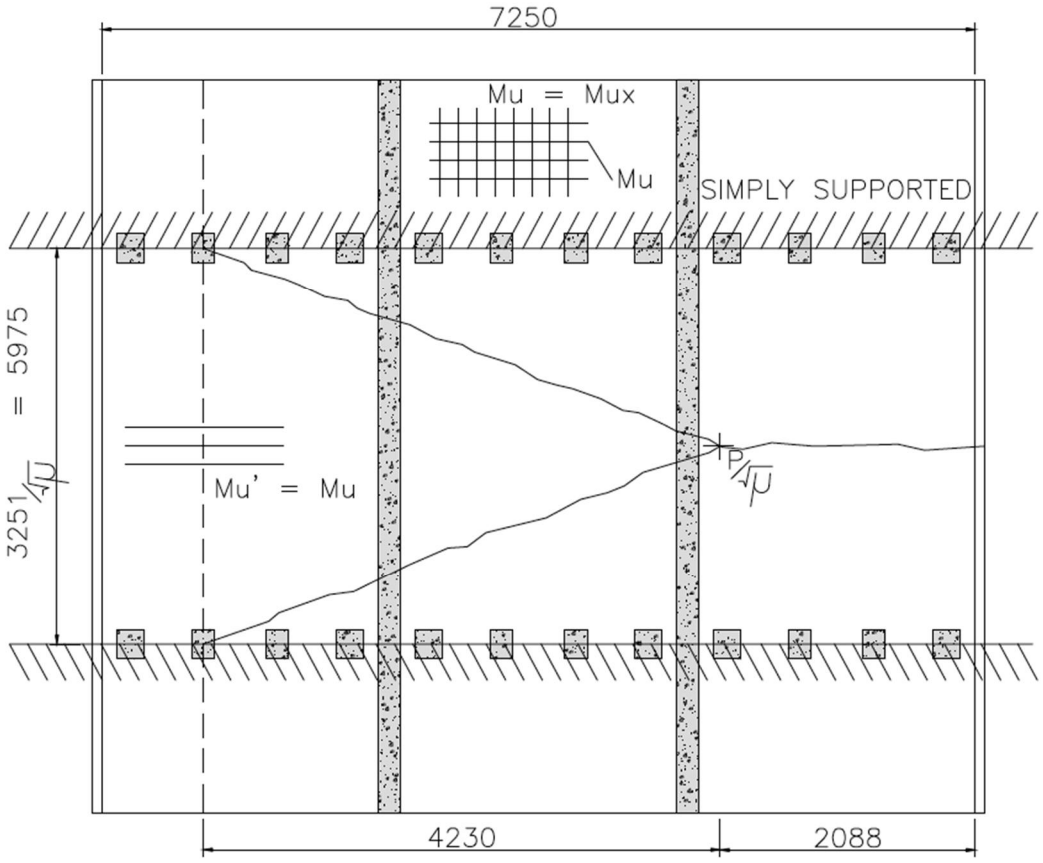

Internal Work:

$$\boldsymbol{Internal\ work = 4 * M_u * (a + b) * \frac{\delta}{0.5 * L_x} + (M_u + M_{u'}) * \frac{L_x}{a}}$$

$$\boldsymbol{b = 2.088\ m\ (distance\ from\ loading\ point\ to\ free\ edge)}$$

Take the derivative of the internal work and set to zero to determine the distance 'a' corresponding to the minimum.

$$\boldsymbol{0 = \frac{dInternal\ work}{da} = 4 * \frac{M_u}{L_x} - \frac{(M_{u'} + M_u) * L_x}{a^2}}$$

Therefore,

$$\boldsymbol{a = 4.230\ m}$$

External Work:

$$External\ work = \frac{P}{\sqrt{\mu}} * \delta$$

Where:

$$M_{ux} = 358\ kNm/m$$
$$M_{uy} = 106\ kN\ m/m$$

$$\mu = \frac{M_{uy}}{M_{ux}} = 0.296$$

$$M_u = M_{u'} = M_{ux}$$
$$L_x = 5.975\ m$$
$$L_y = 2.415\ m$$

Equate *Internal* and *External Work* → solve for P:

$$4 * M_u * (a + b) * \frac{\delta}{0.5 * L_x} + (M_u + M_{u'}) * \frac{L_x}{a} = \frac{P}{\sqrt{\mu}} * \delta$$

Therefore:

$$P = 2198\ kN$$

MODE (f)

Diagram:

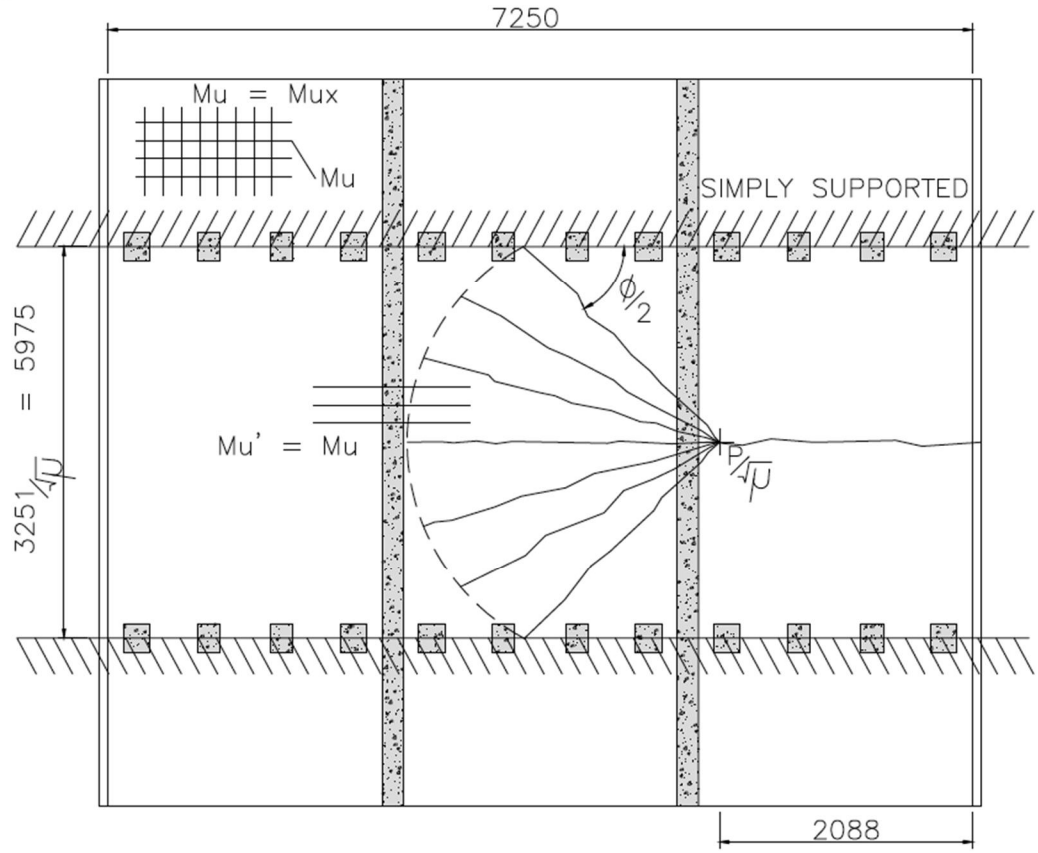

Internal Work:

$$\boldsymbol{Internal\ work = 2 * M_u * (b + \frac{L_x}{2} * cot\frac{\emptyset}{2}) * \frac{\delta}{0.5 * L_x} + (M_u + M_{u'}) * \emptyset * \delta}$$

$$\boldsymbol{b = 2.088\ m\ (distance\ from\ loading\ point\ to\ free\ edge)}$$

Take the derivative of the internal work and set to zero to determine the angle 'Φ' corresponding to the minimum.

$$\boldsymbol{0 = \frac{dInternal\ work}{d\emptyset} = -M_u * csc^2\frac{\emptyset}{2} + (M_u + M_{u'})}$$

Therefore,

$$\boldsymbol{\emptyset = 90^\circ\ or\ \pi/2\ radians}$$

External Work:

$$External\ work = \frac{P}{\sqrt{\mu}} * \delta$$

Where:

$$M_{ux} = 358\ kNm/m$$
$$M_{uy} = 106\ kN\ m/m$$

$$\mu = \frac{M_{uy}}{M_{ux}} = 0.296$$

$$M_u = M_{u'} = M_{ux}$$
$$L_x = 5.975\ m$$
$$L_y = 2.415\ m$$

Equate *Internal* and *External Work* → solve for P:

$$2 * M_u * (b + \frac{L_x}{2} * cot\frac{\emptyset}{2}) * \frac{\delta}{0.5 * L_x} + (M_u + M_{u'}) * \emptyset * \delta = \frac{P}{\sqrt{\mu}} * \delta$$

Therefore:

$$P = 2341\ kN$$